NASA/TM–2015–218990

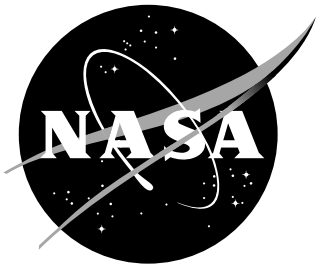

Entropy Stable Staggered Grid Spectral Collocation for the Burgers' and Compressible Navier-Stokes Equations

Mark H. Carpenter and Matteo Parsani
Langley Research Center, Hampton, Virginia

Travis C. Fisher
Sandia National Laboratories, Albuquerque, New Mexico

Eric J. Nielsen
Langley Research Center, Hampton, Virginia

December 2015

NASA STI Program . . . in Profile

Since its founding, NASA has been dedicated to the advancement of aeronautics and space science. The NASA scientific and technical information (STI) program plays a key part in helping NASA maintain this important role.

The NASA STI program operates under the auspices of the Agency Chief Information Officer. It collects, organizes, provides for archiving, and disseminates NASA's STI. The NASA STI program provides access to the NTRS Registered and its public interface, the NASA Technical Reports Server, thus providing one of the largest collections of aeronautical and space science STI in the world. Results are published in both non-NASA channels and by NASA in the NASA STI Report Series, which includes the following report types:

- TECHNICAL PUBLICATION. Reports of completed research or a major significant phase of research that present the results of NASA Programs and include extensive data or theoretical analysis. Includes compilations of significant scientific and technical data and information deemed to be of continuing reference value. NASA counter-part of peer-reviewed formal professional papers but has less stringent limitations on manuscript length and extent of graphic presentations.

- TECHNICAL MEMORANDUM. Scientific and technical findings that are preliminary or of specialized interest, e.g., quick release reports, working papers, and bibliographies that contain minimal annotation. Does not contain extensive analysis.

- CONTRACTOR REPORT. Scientific and technical findings by NASA-sponsored contractors and grantees.

- CONFERENCE PUBLICATION. Collected papers from scientific and technical conferences, symposia, seminars, or other meetings sponsored or co-sponsored by NASA.

- SPECIAL PUBLICATION. Scientific, technical, or historical information from NASA programs, projects, and missions, often concerned with subjects having substantial public interest.

- TECHNICAL TRANSLATION. English-language translations of foreign scientific and technical material pertinent to NASA's mission.

Specialized services also include organizing and publishing research results, distributing specialized research announcements and feeds, providing information desk and personal search support, and enabling data exchange services.

For more information about the NASA STI program, see the following:

- Access the NASA STI program home page at http://www.sti.nasa.gov

- E-mail your question to help@sti.nasa.gov

- Phone the NASA STI Information Desk at 757-864-9658

- Write to:
  NASA STI Information Desk
  Mail Stop 148
  NASA Langley Research Center
  Hampton, VA 23681-2199

NASA/TM–2015–218990

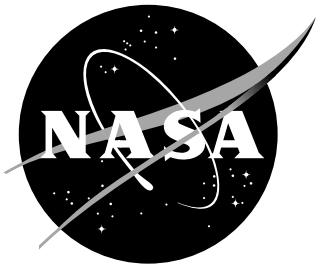

Entropy Stable Staggered Grid Spectral Collocation for the Burgers' and Compressible Navier-Stokes Equations

Mark H. Carpenter and Matteo Parsani
Langley Research Center, Hampton, Virginia

Travis C. Fisher
Sandia National Laboratories, Albuquerque, New Mexico

Eric J. Nielsen
Langley Research Center, Hampton, Virginia

National Aeronautics and
Space Administration

NASA Langley Research Center
Hampton, Virginia 23681-2199

December 2015

Acknowledgments

Special thanks are extended to Dr. Mujeeb R. Malik for funding this work as part of NASA's Transformational Tools and Technologies (T3) project. This research was also supported by an appointment to the NASA Postdoctoral Program at the NASA Langley Research Center, administered by Oak Ridge Associated Universities through a contract with NASA. Our gratitude also goes to the IT support of our system administrators Steve Carrithers and Jim Matthews of the NASA Langley Computational AeroSciences Branch.

Available from:

NASA STI Program / Mail Stop 148
NASA Langley Research Center
Hampton, VA 23681-2199
Fax: 757-864-6500

Abstract

Staggered grid, entropy stable discontinuous spectral collocation operators of any order are developed for Burgers' and the compressible Navier-Stokes equations on unstructured hexahedral elements. This generalization of previous entropy stable spectral collocation work [1, 2], extends the applicable set of points from tensor product, Legendre-Gauss-Lobatto (LGL) to a combination of tensor product Legendre-Gauss (LG) and LGL points. The new semi-discrete operators discretely conserve mass, momentum, energy and satisfy a mathematical entropy inequality for both Burgers' and the compressible Navier-Stokes equations in three spatial dimensions. They are valid for smooth as well as discontinuous flows. The staggered LG and conventional LGL point formulations are compared on several challenging test problems. The staggered LG operators are significantly more accurate, although more costly to implement. The LG and LGL operators exhibit similar robustness, as is demonstrated using test problems known to be problematic for operators that lack a nonlinearly stability proof for the compressible Navier-Stokes equations (e.g., discontinuous Galerkin, spectral difference, or flux reconstruction operators).

Contents

1 Introduction

Beginning with a high-order solution polynomial, numerous approaches exist for constructing discontinuous Galerkin (DG) spectral element methods. Popular variants adopt either the weak (integral) or strong (differential) form of the governing equations derived by integrating the equations once or twice against a test function. Various interior and interface flux approximations are used (e.g., quadrature free fluxes [3], or skew-symmetric operators [4]), as are various quadrature rules (e.g., Legendre-Gauss,[1] Legendre-Gauss-Lobatto, or Legendre-Gauss-Radau points). Each design choice is motivated by desirable goals, such as efficiency, accuracy, data locality, flexibility, etc. Kopriva and Gassner [5] presented a survey of design decisions made when constructing nodal DG algorithms, as well as their advantages and disadvantages.

A popular design philosophy for the incompressible Navier-Stokes equations is to stagger the solution and fluxes at independent point sets. For example, Bernardi and Maday use a staggered approach for the Stokes problem [6]. For the compressible Navier-Stokes equations, Kopriva and Kolias [7] collocate the solution variables at the Legendre-Gauss-Chebyshev quadrature points $(0, \cdots, N-1)$, and evaluate the fluxes at the Legendre-Gauss-Chebyshev points $(0, \cdots, N)$. This conservative combination of over-collocated fluxes proves to be more robust in practical problems than conventional Legendre-Gauss-Lobatto (LGL) techniques [7]. (The number of flux points exceeds the solution points by one, and is reminiscent of the spectral finite volume method of Cai, Gottlieb, and Harten [8]). Staggered collocation operators have evolved over the past two decades to include a rich set of approaches. For example, the spectral difference (SD) [9,10] and flux reconstruction (FR) [11, 12] approaches, discretize the compressible Navier-Stokes equations in strong form on a staggered set of solution (order p) and flux points (order $p+1$). The observed convergence rate is reported to be $(p+1)$, for a sequence of nested uniform and quasi-uniform grids.

An alternate design strategy based on a summation-by-parts (SBP), simultaneous-approximation-term (SAT) framework (i.e., SBP-SAT operators), is used in references 1, 2 to construct discontinuous collocation spectral element methods of any order, and are referred to as entropy stable (SS) discontinuous collocation (DC) algorithms (i.e., SSDC algorithms). Therein, the primary design motivation is a semi-discrete spatial operator that supports a nonlinear (entropy) stability proof for the compressible three-dimensional (3D) Navier-Stokes equations, on curvilinear unstructured hexahedral elements.

The SSDC operators discretize the governing equations in strong form at the 3D tensor product LGL points, and adjoining elements are coupled using a provably nonlinearly stable SAT penalty approach technique [13]. The resulting algorithm is similar to the strong form nodal DG method reported in reference 14, although it differs in the treatment of the nonlinear Euler fluxes and the interface couplings. A novel choice of nonlinear fluxes ensures conservation of mass, momentum and energy as well as the entropy inequality within each element; hence element-wise entropy stability.[2] Carefully constructed interface fluxes then guarantee boundedness of the entropy throughout the entire domain. The nonlinear stability is achieved without additional hyper-viscosity dissipation, de-aliasing or filtering, and over-integration of the fluxes or solution. Other important differences with respect to the DG, SD, and FR schemes appear in the treatment of boundary conditions, which are designed to preserve the nonlinear stability of the interior operators (see, references 2, 15).

[1] These points are also referred to as Gauss points in literature.

[2] Dissipation is required for shocked flows to enforce a physical entropy inequality, and density and pressure (or temperature) are assumed to remain positive.

Entropy stable spectral collocation operators are robust for shocks of moderate strength (e.g., normal shock strengths $M \leq 1.75$), and are fully consistent with the Lax-Wendroff theorem [16] for weak solutions. The robustness stems from a semi-discrete thermodynamic entropy that is provably bounded for all time in the L^2 norm, provided that boundary data preserves the entropy estimate of the interior operator (and density and temperature remain positive). The nonlinear stability proof is sharp; indeed entropy conservative interface fluxes guarantee global entropy conservation (neutral nonlinear stability). This sharp estimate is achieved because hyper-viscosity dissipation, de-aliasing or filtering of the fluxes/solution is not needed. Furthermore, assumptions of integral exactness are unnecessary to justify the proof (commonly used in weak form finite element methods (FEM)), because strong conservation form derivatives are approximated using diagonal-norm SBP operators, rather than weak form integrals. Thus, over-integration of the nonlinear fluxes is unnecessary to more closely approximate integral exactness.

Although the formulations presented in references 1, 2 are a significant step towards operational entropy stable discontinuous collocation spatial discretizations of any order, noteworthy challenges remain: 1) arbitrary collocation points, 2) spatial- (h) and order- (p) adaptive refinement of hexahedral elements, and 3) triangular, prismatic and tetrahedral elements. Herein, an SBP-SAT framework is used to develop a staggered grid, entropy stable spectral element formulation that includes a broader selection of collocation points. The entropy stable mechanics developed in references 1, 2 are extended to include solutions collocated at the Legendre-Gauss (LG) points with fluxes computed at the LGL points. The competitive advantages of the new entropy stable staggered algorithm relative to the algorithms presented in references 1, 2 are then established.

The new staggered operators based on the LG points have several advantages relative to the pure LGL operators. First, the integral exactness of the LG points exceeds that of the LGL points: $(2p + 1)$ vs. $(2p - 1)$, and it is shown elsewhere [5] that the LG points have superior accuracy properties. Second, the LG points are an interior point distribution and as such, the solution data is not duplicated on adjoining element interfaces. Neither are variables collocated at the corners of the element. Thus, geometric boundary discontinuities are handled in an integral sense without explicit knowledge of the boundary singularity. In more general terms, moving data around an element while maintaining entropy stability is an important capability when developing additional element types and connectivities. For example, consider the closely related problems of h-refinement at a $2:1$ element interface compression or a p-refinement interface. These scenarios require data movement from adjoining interfaces onto a common intermediate mortar [17]. The quadrature points do not in general coincide on either side of the interface. Thus, the nonlinear stability proofs presented in references 1, 2 do not immediately extend to this extremely important capability.

Extensive numerical tests presented herein, reveal that the new staggered entropy stable discontinuous collocation (staggered SSDC) operators are significantly more accurate than the LGL SSDC operators [1,2], of equivalent polynomial order. They are however, more costly to implement. Simple counting arguments based on inviscid and viscous flux evaluations, indicate that the cost of the staggered algorithm for a solution polynomial order p is comparable to that of an LGL operator [1,2], with a solution polynomial order of $(p+1)$. Preliminary studies using an explicit temporal integrator indicate that the increased accuracy of the staggered approach partially offsets the additional cost, particularly at low polynomial order. Further investigation is needed to convincingly establish whether over-collocating the fluxes (including the SD [7, 9] or FR [11, 12] operators) can be justified from a cost perspective. An ongoing investigation continues that includes the effects of implicit temporal integrators as well as the impact of data movement; computationally intensive

yet extremely accurate, low memory footprint algorithms will be competitive in the future.

The paper is organized as follows. Section 2 includes the general theory of SBP operators, and differentiation and interpolation spectral collocation operators. Section 3 includes a brief survey of entropy stability at the continuous and semi-discrete level, the data mechanics and the interface SAT coupling approach for the staggered SSDC operator in multiple spatial dimensions. Section 4 includes the mechanics of the staggered SSDC operator. Both energy and entropy proof are presented for the 1D Burgers' equation. Section 5 extends the 1D staggered SSDC operator to multiple spatial dimensions in the context of the compressible Navier-Stokes equations. Section 6 extends the staggered SSDC operator to multiple elements. In Section 7, a theoretical cost comparison is made between the conventional collocated [1, 2] and the staggered SSDC operators. Section 8 presents numerous numerical studies. The Euler vortex and viscous shock propagation problems are used to demonstrate the superior accuracy of the staggered algorithm. The Taylor-Green vortex problem and supersonic flow past a 3D square cylinder (Mach = 1.5, and $Re = 10^4$), are used to demonstrate the robustness in the limit of order one discretization errors. Section 9 summarizes the results of the paper. Two appendices are included. Appendix A includes a more detailed discussion on SBP-SAT operators, while a derivation of spectral derivative and interpolation operators is included in Appendix B.

2 Summation-by-parts operators

2.1 First derivative

First derivative operators that satisfy the summation-by-parts (SBP) convention, discretely mimic the integration-by-parts property

$$\int_{x^L}^{x^H} \phi \, \frac{\partial q}{\partial x} \, \mathrm{d}x = \phi \, q|_{x^L}^{x^H} - \int_{x^L}^{x^H} \frac{\partial \phi}{\partial x} \, q \, \mathrm{d}x, \tag{1}$$

with ϕ an arbitrary scalar test function. At the discrete level, this mimetic property is achieved by constructing the first derivative approximation, $\mathcal{D}\boldsymbol{\phi}$, with an operator in the form

$$\begin{gathered} \mathcal{D} = \mathcal{P}^{-1} \, \mathcal{Q}, \quad \mathcal{P} = \mathcal{P}^{\top}, \quad \boldsymbol{\zeta}^{\top} \mathcal{P} \boldsymbol{\zeta} > 0, \quad \boldsymbol{\zeta} \neq \mathbf{0}, \\ \mathcal{Q}^{\top} = \mathcal{B} - \mathcal{Q}, \quad \mathcal{B} = \mathrm{Diag}\left(-1, 0, \ldots, 0, 1\right), \end{gathered} \tag{2}$$

where $\boldsymbol{\zeta}$ is an arbitrary vector. The matrix $\mathcal{P}$ can be thought of as a mass matrix (or integrator) much like in the finite element framework, or a volume that contains local grid information in the context of finite volume or finite difference numerical methods. The nearly skew-symmetric matrix $\mathcal{Q}$, is an undivided differencing operator; all rows sum to zero, as do all columns save the first and last, which sum to -1 and 1, respectively. The special structure of $\mathcal{Q}$ guarantees conservation as is proven in the following lemma.

Lemma 2.1. *All differentiation matrices, $\mathcal{D}$, satisfying the SBP convention given in equation* (2) *are discretely conservative in the $\mathcal{P}$-norm.*

Proof. The proof of this lemma can be found in reference 18. □

While the matrix $\mathcal{P}$ need not be diagonal, the class of diagonal norm SBP operators play a crucial roll in the development of entropy stable (SS) SBP simultaneous-approximation-term (SAT) operators (see references 1, 2, 15, 19, 20).

The accuracy of the first derivative operator, $\mathcal{D}$, can be expressed as

$$\frac{\partial \boldsymbol{\phi}}{\partial x}(\mathbf{x}) = \mathcal{D}\boldsymbol{\phi}(\mathbf{x}) + \mathcal{T}_{p+1}, \tag{3}$$

where

$$\mathbf{x} = (x_1, \ldots, x_N), \quad x_1 = x^L, \quad x_N = x^H \tag{4}$$

are the collocated points, and

$$\begin{aligned} \boldsymbol{\phi}(\mathbf{x}) &= (\phi(x_1), \phi(x_2), \ldots, \phi(x_N))^\top \\ \frac{\partial \boldsymbol{\phi}}{\partial x}(\mathbf{x}) &= \left(\frac{d\phi}{dx}(x_1), \frac{d\phi}{dx}(x_2), \ldots, \frac{d\phi}{dx}(x_N)\right)^\top \end{aligned} \tag{5}$$

are the projections of the test function ϕ and its derivative onto the grid $\mathbf{x}$. $\mathcal{T}_{p+1}$ is the truncation error of the approximation of the first derivative, which is p-th order accurate. Integration in the approximation space is conducted using an inner product with the integration weights contained in the norm $\mathcal{P}$,

$$\int_{x^L}^{x^H} \phi \frac{\partial q}{\partial x} \, \mathrm{d}x \approx \boldsymbol{\phi}^\top \mathcal{P}\mathcal{D}\mathbf{q}, \tag{6}$$

where

$$\mathbf{q}(\mathbf{x}) = (q(x_1), q(x_2), \ldots, q(x_N))^\top, \quad \text{with} \quad \mathbf{x} = (x_1, \ldots, x_N), \quad x_1 = x^L, \quad x_N = x^H, \tag{7}$$

is the projection of continuous variables q onto the grid $\mathbf{x}$. Substituting equation (2) into equation (6), the mimetic SBP property is demonstrated,

$$\boldsymbol{\phi}^\top \mathcal{P}\mathcal{P}^{-1}\mathcal{Q}\mathbf{q} = \boldsymbol{\phi}^\top \left(\mathcal{B} - \mathcal{Q}^\top\right)\mathbf{q} = \phi_N q_N - \phi_1 q_1 - \boldsymbol{\phi}^\top \mathcal{D}^\top \mathcal{P}\mathbf{q}. \tag{8}$$

2.2 Discontinuous spectral collocation operators

2.2.1 Differentiation

Consider the SBP operators constructed at the Legendre-Gauss-Lobatto (LGL) points [21], which include the end points of the interval, x^L and x^H. The complete discretization operator for the fourth-order accurate polynomial interpolation ($p = 4$) in the standard one-dimensional (1D) element ($x^L = -1$, $x^H = +1$) is illustrated in Figure 1. In this figure, the solution points are identified with $\bullet$ and the flux points are identified with $|$. The latter points are similar in nature to the control volume edges employed in the finite volume method and are used to prove the nonlinear stability (entropy stability) as briefly shown in Section 3.3, (see references 1,2 for a more detailed discussion).

Define the Lagrange basis polynomials relative to the N discrete LGL points, $\mathbf{x}$, as

$$L_j(x) = \prod_{\substack{k=1 \\ k \neq j}}^{N} \frac{x - x_k}{x_j - x_k}, \qquad 1 \leq j \leq N. \tag{9}$$

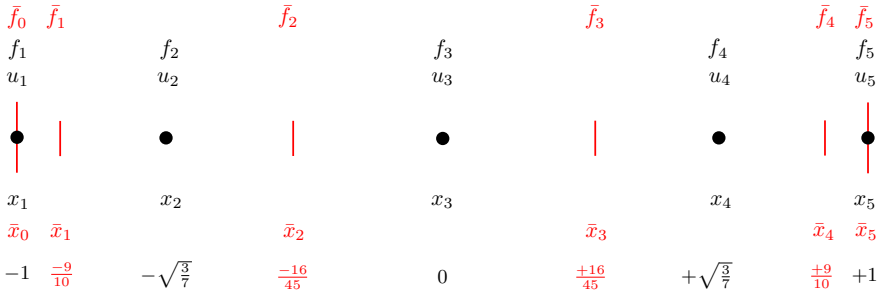

Figure 1. The one-dimensional discretization for the fourth-order accurate polynomial interpolation ($p = 4$) LGL collocation is illustrated. Solution points are identified with • and the flux points are identified with |.

Assume that a smooth and (infinitely) differentiable function $f(x)$ is defined on the interval $x^L = -1 \leq x \leq 1 = x^H$. Reading the function f and its derivative $\frac{df}{dx}$ at the discrete points, $\mathbf{x}$, yields the vectors

$$\begin{aligned} \mathbf{f}(\mathbf{x}) &= (f(x_1), f(x_2), \cdots, f(x_{N-1}), f(x_N))^\top, \\ \frac{d\mathbf{f}}{dx}(\mathbf{x}) &= \left(\frac{df}{dx}(x_1), \frac{df}{dx}(x_2), \cdots, \frac{df}{dx}(x_{N-1}), \frac{df}{dx}(x_N)\right)^\top. \end{aligned} \tag{10}$$

The interpolation polynomial $f_N(x)$ (of order $p = N - 1$) that collocates $f(x)$ at the discrete points, $\mathbf{x}$, is given by the contraction

$$f(x) \approx f_N(x) = \mathbf{L}(x; \mathbf{x})^\top \mathbf{f}(\mathbf{x}), \tag{11}$$

where $\mathbf{L}(x; \mathbf{x})$ is a column vector whose components are the Lagrange basis polynomials relative to the nodes $\mathbf{x}$ (i.e., $L_j(x)$ in equation (9)). Note that the explicit dependence of $\mathbf{L}$ on the independent variable x and the set of point $\mathbf{x}$ is indicated for completeness.[3]

Theorem 2.1. *The derivative operator that exactly differentiates an arbitrary p-th order polynomial ($p = N - 1$) at the collocation points, $\mathbf{x}$, is*

$$\mathcal{D} \;=\; (d_{ij}) = \left(\frac{dL_j}{dx}(x_i)\right), \tag{12}$$

where $\frac{dL_j}{dx}(x_i)$ denotes the derivatives of the L_j Lagrange basis polynomial with respect to x evaluated at the collocated node x_i. This element corresponds to the element in the j-th column and i-th row of the differentiation matrix $\mathcal{D}$.

Proof. The proof to this theorem can be found in Appendix B (see also reference 21). □

A representation of the differentiation operator $\mathcal{D}$, which satisfies all the requirements for being an SBP operator is given in the following theorem

[3] f_N is a polynomial of order p in the independent variable x.

Theorem 2.2. *The derivative operator that exactly differentiates an arbitrary p-th order polynomial ($p = N - 1$) at the collocation points,* $\mathbf{x}$*, can be expressed as*

$$\mathcal{D} \;=\; \mathcal{P}^{-1}\,\mathcal{Q} \tag{13}$$

with

$$\mathcal{P} \;=\; \textstyle\sum_\ell \mathbf{L}(\eta_l;\mathbf{x})\mathbf{L}(\eta_l;\mathbf{x})^\top\omega_\ell \quad , \quad \mathcal{Q} \;=\; \sum_\ell \mathbf{L}(\eta_l;\mathbf{x})\tfrac{d\mathbf{L}}{dx}(\eta_l;\mathbf{x})^\top\omega_\ell, \tag{14}$$

where η_ℓ and ω_ℓ, $1 \le l \le N$, are the abscissae of the LGL points and their quadrature weights, respectively. $\mathbf{L}(x;\mathbf{x})$ *is a column vector whose components are the Lagrange basis polynomials relative to the discrete nodes* $\mathbf{x}$ *(i.e., $L_j(x)$ in equation* (9)*)*

Proof. The proof to this theorem can be found in Appendix B. □

The matrix $\mathcal{P}$ in (14) is symmetric and positive definite for any vector $\mathbf{x}$ [21]. When the LGL points are used for $\mathbf{x}$, then $\mathcal{P}$ is a diagonal approximation (i.e., the so-called "mass lumped" approximation) of the full $\mathcal{P}$-norm (see Appendix B). A diagonal norm SBP operator is necessary to achieve strict entropy stability [22, 23]. This constraint on the norm $\mathcal{P}$ is reiterated in section 3.3.1.

2.2.2 Interpolation

Define on the interval $-1 \le x \le 1$, the vectors of discrete point,

$$\begin{aligned} \widetilde{\mathbf{x}} &= (\widetilde{x}_1, \widetilde{x}_2, \cdots, \widetilde{x}_{M-1}, \widetilde{x}_M)^\top, \quad -1 \le \widetilde{x}_1, \widetilde{x}_2, \cdots, \widetilde{x}_{M-1}, \widetilde{x}_M \le 1; \\ \mathbf{x} &= (x_1, x_2, \cdots, x_{N-1}, x_N)^\top, \quad -1 \le x_1, x_2, \cdots, x_{N-1}, x_N \le 1. \end{aligned} \tag{15}$$

Herein, the discrete points $\widetilde{\mathbf{x}}$ and $\mathbf{x}$ are the Legendre-Gauss (LG) points (i.e., the so called Gauss points) and the LGL points, respectively. All the scalars, vectors, and matrices associated to the LG points are denoted with a "tilde" symbol. Next, define the interpolation operators that move data between $\widetilde{\mathbf{x}}$ and $\mathbf{x}$:

$$\begin{aligned} \mathcal{I}_{LGL\to LG} &= \widetilde{\mathcal{P}}^{-1}\,\mathcal{R}_{LG-LGL}, \\ \mathcal{I}_{LG\to LGL} &= \mathcal{P}^{-1}\mathcal{R}_{LG-LGL}^\top, \\ \widetilde{\mathcal{P}}\,\mathcal{I}_{LGL\to LG} &= \mathcal{I}_{LG\to LGL}^\top\,\mathcal{P}, \end{aligned} \tag{16}$$

where

$$\mathcal{R}_{LG-LGL} \;=\; \int_{-1}^{1} \mathbf{L}(x;\widetilde{\mathbf{x}})\,\mathbf{L}(x;\mathbf{x})^\top\,dx. \tag{17}$$

In Appendix B.3, we prove that these polynomial interpolation operators exist and satisfy the relations (16), provided that the LGL points are of higher polynomial orders than the LG points (i.e., $N > M$).

3 Entropy consistent and entropy stable SBP operators

3.1 Governing equations

Consider the three-dimensional (3D) compressible Navier-Stokes equations for a calorically perfect gas expressed in the form

$$\begin{aligned} &\frac{\partial q}{\partial t} + \frac{\partial f_i}{\partial x_i} = \frac{\partial f_i^{(V)}}{\partial x_i}, \quad x \in \Omega, \quad t \in [0, \infty), \\ &Bq = g^{(B)}(x,t), \quad x \in \partial\Omega, \quad t \in [0, \infty), \\ &q(x,0) = g^{(0)}(x), \quad x \in \Omega, \end{aligned} \tag{18}$$

where the Cartesian coordinates, $x = (x_1, x_2, x_3)^\top$, and time, t, are independent variables, and index sums are implied. The vectors q, f_i, and $f_i^{(V)}$ are the conserved variables, and the conserved inviscid and viscous fluxes, respectively. Without loss of generality, a 3D box

$$\Omega = [x_1^L, x_1^H] \times [x_2^L, x_2^H] \times [x_3^L, x_3^H]$$

is chosen as our computational domain with $\partial\Omega$ representing the boundary of the domain. The boundary vector $g^{(B)}$ is assumed to contain linearly well-posed Dirichlet and/or Neumann data. Herein, we have omitted a detailed description of the 3D compressible Navier-Stokes equations because it can easily be found in literature.

3.2 Continuous analysis

Consider the (nonlinear) compressible Navier-Stokes equations given in equation (18). This system of incomplete parabolic partial differential equations (PDEs) have a quadratic or otherwise convex extension of its original form, that when integrated over the physical domain, Ω, depends only on boundary data and dissipative terms. This convex extension yields the entropy function and provides a mechanism for proving the stability in the L^2 norm of the nonlinear system of PDEs (18). In fact, Dafermos [24] showed that if a system of conservation laws is endowed with a convex entropy function, $S = S(q)$, a bound on the global estimate of S can be converted into an a priori estimate on the solution vector q (e.g., the solution of system (18)).

Definition 3.1. *A scalar function $S = S(q)$ is an entropy function of system* (18) *if it satisfies the following conditions:*

- *Differentiation of the convex function $S(q)$, simultaneously contracts all the inviscid spatial fluxes as follows*

$$\frac{\partial S}{\partial q}\frac{\partial f_i}{\partial x_i} = \frac{\partial S}{\partial q}\frac{\partial f_i}{\partial q}\frac{\partial q}{\partial x_i} = \frac{\partial F_i}{\partial q}\frac{\partial q}{\partial x_i} = \frac{\partial F_i}{\partial x_i}, \quad i = 1, 2, 3. \tag{19}$$

  The components of the contracting vector, $\partial S/\partial q$, are the entropy variables denoted as $w^\top = \partial S/\partial q$. $F_i(q)$ are the entropy fluxes in the i-direction.

- *The entropy variables, w, symmetrize system* (18) *if w assumes the role of a new independent variable (i.e., $q = q(w)$). Expressing equations* (18) *in terms of w yields*

$$\frac{\partial q}{\partial t} + \frac{\partial f_i}{\partial x_i} - \frac{\partial f_i^{(V)}}{\partial x_i} = \frac{\partial q}{\partial w}\frac{\partial w}{\partial t} + \frac{\partial f_i}{\partial w}\frac{\partial w}{\partial x_i} - \frac{\partial}{\partial x_i}\left(\widehat{c}_{ij}\frac{\partial w}{\partial x_j}\right) = 0, \quad i = 1, 2, 3, \tag{20}$$

with the symmetry conditions: $\partial q/\partial w = (\partial q/\partial w)^\top$, $\partial f_i/\partial w = (\partial f_i/\partial w)^\top$ and $\widehat{c}_{ij} = \widehat{c}_{ij}^\top$.

Because the entropy is convex, the Hessian $\partial^2 S/\partial q^2 = \partial w/\partial q$ is positive definite[4]*,*

$$\zeta^\top \frac{\partial^2 S}{\partial q^2}\zeta > 0, \quad \forall \zeta \neq 0, \tag{21}$$

and yields a one-to-one mapping from conservation variables, q, to entropy variables, w. Likewise, $\partial w/\partial q$ is symmetric positive definite (SPD) because $\partial q/\partial w = (\partial w/\partial q)^{-1}$ and SPD matrices are invertible. The entropy and corresponding entropy flux are often denoted an entropy-entropy flux pair, (S, F) [25].

The symmetry of the matrices $\partial q/\partial w$ and $\partial f_i/\partial w$, indicates that the conservation variables, q, and inviscid fluxes, f_i, are Jacobians of scalar functions with respect to the entropy variables,

$$q^\top = \frac{\partial \varphi}{\partial w}, \quad {f_i}^\top = \frac{\partial \psi_i}{\partial w}, \tag{22}$$

where the nonlinear function, φ, is called the potential and ψ_i are called the potential fluxes [25]. The potential and the corresponding potential flux are denoted a potential-potential flux pair, (φ, ψ) [25].

Just as the entropy function is convex with respect to the conservative variables ($\partial^2 S/\partial q^2$ is SPD), the potential function is convex with respect to the entropy variables, w.

The two elements of Definition 3.1 are closely related, as is shown by Godunov [26] and Mock [27]. Godunov proves that:

Theorem 3.1. *If equation* (18) *can be symmetrized by introducing new variables w, and q is a convex function of φ, then an entropy function $S = S(q)$ is given by*

$$\varphi = w^\top q - S, \tag{23}$$

and the entropy fluxes $F_i(q)$ satisfy

$$\psi_i = w^\top f_i - F_i. \tag{24}$$

Proof. The proof of this theorem can be found in references 26, 28. □

Mock proves the converse to be true:

Theorem 3.2. *If $S = S(q)$ is an entropy function of system* (18)*, then $w^\top = \partial S/\partial q$ symmetrizes* (18)*.*

Proof. The proof of this theorem can be found in references 27, 28. □

[4]The Hessian, $\partial^2 S/\partial q^2$, is actually symmetric positive definite (SPD).

Contracting system (18) with the entropy variables, w, results in the differential form of the (scalar) entropy equation,

$$\begin{aligned}\frac{\partial S}{\partial q}\frac{\partial q}{\partial t}+\frac{\partial S}{\partial q}\frac{\partial f_i}{\partial x_i}=\frac{\partial S}{\partial t}+\frac{\partial F_i}{\partial x_i}=\frac{\partial S}{\partial q}\frac{\partial f_i^{(V)}}{\partial x_i}&=\frac{\partial}{\partial x_i}\left(w^\top f_i^{(V)}\right)-\left(\frac{\partial w}{\partial x_i}\right)^\top f_i^{(V)}\\&=\frac{\partial}{\partial x_i}\left(w^\top f_i^{(V)}\right)-\left(\frac{\partial w}{\partial x_i}\right)^\top \widehat{c}_{ij}\,\frac{\partial w}{\partial x_j}.\end{aligned}\tag{25}$$

Integrating equation (25) over the domain yields a global conservation statement for the entropy in the domain

$$\frac{d}{dt}\int_\Omega S\,\mathrm{d}\mathbf{x}=\left[w^\top f_i^{(V)}-F_i\right]_{\partial\Omega}-\int_\Omega w_{x_i}^\top\widehat{c}_{ij}\,w_{x_j}\,\mathrm{d}\mathbf{x}.\tag{26}$$

References 22, 23 prove that the five-by-five matrices $\widehat{c}_{ij}$ in the last term in the integral are positive semi-definite. Note that the entropy can only increase in the domain based on data that convects and diffuses through the boundaries, $\partial\Omega$. The sign of the entropy change from viscous dissipation is always negative.

Remark 3.1. *The scalar equation* (26) *is an integral statement of entropy conservation but it is not strictly valid in the presence of discontinuities (i.e., shocks). In fact, it does not account for the dissipation of the entropy at a shock. Although the precise amount of entropy dissipated at a discontinuity is not known a priori, what is known is the sign of the jump in entropy. Thus, a general but not sharp statement of the global behavior of entropy in the entire domain is*

$$\frac{d}{dt}\int_\Omega S\,\mathrm{d}\mathbf{x}\le\left[w^\top f_i^{(V)}-F_i\right]_{\partial\Omega}-\int_\Omega w_{x_i}^\top\,\widehat{c}_{ij}\,w_{x_j}\,\mathrm{d}\mathbf{x}.\tag{27}$$

Remark 3.2. *A sufficient condition to ensure the convexity of the entropy function $S=S(q)$ (and, hence, a one-to-one mapping between the entropy variables, w, and the conservative variables, q, is that $\rho,T>0$ (for the proof see for instance, Appendix B.1 in reference 19). Expressly:*

$$\boldsymbol{\zeta}^\top\frac{\partial^2 S}{\partial q^2}\,\boldsymbol{\zeta}^\top>0,\quad\forall\boldsymbol{\zeta}\neq 0,\quad\rho,T>0.$$

This (physical and mathematical) restriction on density, ρ, and temperature, T, weakens the entropy proof, making it less than full measure of nonlinear stability. Another mechanism must be employed to bound ρ and T away from zero to guarantee positivity; positivity preservation will not be considered herein.

3.3 Overview of the semi-discrete entropy analysis for the LGL points

The semi-discrete entropy estimate is achieved by mimicking term by term the continuous estimate given in equation (26). As for the continuous case, the nonlinear stability (entropy stability) analysis begins by contracting the discrete entropy variables, $\mathbf{w}^\top$, with the semi-discrete version of the system (18) (see for instance, references 1, 2). (For clarity of presentation, but without loss of generality, the derivation is simplified to one spatial dimension. Tensor product algebra allows the

results to be extended directly to three-dimensions.) The resulting global equation that governs the semi-discrete decay of entropy is given by [1]

$$\mathbf{w}^\top \mathcal{P}\mathbf{q}_t + \mathbf{w}^\top \Delta\overline{\mathbf{f}} = \mathbf{w}^\top \Delta\overline{\mathbf{f}}^{(V)} + \mathbf{w}^\top \mathbf{g}^{(B)} + \mathbf{w}^\top \mathbf{g}^{(Int)}, \tag{28}$$

where

$$\mathbf{w} = \left(w(q_1)^\top, w(q_2)^\top, \ldots, w(q_N)^\top\right)^\top.$$

The source terms $\mathbf{g}^{(B)}$ and $\mathbf{g}^{(Int)}$ contain the enforcement of boundary and interface conditions, respectively. (Herein, the solution between adjoining elements or cells is allowed to be discontinuous. Therefore, interface penalties $\mathbf{g}^{(Int)}$ are needed to patch interfaces together). The entropy variables, $\mathbf{w}$, are defined at the solution points whereas the quantities with an over-bar, i.e., $\overline{\mathbf{f}}$ and $\overline{\mathbf{F}}$, are defined at the flux points (see Figure 1). The analysis of each semi-discrete term is presented elsewhere [19]. The stability of the viscous $\left(\mathbf{w}^\top \Delta\overline{\mathbf{f}}^{(V)}\right)$ terms follow immediately by conventional approaches for diagonal norm SBP operators and will not be repeated herein. The analysis of the time derivative and inviscid terms is summarized next, while the form of the penalty terms is presented in Section 6.

3.3.1 Time derivative

The time derivative in (28) is in mimetic form for diagonal norm SBP operators. The entropy variables are defined by the expression $w^\top = \partial S/\partial q$. Define the diagonal matrices $\partial\mathbf{S}/\partial\mathbf{q} = \mathbf{W} = \text{Diag}[\mathbf{w}]$. Since $\mathcal{P}$ is a diagonal matrix (see equation (14)) and arbitrary diagonal matrices commute, the semi-discrete rate of change of entropy becomes

$$\mathbf{w}^\top \mathcal{P}\frac{\partial \mathbf{q}}{\partial t} \;=\; \mathbf{1}^\top \mathbf{W}\mathcal{P}\frac{\partial \mathbf{q}}{\partial t} \;=\; \mathbf{1}^\top \mathcal{P}\mathbf{W}\frac{\partial \mathbf{q}}{\partial t} \;=\; \mathbf{1}^\top \mathcal{P}\frac{\partial \mathbf{S}}{\partial \mathbf{q}}\frac{\partial \mathbf{q}}{\partial t} \;=\; \mathbf{1}^\top \mathcal{P}\frac{\partial \mathbf{S}}{\partial t},$$

where

$$\mathbf{1} = (1, 1, \ldots, 1)^\top,$$

is a vector with N elements.[5]

3.3.2 Entropy consistent inviscid fluxes

The inviscid portion of equation (28) is entropy conservative if it satisfies

$$\mathbf{w}^\top \Delta\overline{\mathbf{f}} = \overline{F}(q_N) - \overline{F}(q_1) = F(q_N) - F(q_1) = \mathbf{1}^\top \Delta\overline{\mathbf{F}}. \tag{29}$$

Tadmor [25] uses the following rational to construct entropy conservative (entropy consistent) three-point centered operators satisfying equation (29). Consider the term $w_i(\overline{f}_i - \overline{f}_{i-1})$ in the vector relation (29), which can be rewritten as $[\mathbf{w}^\top \Delta\overline{\mathbf{f}} - \Delta\overline{\mathbf{F}}] = 0$. Adding and subtracting equivalent terms yields the expression

$$\begin{aligned} w_i\left(\overline{f}_i - \overline{f}_{i-1}\right) \;&=\; \left[\tfrac{1}{2}\,(w_{i+1} + w_i)\;\overline{f}_i \;-\; \tfrac{1}{2}\,(w_i + w_{i-1})\;\overline{f}_{i-1}\right] \\ &-\; \left[\tfrac{1}{2}\,(w_{i+1} - w_i)\;\overline{f}_i \;+\; \tfrac{1}{2}\,(w_i - w_{i-1})\;\overline{f}_{i-1}\right]. \end{aligned} \tag{30}$$

[5] N is the size of the 1D grid $\mathbf{x}$.

Note that in this section the subscripts $i-1$, i and $i+1$ are used to denote a scalar or vector quantity at the $i-1$, i or $i+1$ collocated point, and should not be confused with the subscript used, for instance, in (18) to indicate the coordinate direction. The first two bracketed terms on the right-hand-side of equation (30) telescope across the domain in their current form (i.e., their contributions within an element sum to zero). The last two terms telescope provided they satisfy a consistency condition of the form

$$(w_{i+1} - w_i)\,\overline{f}_i^{(S)} = \psi_i - \psi_{i-1}, \quad 2 \le i \le N \tag{31}$$

(modulo slight changes at the end points of the domain), where $\overline{f}_i^{(S)}$ denotes an entropy conservative (or entropy consistent) flux.

A general strategy for constructing an entropy conservative flux, $\overline{f}_i^{(S)}$, that satisfies the pointwise conditions

$$(w_{i+1} - w_i)\,\overline{f}_i^{(S)} = \widetilde{\psi}_{i+1} - \widetilde{\psi}_i, \quad i = 1, 2, \ldots, N-1 \quad ; \quad \widetilde{\psi}_1 = \psi_1, \quad \widetilde{\psi}_N = \psi_N \tag{32}$$

is presented elsewhere [23]. Herein, the flux $\overline{f}_i^{(S)}$ is based on linear combinations of q_{ij}-weighted, two-point entropy conservative fluxes $\overline{f}_S = \overline{f}_S(u_\ell, u_k)$, which satisfy the following relation:

$$(w_\ell - w_k)\,\overline{f}_S(u_\ell, u_k) = \psi_\ell - \psi_k. \tag{33}$$

The dyadic shuffle conditions given by equation (33) are known to exist for Burgers' equation and the Euler equations [25, 29].

The following theorem summarizes the work given in reference 23, and provides the general formula for constructing $\overline{f}_i^{(S)}$ of any order from a linear combination of dyadic entropy conservative fluxes $\overline{f}_S(u_\ell, u_k)$.

Theorem 3.3. *A two-point high-order accurate entropy conservative flux satisfying equation* (32) *with formal boundary closures can be constructed as*

$$\overline{f}_i^{(S)} = \sum_{k=i+1}^{N} \sum_{\ell=1}^{i} 2\, q_{\ell k}\, \overline{f}_S(u_\ell, u_k), \quad 1 \le i \le N-1,$$

where $\overline{f}_S(u_\ell, u_k)$ is any two-point non-dissipative flux function that satisfies the entropy conservation condition given by equation (33)*. The two-point high-order accurate entropy conservative flux, $\overline{f}_i^{(S)}$, satisfies an additional local entropy conservation property,*

$$\mathbf{w}^\top \mathcal{P}^{-1} \Delta \overline{\mathbf{f}}^{(S)} = \mathcal{P}^{-1} \Delta \overline{\mathbf{F}} = \frac{\partial \overline{\mathbf{F}}}{\partial x}(\mathbf{q}) + \mathcal{T}_{p+1}, \tag{34}$$

or equivalently,

$$w_i^\top \left(\overline{f}_i^{(S)} - \overline{f}_{i-1}^{(S)} \right) = \left(\overline{F}_i - \overline{F}_{i-1} \right), \quad 1 \le i \le N, \tag{35}$$

where

$$\overline{F}_i = \sum_{k=i+1}^{N} \sum_{\ell=1}^{i} q_{\ell k} \left[(w_\ell + w_k)^\top \overline{f}_S(u_\ell, u_k) - (\psi_\ell + \psi_k) \right], \quad 1 \le i \le N-1. \tag{36}$$

Proof. For brevity, the proof is not included herein, but is reported elsewhere [23]. □

4 Stability on staggered grids: Burgers' equation

An energy/entropy analysis of the 1D Burgers' equation is presented before that of the compressible Navier-Stokes equations.

4.1 Data mechanics of the staggered grid approach

Define a staggered grid algorithm (Sta-Grd-Alg) for building discrete differentiation operators using two sets of collocation points: $\widetilde{\mathbf{x}}$ and $\mathbf{x}$ of dimension M and N, respectively (see Figure 2). The proposed algorithm is similar to that proposed by Kopriva and Kolias [7]. Assume that the time-dependent solution is stored at the points $\widetilde{\mathbf{x}}$. Furthermore, assume that the extrema of $\mathbf{x}$ coincide with the endpoints of the domain: $\mathbf{x}_1 = x^L$, $\mathbf{x}_N = x^H$, to facilitate imposition of interface or boundary data.

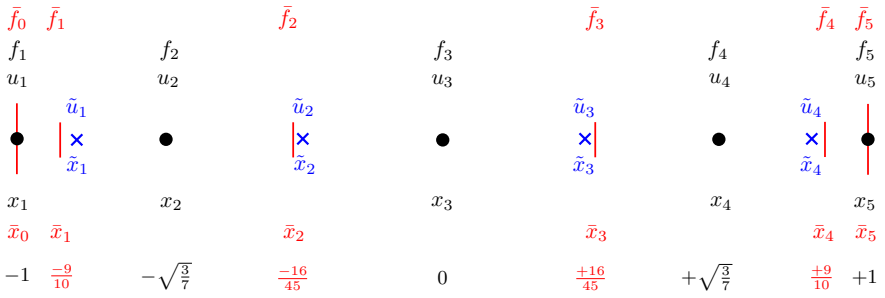

Figure 2. The one-dimensional discretization for the fourth-order accurate polynomial interpolation ($p = 4$) with the staggered approach is illustrated. Solution points $\widetilde{\mathbf{x}}$ are identified with $\times$ and auxiliary points $\mathbf{x}$ are identified with $\bullet$. Flux points $\overline{\mathbf{x}}$ (used to prove the entropy stability) are identified with $|$.

Discrete differentiation of first or second order spatial terms (e.g., $\partial f/\partial x$ or $\partial f^{(V)}/\partial x$), by using the Sta-Grd-Alg is accomplished as follows:

- Interpolate the discrete entropy variables from $\widetilde{\mathbf{x}}$ to $\mathbf{x}$.
- Build the nonlinear fluxes f and $f^{(V)}$ on the set of points $\mathbf{x}$.
- Build the interface and/or boundary penalties at the extrema of $\mathbf{x}$.
- Differentiate the fluxes on $\mathbf{x}$, and impose the penalties by using the SAT approach.
- Interpolate the discrete flux derivatives and penalties back to $\widetilde{\mathbf{x}}$.
- Advance the solution with a time integration scheme by using the interpolated flux derivative on $\widetilde{\mathbf{x}}$.

Tensor product arithmetic extends the approach directly to three spatial dimensions.[6] An SBP-SAT stability proof is now presented for the Sta-Grd-Alg. It is valid for all diagonal-norm SBP operators.

[6]The Sta-Grd-Alg is valid for other grid distributions that do not support tensor product arithmetic.

Define "tilde" variables and operators that act on the set of points $\widetilde{\mathbf{x}}$ (e.g., $\widetilde{\mathbf{u}}$, $\widetilde{\mathcal{P}}$ and $\widetilde{\mathcal{D}}$), and the pair of interpolation operators $\mathcal{I}_{LG\to LGL}$ and $\mathcal{I}_{LGL\to LG}$ introduced in section 2.2.2. The $\mathcal{I}_{LG\to LGL}$ operator transfers data from $\widetilde{\mathbf{x}}$ to $\mathbf{x}$, while the $\mathcal{I}_{LGL\to LG}$ transfers data from $\mathbf{x}$ to $\widetilde{\mathbf{x}}$. Define the interpolated solution vector $\mathbf{u}$, and the diagonal velocity and viscosity matrices $[\sqcap]$ and $[\epsilon]$ as

$$\mathbf{u} \;=\; \mathcal{I}_{LG\to LGL}\,\widetilde{\mathbf{u}} \quad ; \qquad [\sqcap] = \mathrm{Diag}[\mathcal{I}_{LG\to LGL}\widetilde{\mathbf{u}}] \quad ; \qquad [\epsilon] = \mathrm{Diag}[\mathcal{I}_{LG\to LGL}\widetilde{\epsilon}] \quad ; \tag{37}$$

and the boundary operator nomenclature

$$\begin{aligned}
&\mathbf{e}\left(x^L\right) = (1,0,\cdots,0)^\top_M,\\
&u\left(x^L\right) = \mathbf{u}|_{x=-1} = \mathbf{u}^\top \mathbf{e}\left(x^L\right),\\
&\left(\mathcal{D}\mathbf{u}\right)\left(x^L\right) = \left(\mathcal{D}\mathbf{u}\right)|_{x=-1} = \left(\mathcal{D}\mathbf{u}\right)^\top \mathbf{e}\left(x^L\right),\\
&g\left(x^L\right) = \mathbf{g}|_{x=-1} = \mathbf{g}^\top \mathbf{e}\left(x^L\right),
\end{aligned} \tag{38}$$

with similar definitions for $\mathbf{e}\left(x^H\right)$, $u\left(x^H\right)$, $\left(\mathcal{D}\mathbf{u}\right)\left(x^H\right)$, and $g\left(x^H\right)$. The subscript M in (38) denotes the size of the vector $\mathbf{e}\left(x^L\right)$.

4.2 Stability of Burgers' equation

Conventional energy estimates as well as entropy analysis exists for Burgers' equation for all diagonal norm SBP operators [14, 23, 25]. Comparison of the two approaches provides insight on how to proceed with the analysis of the compressible Navier-Stokes equations.

Consider the 1D viscous Burgers' equation

$$\begin{aligned}
&\frac{\partial u}{\partial t} + \frac{\partial f(u)}{\partial x} = \frac{\partial\left(\varepsilon f^{(V)}\left(\frac{\partial u}{\partial x}\right)\right)}{\partial x}, \quad f(u) = \frac{u^2}{2}, \quad f^{(v)}\left(\frac{\partial u}{\partial x}\right) = \frac{\partial u}{\partial x}, \quad x\in[x^L,x^H], \quad t\in[0,\infty),\\
&\frac{u\left(x^L,t\right)+\left|u\left(x^L,t\right)\right|}{3}u\left(x^L,t\right) - \varepsilon\frac{\partial u}{\partial x}\left(x^L,t\right) - g\left(x^L,t\right) = 0,\\
&\frac{u\left(x^H,t\right)-\left|u\left(x^H,t\right)\right|}{3}u\left(x^H,t\right) - \varepsilon\frac{\partial u}{\partial x}\left(x^H,t\right) - g\left(x^H,t\right) = 0,\\
&u\left(x,0\right) = g^{(0)}\left(x\right),
\end{aligned} \tag{39}$$

where $u = u(x,t)$ is the continuous solution vector, $f = f(u)$ is a nonlinear flux function. The boundary conditions in (39) are constructed such that the semi-discrete energy only increases with respect to the imposed data and maintains the same form in the inviscid limit $\varepsilon \to 0$.

A general semi-discretization of (39) suitable for energy or entropy analysis is

$$\begin{aligned}
\tfrac{d}{dt}\widetilde{\mathbf{u}} \;&+\; \mathcal{I}_{LGL\to LG}\mathcal{D}\,\widehat{\mathbf{f}}\left(\mathbf{u}\right) \;=\; \mathcal{I}_{LGL\to LG}\mathcal{D}\mathcal{E}\mathcal{D}\mathbf{u}\\
&-\; \left(\tfrac{u\left(x^L\right)+\left|u\left(x^L\right)\right|}{3}\,u\left(x^L\right) - \epsilon(\mathcal{D}\mathbf{u})\left(x^L\right) - g\left(x^L\right)\right)\,\mathcal{I}_{LGL\to LG}\mathcal{P}^{-1}\,\mathbf{e}\left(x^L\right)\\
&+\; \left(\tfrac{u\left(x^H\right)-\left|u\left(x^H\right)\right|}{3}\,u\left(x^H\right) - \epsilon(\mathcal{D}\mathbf{u})\left(x^H\right) - g\left(x^H\right)\right)\,\mathcal{I}_{LGL\to LG}\mathcal{P}^{-1}\,\mathbf{e}\left(x^H\right)
\end{aligned} \tag{40}$$

where the initial data is $\widetilde{\mathbf{u}}(x,0) = \mathbf{g}^{(0)}(x)$ and $\widehat{\mathbf{f}}(\mathbf{u})$ denotes a numerical discretization of the inviscid flux (to be specified later). To simplify the notation in (40), the dependence on the time, t, has been omitted.

Two stability proofs for Burgers' equation are now presented. The first proof uses conventional energy analysis and a canonical α-flux splitting technique, while the second proof uses entropy analysis. Both proofs assume that the solution is stored at the LG points and is interpolated to the LGL points to achieve a statement of stability.

4.2.1 Energy analysis

The flux $f(u)$ in (39) can be written as the product of two functions, $V(u)$ and $W(u)$, (i.e., $f(u) = V(u)W(u)$). Expressing the divergence term $\frac{\partial f(u)}{\partial x}$ in (39) as a combination of divergence and chain-rule forms, yields the following equation

$$\frac{\partial u}{\partial t} + \alpha \frac{\partial f(u)}{\partial x} + (1-\alpha)\left[V(u)\frac{\partial W(u)}{\partial x} + \frac{\partial V(u)}{\partial x} W(u)\right] = \frac{\partial \left(\varepsilon f^{(V)}\left(\frac{\partial u}{\partial x}\right)\right)}{\partial x}. \tag{41}$$

Equation (41) is referred to as α-splitting and for $\alpha = 2/3$ it is denoted a "canonical" splitting of the Burgers' equation. Therefore, if we canonically split to the quadratic term in the semi-discretized Burgers' equation (40) and apply the Sta-Grd-Alg to all spatial terms, we get the following staggered grid operator

$$\begin{array}{rcl} \frac{d}{dt}\widetilde{\mathbf{u}} & + & \frac{1}{3}\mathcal{I}_{LGL\to LG}\left(\mathcal{D}\left[\sqcap\right] + \left[\sqcap\right]\mathcal{D}\right)\mathbf{u} = \mathcal{I}_{LGL\to LG}\,\mathcal{D}\left[\epsilon\right]\mathcal{D}\,\mathbf{u} \\ & - & \left(\frac{u(x^L)+|u(x^L)|}{3}u\left(x^L\right) - \epsilon\left(\mathcal{D}\mathbf{u}\right)\left(x^L\right) - g\left(x^L\right)\right)\mathcal{I}_{LGL\to LG}\,\mathcal{P}^{-1}\,\mathbf{e}\left(x^L\right) \\ & + & \left(\frac{u(x^H)-|u(x^H)|}{3}u\left(x^H\right) - \epsilon\left(\mathcal{D}\mathbf{u}\right)\left(x^H\right) - g\left(x^H\right)\right)\mathcal{I}_{LGL\to LG}\,\mathcal{P}^{-1}\,\mathbf{e}\left(x^H\right), \end{array} \tag{42}$$

with the initial data $\widetilde{\mathbf{u}}(x,0) = \mathbf{g}^{(0)}(x)$.

Theorem 4.1. *The semi-discrete solution $\widetilde{\mathbf{u}}$ defined in equation (42) is bounded for all time for any diagonal norm SBP operator $\mathcal{D}$, provided there exist interpolation operators $\mathcal{I}_{LG\to LGL}$ and $\mathcal{I}_{LGL\to LG}$ that satisfy the constraint*

$$\widetilde{\mathcal{P}}\,\mathcal{I}_{LGL\to LG} = \mathcal{I}_{LG\to LGL}^{\top}\mathcal{P},$$

and provided the boundary data $\left|g\left(x^L\right)\right|$ and $\left|g\left(x^H\right)\right|$ are bounded.

Proof. The energy method is used to prove Theorem 4.1. The proof begins by contracting equation (42) with the vector $\widetilde{\mathbf{u}}^{\top}\widetilde{\mathcal{P}}$ to yield the expression

$$\begin{array}{rcl} \frac{d}{dt}\left(\widetilde{\mathbf{u}}^{\top}\widetilde{\mathcal{P}}\widetilde{\mathbf{u}}\right) & + & \frac{1}{3}\mathbf{u}^{\top}\left(\mathcal{Q}\left[\sqcap\right] + \left[\sqcap\right]\mathcal{Q}\right)\mathbf{u} = \mathbf{u}^{\top}\mathcal{D}[\epsilon]\,\mathcal{D}\,\mathbf{u} \\ & - & \left(\frac{u(x^L)+|u(x^L)|}{3}u\left(x^L\right) - \epsilon\left(\mathcal{D}\mathbf{u}\right)\left(x^L\right) - g\left(x^L\right)\right)u\left(x^L\right) \\ & + & \left(\frac{u(x^H)-|u(x^H)|}{3}u\left(x^H\right) - \epsilon\left(\mathcal{D}\mathbf{u}\right)\left(x^H\right) - g\left(x^H\right)\right)u\left(x^H\right). \end{array} \tag{43}$$

The constraint given in Theorem 4.1 (see also equation (B29)) is used in all spatial terms to relate the vector contraction $\widetilde{\mathbf{u}}^{\top}\widetilde{\mathcal{P}}$ on $\widetilde{\mathbf{x}}$, to an equivalent vector contraction on $\mathbf{x}$.

Further simplification of equation (43) by using the SBP property $\mathcal{Q}+\mathcal{Q}^\top = \mathcal{B}$ and the boundary data yields the expression

$$\begin{aligned} \tfrac{d}{dt}\left(\widetilde{\mathbf{u}}^\top \widetilde{\mathcal{P}}\widetilde{\mathbf{u}}\right) &= -\varepsilon(\mathcal{D}\mathbf{u})^\top \mathcal{P}\mathcal{D}\mathbf{u} - \tfrac{1}{3}\left(u\left(x^H\right)^3 - u\left(x^L\right)^3\right) \\ &+ \tfrac{1}{3}\left(u\left(x^H\right)^3 - u\left(x^L\right)^3 + \left|u\left(x^H\right)\right| u\left(x^H\right)^2 - \left|u\left(x^L\right)\right| u\left(x^L\right)^2\right) \\ &+ u\left(x^L\right) g\left(x^L\right) + u\left(x^H\right) g\left(x^H\right). \end{aligned} \tag{44}$$

Provided that $u\left(x^L\right) \neq 0$ or $u\left(x^H\right) \neq 0$, the identity

$$yz = -\frac{1}{2}\left(\sqrt{a}y - \frac{1}{\sqrt{a}}z\right)^2 + \frac{a}{2}y^2 + \frac{1}{2a}z^2, \quad a > 0, \tag{45}$$

is used to bound the terms $u\left(x^L\right) g\left(x^L\right) + u\left(x^H\right) g\left(x^H\right)$. The final expression becomes

$$\begin{aligned} \tfrac{d}{dt}\left(\widetilde{\mathbf{u}}^\top \widetilde{\mathcal{P}}\widetilde{\mathbf{u}}\right) &= -\varepsilon(\mathcal{D}\mathbf{u})^\top \mathcal{P}\mathcal{D}\mathbf{u} + \tfrac{1}{2a^L} g\left(x^L\right)^2 + \tfrac{1}{2a^H} g\left(x^H\right)^2 \\ &- \tfrac{1}{2}\left(\sqrt{(a^H)} u\left(x^H\right) - \tfrac{1}{\sqrt{a^H}} g\left(x^H\right)\right)^2 - \tfrac{1}{2}\left(\sqrt{(a^L)} u\left(x^L\right) - \tfrac{1}{\sqrt{a^L}} g\left(x^L\right)\right)^2 \\ &+ \left(\tfrac{a^H}{2} - \tfrac{|u(x^H)|}{3}\right) u\left(x^H\right)^2 + \left(\tfrac{a^L}{2} - \tfrac{|u(x^L)|}{3}\right) u\left(x^L\right)^2, \\ &0 < a^L \leq \tfrac{2}{3}\left|u\left(x^L\right)\right|, \quad 0 < a^H \leq \tfrac{2}{3}\left|u\left(x^H\right)\right|. \end{aligned} \tag{46}$$

Thus, $\tfrac{d}{dt}\left(\widetilde{\mathbf{u}}^\top \widetilde{\mathcal{P}}\widetilde{\mathbf{u}}\right) \leq -\varepsilon(\mathcal{D}\mathbf{u})^\top \mathcal{P}\mathcal{D}\mathbf{u}$ and establishes boundedness of the L^2 norm of $\mathbf{u}$ provided that the boundary data $g\left(x^L\right)^2$ and $g\left(x^H\right)^2$ are well behaved. □

An expression equivalent to (46) is now derived using entropy analysis [25].

4.2.2 Entropy analysis

An entropy-entropy flux pair, (S, F), a potential-potential flux pair, (ϕ, ψ), and the entropy variable, w, for Burgers' equation are [25]

$$(S, F) = \left(\frac{u^2}{2}, \frac{u^3}{3}\right) \quad ; \quad (\phi, \psi) = \left(\frac{u^2}{2}, \frac{u^3}{6}\right) \quad ; \quad u = w. \tag{47}$$

Note that the entropy is guaranteed to be convex for all u (i.e., $\partial^2 S/\partial u^2 = 1$), and that the entropy is (chosen) to be equivalent to the energy used in the SBP analysis.[7]

Consider the entropy analysis of equation (40). Apply the Sta-Grd-Alg to construct the quadratic inviscid and linear viscous fluxes as well as the boundary penalties. As with the collocated approach [1], the entropy and energy analyses of the time, viscous, and SAT terms are equivalent when using the Sta-Grd-Alg, while differences appear in the analysis of the quadratic flux term. In the entropy analysis, the quadratic flux is discretized using a diagonal norm SBP operator: $\mathcal{D} = \mathcal{P}^{-1}\mathcal{Q}$. The $\mathcal{Q}$ operator is then rearranged into telescoping form by using the generalized SBP relation given in Lemma 2.1. The resulting expression for the quadratic term discretized using Sta-Grd-Alg is

$$\frac{1}{2}\frac{\partial u^2}{\partial x} \approx \mathcal{P}^{-1}\Delta\overline{\mathbf{f}}(\mathbf{u}).$$

[7] The entropy is not unique.

The resulting semi-discrete staggered grid operator is then

$$\begin{array}{rcl} \frac{d}{dt}\widetilde{\mathbf{u}} & + & \mathcal{I}_{LGL\to LG}\,\mathcal{P}^{-1}\Delta\,\overline{\mathbf{f}}(\mathbf{u}) \;=\; \mathcal{I}_{LGL\to LG}\,\mathcal{D}\,[\epsilon]\,\mathcal{D}\,\mathbf{u} \\ & - & \left(\frac{u\left(x^L\right)+\left|u\left(x^L\right)\right|}{3}u\left(x^L\right)-\epsilon\left(\mathcal{D}\mathbf{u}\right)\left(x^L\right)-g\left(x^L\right)\right)\,\mathcal{I}_{LGL\to LG}\,\mathcal{P}^{-1}\,\mathbf{e}\left(x^L\right) \\ & + & \left(\frac{u\left(x^H\right)-\left|u\left(x^H\right)\right|}{3}u\left(x^H\right)-\epsilon\left(\mathcal{D}\mathbf{u}\right)\left(x^H\right)-g\left(x^H\right)\right)\,\mathcal{I}_{LGL\to LG}\,\mathcal{P}^{-1}\,\mathbf{e}\left(x^H\right) \end{array} \tag{48}$$

with the initial data $\mathbf{u}(x,0)=\mathbf{g}^{(0)}(x)$. What remains is to construct an entropy conserving flux $\overline{\mathbf{f}}(\mathbf{u})=\overline{\mathbf{f}}_i^{(S)}$.

Theorem 3.3 guarantees the existence of an entropy conserving flux for the delta form operator $\mathcal{P}^{-1}\Delta\overline{\mathbf{f}}(\mathbf{u})$, provided there exists a two-point entropy flux relation and a diagonal norm SBP operator is used for $\mathcal{D}$. Using the definition for the entropy variable u given in equation (47) and Tadmor's integral relation [25]

$$\overline{f}_S\left(u_k,u_\ell\right)=\int_0^1 g\left(w(u_k)+\xi\left(w(u_\ell)-w(u_k)\right)\right)\,\mathrm{d}\xi,\quad g(w(u))=f(u) \tag{49}$$

yields a two-point entropy conservative flux

$$\overline{f}_S\left(u_\ell,u_k\right)=\frac{1}{6}\left(u_\ell^2+u_\ell u_k+u_k^2\right), \tag{50}$$

which satisfies the two-point relation

$$\left(u_\ell-u_k\right)\overline{f}_S\left(u_\ell,u_k\right)=\frac{1}{6}\left(u_\ell^3-u_k^3\right). \tag{51}$$

The high-order accurate entropy conserving flux guaranteed by Theorem 3.3 is given by

$$\overline{f}_i^{(S)} \;=\; \sum_{k=i+1}^{N}\sum_{\ell=1}^{i}2q_{\ell k}\overline{f}_S\left(u_\ell,u_k\right) \;=\; 2\sum_{k=i+1}^{N}\sum_{\ell=1}^{i}q_{\ell k}\frac{1}{6}\left(u_\ell^2+u_\ell u_k+u_k^2\right),\quad 1\le i\le N-1. \tag{52}$$

Contracting the quadratic term $\mathcal{I}_{LGL\to LG}\mathcal{P}^{-1}\Delta\overline{\mathbf{f}}^{(S)}$ in equation (48) with the discrete vector $\left(\widetilde{\mathcal{P}}\widetilde{\mathbf{u}}\right)^\top$ yields the telescoping condition

$$\mathbf{u}^\top\Delta\overline{\mathbf{f}}^{(S)} \;=\; \mathbf{1}^\top[\sqcap]\Delta\overline{\mathbf{f}}^{(S)} \;=\; \mathbf{1}^\top\Delta\overline{\mathbf{F}} \;=\; \left(\overline{F}_N-\overline{F}_1\right) \tag{53}$$

with

$$\begin{array}{c} \overline{F}_i \;=\; \displaystyle\sum_{k=i+1}^{N}\sum_{\ell=1}^{i}q_{\ell k}\left[\left(u_\ell+u_k\right)\overline{f}_S\left(u_\ell,u_k\right)-\frac{1}{6}\left(u_\ell^3+u_k^3\right)\right],\quad 1\le i\le N-1, \\ \overline{F}_0=\frac{1}{3}u_0^3,\qquad \overline{F}_N=\frac{1}{3}u_N^3. \end{array} \tag{54}$$

Collecting all terms in the entropy analysis of Burgers' equation yields an (entropy) estimate that is identical to the energy estimate given in equation (46).

4.2.3 Relating the energy and entropy analyses

The canonical splitting of the inviscid flux ($f(u) = \left(\frac{u^2}{2}\right) = V(u)W(u)$) in Burgers' equation satisfies the necessary conditions of equation (A9). As such, all terms can be rearranged into a single telescoping flux

$$\frac{1}{2}\frac{\partial u^2}{\partial x} = \alpha\frac{\partial f(u)}{\partial x} + (1-\alpha)\left[V(u)\frac{\partial W(u)}{\partial x} + \frac{\partial V(u)}{\partial x}W(u)\right] \approx \mathcal{P}^{-1}\Delta\overline{\mathbf{f}}(\mathbf{u}).$$

The $\alpha-$ splitting of the conservative (equation (55a)) and chain rule (equation (55b)) forms of the flux $\left(\frac{u^2}{2}\right)$ are decomposed as follows:

$$V(u) = \frac{1}{2}\mathcal{U}\,\mathcal{U}\,\mathbf{1} \quad ; \quad W(u) = \mathbf{1} \tag{55a}$$

$$V(u) = \frac{1}{2}\,\mathcal{U}\,\mathbf{1} \quad ; \quad W(u) = \mathcal{U}\,\mathbf{1} \tag{55b}$$

which produce the equivalent fluxes (see equation (A10))

$$\overline{f}_i^a = \sum_{k=i+1}^{N}\sum_{l=1}^{i} q_{\ell k}\left(\frac{u_k u_k + u_\ell u_\ell}{2}\right) \quad , \quad 1 \le i \le N-1, \tag{56a}$$

$$\overline{f}_i^b = \sum_{k=i+1}^{N}\sum_{l=1}^{i} q_{\ell k}\left(\frac{u_k u_\ell + u_\ell u_k}{2}\right) \quad , \quad 1 \le i \le N-1. \tag{56b}$$

Combining the split Burgers' fluxes (56) into equation (A10) yields the expression

$$\begin{gathered}\overline{f}_i = \overline{f}_i^a + \overline{f}_i^b = 2\sum_{k=i+1}^{N}\sum_{l=1}^{i} q_{\ell k}\frac{1}{6}(u_\ell^2 + u_\ell u_k + u_k^2), \\ 1 \le i \le N-1, \quad \overline{f}_0 = \frac{1}{2}u_1^2, \quad \overline{f}_N = \frac{1}{2}u_N^2,\end{gathered} \tag{57}$$

for a splitting parameter $\alpha = 2/3$.

*R*emark. Equation (40) invokes a canonical splitting of Burgers' equation to facilitate the energy analysis, and is valid for any diagonal norm SBP operator. Equation (53) relies on a two-point dyadic entropy conservative flux of the form given as a necessary condition in Theorem 32. Choosing u as the entropy variable in equation (47), enforces equality of the entropy and α-split fluxes. (Compare the fluxes $\overline{f}_i^{(S)}$ in equations (57) and (52).)

*R*emark. The compressible Navier-Stokes equations do not support a canonical decomposition based on the α-split flux technique. Thus, conventional nonlinear energy analysis is not applicable (to our knowledge). Nevertheless, the existence of a two-point entropy conservative flux satisfying equation (32) enables entropy analysis to be used for all diagonal norm SBP operators.

*R*emark. The numerical approach is conservative. The inviscid and viscous fluxes are explicitly conserved on the LGL points.

5 The compressible Navier-Stokes equations in multiple dimensions on staggered grids

5.1 Staggered grid in two dimensions

Extension of a 1D staggered operator to multiple dimensions can proceed in several ways. Figure 3 shows two popular staggered data structures in two spatial dimensions. Both approaches store the solution at the tensor product LG points (i.e., the so called Gauss points) of order p (blue crosses).

The fully-staggered approach moved the data via 3D tensor product interpolations from LG (supporting a polynomial of order p) to LGL (supporting a polynomial of order $p+1$) points (black circles). The discrete operators reported in references $1, 2, 13, 30$, are used on the LGL points to construct the spatial residual. The temporal updates needed on the LG points are obtained by restricting the LGL residuals back to the LG points. Extension to general curvilinear coordinates follows immediately on the LGL points [1, 13].

The semi-staggered approach moves the data via 1D interpolations from the LG to LGL points (black circles and green triangles). The inviscid terms are constructed via three 1D operations on the semi-staggered LG-LGL points. The viscous terms are most easily formed by using a fully-staggered approach. The semi-staggered operator has the advantage of not requiring corner data in the inviscid operators. However, its extension to curvilinear coordinates is not straight forward because of ambiguities in the geometric conservation law (GCL) terms. For this reason, the fully-staggered approach is used exclusively herein.

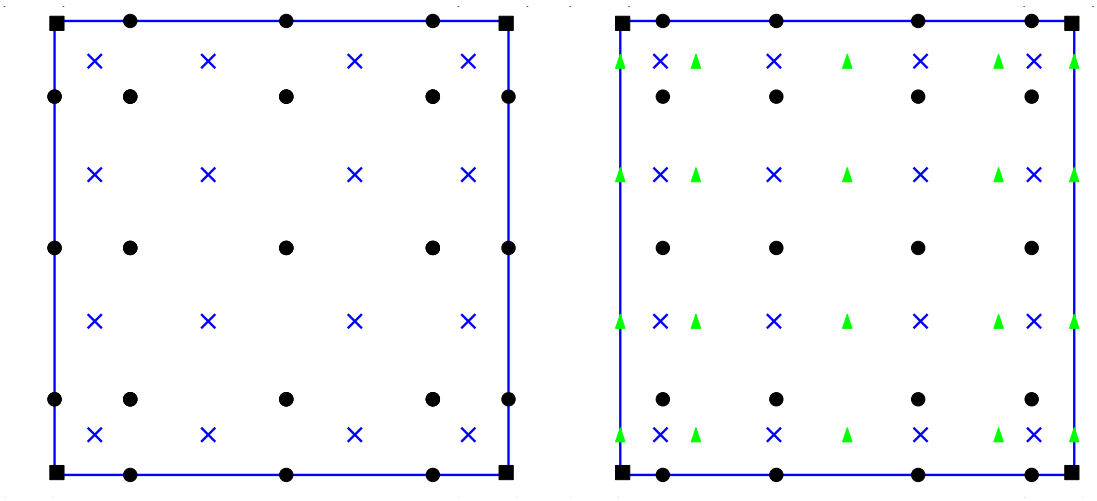

(a) Fully-staggered. (b) Semi-staggered.

Figure 3. Fully- and semi-staggered 2D tensor product elements.

5.2 Tensor operators in three dimensions

Consider a single tensor product element and an entropy stable spatially discontinuous collocation (SSDC) discretization with $M = p+1$ LG solution points in each coordinate direction[8] [1,2,30,31]; the following element-wise matrices will be used:

$$\widetilde{\boldsymbol{\mathcal{P}}} = \left(\widetilde{\mathcal{P}}_M \otimes \widetilde{\mathcal{P}}_M \otimes \widetilde{\mathcal{P}}_M \otimes I_5\right),$$

$$\boldsymbol{\mathcal{I}}_{LG\to LGL} = \left(\mathcal{I}_{LG\to LGL}\right)_{x_1x_2x_3} = \left(\mathcal{I}_{LG\to LGL} \otimes \mathcal{I}_{LG\to LGL} \otimes \mathcal{I}_{LG\to LGL} \otimes I_5\right),$$

$$\boldsymbol{\mathcal{I}}_{LGL\to LG} = \left(\mathcal{I}_{LGL\to LG}\right)_{x_1x_2x_3} = \left(\mathcal{I}_{LGL\to LG} \otimes \mathcal{I}_{LGL\to LG} \otimes \mathcal{I}_{LGL\to LG} \otimes I_5\right),$$

$$\begin{aligned}
\mathcal{D}_{x_1} &= \left(\mathcal{D}_N \otimes I_N \otimes I_N \otimes I_5\right), \quad \cdots \quad \mathcal{D}_{x_3} = \left(I_N \otimes I_N \otimes \mathcal{D}_N \otimes I_5\right), \\
\mathcal{P}_{x_1} &= \left(\mathcal{P}_N \otimes I_N \otimes I_N \otimes I_5\right), \quad \cdots \quad \mathcal{P}_{x_3} = \left(I_N \otimes I_N \otimes \mathcal{P}_N \otimes I_5\right), \\
\mathcal{P}_{x_1x_2} &= \left(\mathcal{P}_N \otimes \mathcal{P}_N \otimes I_N \otimes I_5\right), \quad \cdots \quad \mathcal{P}_{x_2x_3} = \left(I_N \otimes \mathcal{P}_N \otimes \mathcal{P}_N \otimes I_5\right), \\
\boldsymbol{\mathcal{P}} &= \mathcal{P}_{x_1x_2x_3} = \left(\mathcal{P}_N \otimes \mathcal{P}_N \otimes \mathcal{P}_N \otimes I_5\right), \\
\mathcal{B}_{x_1} &= \left(\mathcal{B}_N \otimes I_N \otimes I_N \otimes I_5\right), \quad \cdots \quad \mathcal{B}_{x_3} = \left(I_N \otimes I_N \otimes \mathcal{B}_N \otimes I_5\right), \\
\Delta_{x_1} &= \left(\Delta_N \otimes I_N \otimes I_N \otimes I_5\right), \quad \cdots \quad \Delta_{x_3} = \left(I_N \otimes I_N \otimes \Delta_N \otimes I_5\right),
\end{aligned} \tag{58}$$

where $\widetilde{\mathcal{P}}_M$ is the norm of the LG points, while $\mathcal{D}_N$, $\mathcal{P}_N$, Δ_N, and $\mathcal{B}_N$ are the 1D SBP operators [31] defined on the LGL points, and I_N is the identity matrix of dimension N. I_5 denotes the identity matrix of dimension five.[9] The subscripts in (58) indicate the coordinate directions to which the operators apply (e.g., $\mathcal{D}_{x_1}$ is the differentiation matrix in the x_1 direction). The symbol $\otimes$ represents the Kronecker product. When applying these operators to the scalar entropy equation in space at the LG points, a hat is used to differentiate the scalar operator from the full vector operator. For example,

$$\widehat{\widetilde{\boldsymbol{\mathcal{P}}}} = \left(\widetilde{\mathcal{P}}_M \otimes \widetilde{\mathcal{P}}_M \otimes \widetilde{\mathcal{P}}_M\right) \quad ; \quad \widehat{\boldsymbol{\mathcal{P}}} = \left(\mathcal{P}_M \otimes \mathcal{P}_M \otimes \mathcal{P}_M\right). \tag{59}$$

The vector of conservative variables of each element is ordered as

$$\widetilde{\mathbf{q}} = \left(\widetilde{q}\left(\widetilde{x}_{(1)(1)(1)}\right)^\top, \widetilde{q}\left(\widetilde{x}_{(1)(1)(2)}\right)^\top, \ldots, \widetilde{q}\left(\widetilde{x}_{(M)(M)(M)}\right)^\top\right) = \left(\widetilde{q}_{(1)}^\top, \widetilde{q}_{(2)}^\top, \ldots, \widetilde{q}_{(M^3)}^\top\right), \tag{60}$$

[8] Recall from Section 2.2.2 that with the staggered algorithm the number of LG and LGL points in 1D is denoted by M and N, respectively.

[9] The 3D compressible Navier-Stokes equations form a system of five nonlinear partial differential equations.

where the subscripts denote the ordering of the solution points in the coordinate directions. Assume an equivalent definition and order for the entropy variables $\widetilde{\mathbf{w}}$; and an analogous definition for the variables at the LGL points.[10]

The $\mathcal{I}_{LG\to LGL}$ operator transfers data from $\widetilde{\mathbf{x}}$ to $\mathbf{x}$, while the $\mathcal{I}_{LGL\to LG}$ transfers data from $\mathbf{x}$ to $\widetilde{\mathbf{x}}$. Define

$$\mathbf{w} \;=\; \mathcal{I}_{LG\to LGL}\,\widetilde{\mathbf{w}} \quad ; \qquad \widehat{c}_{ij} \;=\; \mathcal{I}_{LG\to LGL}\,\widetilde{c}_{ij} \quad ; \qquad [\widehat{c}_{ij}] \;=\; \mathrm{Diag}[\mathcal{I}_{LG\to LGL}\,\widetilde{c}_{ij}]. \tag{61}$$

Using these definitions and the SBP operators (58), system (18) is discretized locally on an isolated element as [13, 31]

$$\frac{d\widetilde{\mathbf{q}}}{dt} + \mathcal{I}_{LGL\to LG}\left[\mathcal{P}_{x_i}^{-1}\,\Delta_{x_i}\,\overline{\mathbf{f}}_i - \mathcal{D}_{x_i}\,\overline{\mathbf{f}}_i^{(V)}\right] \;= \mathcal{I}_{LGL\to LG}\,\mathcal{P}_{x_i}^{-1}\,\mathbf{g}_i^{(Int)}, \tag{62}$$

where Einstein notation is used to express the coordinate directions. The penalty interface terms $\mathbf{g}_i^{(Int)}$ with $i = 1, 2, 3$ are used to connect neighboring elements (see Section 6).

An entropy conservative reconstruction is used for the inviscid fluxes $\overline{\mathbf{f}}_i$ in equation (62) based on the expression given in theorem 3.3 and the two-point entropy conservative flux, $\overline{f}_S\,(u_\ell, u_k)$, of Ismail and Roe [29]. The interpolated entropy variables $\mathbf{w} = \mathcal{I}_{LG\to LGL}\,\widetilde{\mathbf{w}}$ are used to build the fluxes on the LGL points. The viscous fluxes are also computed using interpolated entropy variables and the operators $\mathcal{D}_{x_i}$, $i = 1, 2, 3$, defined in (58). The viscous coefficient matrices $\widehat{c}_{ij}$ are again formed using interpolated data on the LGL points.

Remark 5.1. *The interpolations from and to the LG points are carried out in computational space by using an efficient tensor-product algorithm that requires only the knowledge of the 1D $\mathcal{I}_{LG\to LGL}$ and $\mathcal{I}_{LGL\to LG}$ operators. The extension to general curvilinear coordinates follows immediately on the LGL points [1, 2].*

6 Entropy stable interface coupling

Consider two cubic tensor product elements by extending equation (62) to two adjoining elements. Without loss of generality assume that all their faces are orthogonal to the three coordinate directions and are not boundary faces, i.e., they are not part of the boundary surface $\partial\Omega$. The resulting expressions become [13, 31]

$$\frac{d\widetilde{\mathbf{q}}_\ell}{dt} + \mathcal{I}_{LGL\to LG\ell}\left[\mathcal{P}_{x_i,\ell}^{-1}\,\Delta_{x_i,\ell}\,\overline{\mathbf{f}}_{i,\ell} - \mathcal{D}_{x_i,\ell}\,[\widehat{c}_{ij,\ell}]\,\mathbf{\Theta}_{j,\ell}\right] = \mathcal{I}_{LGL\to LG\ell}\mathcal{P}_{x_i,\ell}^{-1}\,\mathbf{g}_{i,\ell}^{(Int),q}, \tag{63a}$$

$$\mathbf{\Theta}_{i,\ell} - \mathcal{D}_{x_i}\mathbf{w}_l = \mathcal{P}_{x_i,\ell}^{-1}\,\mathbf{g}_{i,\ell}^{(Int),\Theta}, \tag{63b}$$

$$\frac{d\widetilde{\mathbf{q}}_r}{dt} + \mathcal{I}_{LGL\to LGr}\left[\mathcal{P}_{x_i,r}^{-1}\,\Delta_{x_i,r}\,\overline{\mathbf{f}}_{i,r} - \mathcal{D}_{x_i,r}\,[\widehat{c}_{ij,r}]\,\mathbf{\Theta}_{j,r}\right] = \mathcal{I}_{LGL\to LGr}\mathcal{P}_{x_i,r}^{-1}\,\mathbf{g}_{i,r}^{(Int),q}, \tag{63c}$$

$$\mathbf{\Theta}_{i,r} - \mathcal{D}_{x_i}\mathbf{w}_l = \mathcal{P}_{x_i,r}^{-1}\,\mathbf{g}_{i,r}^{(Int),\Theta}, \tag{63d}$$

where the subscripts l and r denote the "left" and "right" elements. $\mathbf{\Theta}_{i,\ell}$ and $\mathbf{\Theta}_{i,r}$ are the vectors of the gradient of the entropy variables on the left and right elements in the i direction, whereas

[10] With the staggered algorithm, the number of LGL points in 1D is denoted by N (see Section 2.2.2). Thus, N^3 is the number of LGL points in a 3D tensor-product element.

$\mathbf{g}_{i,(\cdot)}^{(Int),q}$ and $\mathbf{g}_{i,(\cdot)}^{(Int),\Theta}$ are the penalty interface terms on the conservative variable and the gradient of the entropy variable, respectively [31]. As indicated in (61), the matrices $[\widehat{c}_{ij}]$ are block diagonal matrices with N^3 five-by-five blocks corresponding to the viscous coefficients of each LGL point.[11] Note that (63) is obtained by using $f_i^{(V)} = \widehat{c}_{ij}\, w_{x_j} = \widehat{c}_{ij}\, \Theta_j$.

To obtain an equation for the entropy of the system, we follow the entropy stability analysis presented in [1,31]. Therefore, multiplying the two discrete equations in the left element by $\widetilde{\mathbf{w}}_l^\top \widetilde{\boldsymbol{\mathcal{P}}}_l$ and $([\widehat{c}_{ij,l}]\boldsymbol{\Theta}_{j,l})^\top \boldsymbol{\mathcal{P}}_l$, respectively, and the two discrete equations in the right element by $\widetilde{\mathbf{w}}_r^\top \widetilde{\boldsymbol{\mathcal{P}}}_r$ and $([\widehat{c}_{ij,r}]\boldsymbol{\Theta}_{j,r})^\top \boldsymbol{\mathcal{P}}_r$, respectively, the expression for the time derivative of the entropy function S in each element is

$$
\begin{aligned}
&\frac{d}{dt}\widetilde{\mathbf{1}}^\top \widehat{\widetilde{\boldsymbol{\mathcal{P}}}}_l \widetilde{\mathbf{S}}_l + 2\left\|\sqrt{[\widehat{c}_{ij,l}]}\,\boldsymbol{\Theta}_{j,l}\right\|_{\boldsymbol{\mathcal{P}}_l}^2 + \mathbf{1}^\top\left(\widehat{\mathcal{P}}_{x_2x_3,l}\,\widehat{\mathcal{B}}_{x_1,l}\overline{\mathbf{F}}_{1,l} + \widehat{\mathcal{P}}_{x_1x_3,l}\,\widehat{\mathcal{B}}_{x_2,l}\overline{\mathbf{F}}_{2,l} + \widehat{\mathcal{P}}_{x_1x_2,l}\,\widehat{\mathcal{B}}_{x_3,l}\overline{\mathbf{F}}_{3,l}\right)\\
&\quad = \mathbf{w}_l^\top\left(\mathcal{P}_{x_2x_3,l}\,\mathcal{B}_{x_1,l}\,[\widehat{c}_{1j,l}]\boldsymbol{\Theta}_{j,l} + \mathcal{P}_{x_1x_3,l}\,\mathcal{B}_{x_2,l}\,[\widehat{c}_{2j,l}]\boldsymbol{\Theta}_{j,l} + \mathcal{P}_{x_1x_2,l}\,\mathcal{B}_{x_3,l}\,[\widehat{c}_{3j,l}]\boldsymbol{\Theta}_{j,l}\right)\\
&\quad + \mathbf{w}_l^\top\left(\mathcal{P}_{x_2x_3,l}\,\mathbf{g}_{1,l}^{(Int),q} + \mathcal{P}_{x_1x_3,l}\,\mathbf{g}_{2,l}^{(Int),q} + \mathcal{P}_{x_1x_2,l}\,\mathbf{g}_{3,l}^{(Int),q}\right)\\
&\quad + ([\widehat{c}_{1j,l}]\boldsymbol{\Theta}_{j,l})^\top\,\mathcal{P}_{x_2x_3,l}\,\mathbf{g}_{1,l}^{(Int),\Theta} + ([\widehat{c}_{2j,l}]\boldsymbol{\Theta}_{j,l})^\top\,\mathcal{P}_{x_1x_3,l}\,\mathbf{g}_{2,l}^{(Int),\Theta} + ([\widehat{c}_{3j,l}]\boldsymbol{\Theta}_{j,l})^\top\,\mathcal{P}_{x_1x_2,l}\,\mathbf{g}_{3,l}^{(Int),\Theta},
\end{aligned}
\tag{64a}
$$

$$
\begin{aligned}
&\frac{d}{dt}\widetilde{\mathbf{1}}^\top \widehat{\boldsymbol{\mathcal{P}}}_r \widetilde{\mathbf{S}}_r + 2\left\|\sqrt{[\widehat{c}_{ij,r}]}\,\boldsymbol{\Theta}_{j,r}\right\|_{\boldsymbol{\mathcal{P}}_r}^2 + \mathbf{1}^\top\left(\widehat{\mathcal{P}}_{x_2x_3,r}\,\widehat{\mathcal{B}}_{x_1,r}\overline{\mathbf{F}}_{1,r} + \widehat{\mathcal{P}}_{x_1x_3,r}\,\widehat{\mathcal{B}}_{x_2,r}\overline{\mathbf{F}}_{2,r} + \widehat{\mathcal{P}}_{x_1x_2,r}\,\widehat{\mathcal{B}}_{x_3,r}\overline{\mathbf{F}}_{3,r}\right)\\
&\quad = \mathbf{w}_r^\top\left(\mathcal{P}_{x_2x_3,r}\,\mathcal{B}_{x_1,r}\,[\widehat{c}_{1j,r}]\boldsymbol{\Theta}_{j,r} + \mathcal{P}_{x_1x_3,r}\,\mathcal{B}_{x_2,r}\,[\widehat{c}_{2j,r}]\boldsymbol{\Theta}_{j,r} + \mathcal{P}_{x_1x_2,r}\,\mathcal{B}_{x_3,r}\,[\widehat{c}_{3j,r}]\boldsymbol{\Theta}_{j,r}\right)\\
&\quad + \mathbf{w}_r^\top\left(\mathcal{P}_{x_2x_3,r}\,\mathbf{g}_{1,r}^{(Int),q} + \mathcal{P}_{x_1x_3,r}\,\mathbf{g}_{2,r}^{(Int),q} + \mathcal{P}_{x_1x_2,r}\,\mathbf{g}_{3,r}^{(Int),q}\right)\\
&\quad + ([\widehat{c}_{1j,r}]\boldsymbol{\Theta}_{j,r})^\top\,\mathcal{P}_{x_2x_3,r}\,\mathbf{g}_{1,r}^{(Int),\Theta} + ([\widehat{c}_{2j,r}]\boldsymbol{\Theta}_{j,r})^\top\,\mathcal{P}_{x_1x_3,r}\,\mathbf{g}_{2,r}^{(Int),\Theta} + ([\widehat{c}_{3j,r}]\boldsymbol{\Theta}_{j,r})^\top\,\mathcal{P}_{x_1x_2,r}\,\mathbf{g}_{3,r}^{(Int),\Theta},
\end{aligned}
\tag{64b}
$$

where the vectors $\widetilde{\mathbf{1}}$ and $\mathbf{1}$ represent a vectors with M^3 and N^3 elements, respectively (i.e., $\widetilde{\mathbf{1}} = (1,1,\ldots,1)_{M^3}^\top$).

To simplify the notation, assume that the interface between the two tensor product cells lies at $x_1 = 0$. We also assume that all the points that lie on the other faces of the two cubes are treated in an entropy stable fashion; their contribution can then be neglected without loss of generality. Then, for our analysis, we can just focus on a pair of LGL interface nodes at $x_1 = 0$. We then introduce the operators $\mathbf{e}^{(-)}$ and $\mathbf{e}^{(+)}$, which "extract" from the cell-wise solution and flux vectors only the variables associated to these LGL points (i.e., the node at the left, $(-)$, and at the right, $(+)$, of the interface).[12] Therefore, equations (64) reduce to

$$
\begin{aligned}
\frac{d}{dt}\widetilde{\mathbf{1}}^\top \widehat{\widetilde{\boldsymbol{\mathcal{P}}}}_l \widetilde{\mathbf{S}}_l + \mathbf{1}^\top\widehat{\mathcal{P}}_{x_2x_3,l}\,\overline{\mathbf{F}}_{1,l} + 2\left\|\sqrt{[\widehat{c}_{ij,l}]}\boldsymbol{\Theta}_{j,l}\right\|_{\boldsymbol{\mathcal{P}}_l}^2 &= \mathbf{w}_l^\top\mathcal{P}_{x_2x_3,l}\,[\widehat{c}_{1j,l}]\boldsymbol{\Theta}_{j,l}\,\mathbf{e}^{(-)} + \mathbf{w}_l^\top\mathcal{P}_{x_2x_3,l}\,\mathbf{g}_{1,l}^{(Int),q}\\
&\quad + ([\widehat{c}_{1j,l}]\boldsymbol{\Theta}_{j,l})^\top\,\mathcal{P}_{x_2x_3,l}\,\mathbf{g}_{1,l}^{(Int),\Theta},
\end{aligned}
\tag{65a}
$$

[11] In the staggered algorithm framework, N^3 is the number of LGL points in a 3D tensor-product element.

[12] These two vectors are zero at all points except at the "$(-),(+)$" interface points.

$$\frac{d}{dt}\widetilde{\mathbf{1}}^{\top}\widehat{\widetilde{\boldsymbol{\mathcal{P}}}}_r\,\widetilde{\mathbf{S}}_r - \mathbf{1}^{\top}\widehat{\mathcal{P}}_{x_2x_3,r}\,\overline{\mathbf{F}}_{1,r} + 2\left\|\sqrt{[\widehat{c}_{ij,r}]}\boldsymbol{\Theta}_{j,r}\right\|^2_{\boldsymbol{\mathcal{P}}_r} = -\mathbf{w}_r^{\top}\mathcal{P}_{x_2x_3,r}\,[\widehat{c}_{1j,r}]\boldsymbol{\Theta}_{j,r}\,\mathbf{e}^{(+)} + \mathbf{w}_r^{\top}\mathcal{P}_{x_2x_3,r}\,\mathbf{g}_{1,r}^{(Int),q} + \left([\widehat{c}_{1j,r}]\boldsymbol{\Theta}_{j,r}\right)^{\top}\mathcal{P}_{x_2x_3,r}\,\mathbf{g}_{1,r}^{(Int),\Theta}. \tag{65b}$$

The interface penalty terms are constructed as a combination of a local discontinuous Galerkin-type (LDG-type) approach and an interior penalty (IP) technique [13]:

$$\mathbf{g}_{1,l}^{(Int),q} = \left[+\overline{\mathbf{f}}_1^{(-)} - f^{(SS)}\left(q^{(-)},q^{(+)}\right)\right]\mathbf{e}^{(-)} + \left[-\frac{1}{2}(1+\alpha)\left(\left[\widehat{c}_{1,j}^{(-)}\right]\boldsymbol{\Theta}_j^{(-)} - \left[\widehat{c}_{1,j}^{(+)}\right]\boldsymbol{\Theta}_j^{(+)}\right)\right]\mathbf{e}^{(-)} + \left[\frac{1}{2}[L]\left(\mathbf{w}^{(-)} - \mathbf{w}^{(+)}\right)\right]\mathbf{e}^{(-)}, \tag{66a}$$

$$\mathbf{g}_{1,l}^{(Int),\Theta} = \left[-\frac{1}{2}(1-\alpha)\left(\mathbf{w}^{(-)} - \mathbf{w}^{(+)}\right)\right]\mathbf{e}^{(-)}, \tag{66b}$$

$$\mathbf{g}_{1,r}^{(Int),q} = \left[-\overline{\mathbf{f}}_1^{(+)} + f^{(SS)}\left(q^{(-)},q^{(+)}\right)\right]\mathbf{e}^{(+)} + \left[+\frac{1}{2}(1-\alpha)\left(\left[\widehat{c}_{1,j}^{(+)}\right]\boldsymbol{\Theta}_j^{(+)} - \left[\widehat{c}_{1,j}^{(-)}\right]\boldsymbol{\Theta}_j^{(-)}\right)\right]\mathbf{e}^{(+)} + \left[\frac{1}{2}[L]\left(\mathbf{w}^{(+)} - \mathbf{w}^{(-)}\right)\right]\mathbf{e}^{(+)}, \tag{66c}$$

$$\mathbf{g}_{1,r}^{(Int),\Theta} = \left[+\frac{1}{2}(1+\alpha)\left(\mathbf{w}^{(+)} - \mathbf{w}^{(-)}\right)\right]\mathbf{e}^{(+)}. \tag{66d}$$

The LDG penalty terms involve the coefficients $\frac{1}{2}(1\pm\alpha)$ and act only in the normal direction to the face. The IP terms involve the block diagonal parameter matrix, $[L] = \mathrm{Diag}\,[L]$, with N^3 five-by-five blocks, L, which are left unspecified for the moment.[13]

Herein, the solution between adjoining elements is allowed to be discontinuous. An inviscid interface flux that preserves the entropy consistency of the interior high-order accurate spatial operators [1] on either side of the interface $f^{(SS)}\left(q^{(-)},q^{(+)}\right)$ is constructed as

$$f^{(SS)}\left(q^{(-)},q^{(+)}\right) \;=\; f^{(SC)}\left(q^{(-)},q^{(+)}\right) \;+\; \Lambda\left(w^{(+)} - w^{(-)}\right), \tag{67}$$

where $f^{(SC)}\left(q^{(-)},q^{(+)}\right)$ is the entropy *conservative* inviscid interface flux of any order [1,2,19,30,31] (i.e., $\overline{f}^{(S)}$). This flux is constructed as in Theorem 3.3 by using the two-point entropy conservative flux, $\overline{f}_S\left(u_\ell,u_k\right)$, of Ismail and Roe [29]. Λ is a negative semi-definite interface matrix with zero or negative eigenvalues. The superscripts $(-)$ and $(+)$ denote the collocated values on the left and right side of the interface, respectively. The entropy stable flux $f^{(SS)}\left(q^{(-)},q^{(+)}\right)$ is more dissipative than the entropy conservative inviscid flux $f^{(SC)}\left(q^{(-)},q^{(+)}\right)$, as can be easily verified by contracting $f^{(SS)}\left(q^{(-)},q^{(+)}\right)$ against the entropy variables [1]. Note that in reference 15, grid interfaces for entropy stable finite difference schemes are studied and interface fluxes similar to (67) are proposed.

[13] In the staggered algorithm framework, N^3 is the number of LGL points in a 3D tensor-product element.

Substituting expressions (66) and (67) in (65) and summing all the contributions of the two elements results in

$$\frac{d}{dt}\widetilde{\mathbf{1}}^{\top}\widehat{\widetilde{\boldsymbol{\mathcal{P}}}}_{l}\,\widetilde{\mathbf{S}}_{l}+\frac{d}{dt}\widetilde{\mathbf{1}}^{\top}\widehat{\widetilde{\boldsymbol{\mathcal{P}}}}_{r}\,\widetilde{\mathbf{S}}_{r}+2\left[\left\|\sqrt{[\widehat{c}_{ij,l}]}\boldsymbol{\Theta}_{j,l}\right\|^{2}_{\boldsymbol{\mathcal{P}}_{l}}+\left\|\sqrt{[\widehat{c}_{ij,r}]}\boldsymbol{\Theta}_{j,r}\right\|^{2}_{\boldsymbol{\mathcal{P}}_{r}}\right]=\boldsymbol{\Upsilon}^{(I)}+\boldsymbol{\Upsilon}^{(V)},\tag{68}$$

where $\boldsymbol{\Upsilon}^{(I)}$ and $\boldsymbol{\Upsilon}^{(V)}$ are the inviscid and the viscous interface terms. At the two interface nodes, these terms are

$$\Upsilon^{(I)}\;=\;\left(w^{(+)}-w^{(-)}\right)^{\top}f^{(SS)}\left(q^{(-)},q^{(+)}\right)\;-\;\left(\psi^{(+)}-\psi^{(-)}\right)=\left(w^{(+)}-w^{(-)}\right)^{\top}\Lambda\left(w^{(+)}-w^{(-)}\right),\tag{69}$$

$$\Upsilon^{(V)}=\left(w^{(+)}-w^{(-)}\right)^{\top}L\left(w^{(+)}-w^{(-)}\right).\tag{70}$$

Clearly, the interface contributions are dissipative if both the five-by-five matrices Λ and L are negative semi-definite. The matrix Λ can be constructed using different approaches, e.g., using an upwind operator that dissipates each characteristic wave based on the magnitude of its eigenvalue:

$$\begin{aligned}
&f^{ssc}\left(q^{(-)},q^{(+)}\right)\;=\;f^{(SC)}\left(q^{(-)},q^{(+)}\right)\;+\;1/2\,\mathcal{Y}\,|\lambda|\,\mathcal{Y}^{\top}\left(w^{(+)}-w^{(-)}\right),\\
&\frac{\partial}{\partial q}f\left(q\right)\;=\;\mathcal{Y}\,\lambda\,\mathcal{Y}^{\top},\\
&\frac{\partial q}{\partial w}\;=\;\mathcal{Y}\mathcal{Y}^{\top},
\end{aligned}\tag{71}$$

where λ and $\mathcal{Y}$ are the diagonal matrix of the eigenvalues and the matrix of the eigenvectors, respectively. Note that the relation $\partial q/\partial w\;=\;\mathcal{Y}\mathcal{Y}^{\top}$ is achieved by an appropriate scaling of the rotation eigenvectors. Reference 1 constructs the matrix $\partial q/\partial w$ using the scaled eigenvectors introduced by Merriam [32]. The imposed artificial viscosity satisfies the semi-discrete second law of thermodynamics.

We are then left with the viscous interface term, $\boldsymbol{\Upsilon}^{(V)}$. The parameter values $\alpha=0$ and $\alpha=\pm1$ yield a symmetric LDG and a "flip-flop" narrow stencil (nearest neighbor) LDG penalty, respectively [2,31]. An LDG value of $\alpha=0$ produces a global discrete operator that has a neutrally damped spurious eigenmode. Herein, when $\alpha=0$, this mode is damped using the IP dissipation. For a Reynolds number that approaches ∞, we would like the five-by-five matrix L to go to zero so that only the inviscid entropy stable penalty contributions in (66) are recovered. To achieve that, the matrix L is constructed as

$$L=-\beta^{(Int)}\frac{\widehat{c}_{11}^{(-)}+\widehat{c}_{11}^{(+)}}{2\,\left(\mathcal{P}_{x_1}\right)_{(1)(1)}},\quad\beta^{(Int)}>0,\tag{72}$$

where $\widehat{c}_{11}^{(-)}$ and $\widehat{c}_{11}^{(+)}$ are the positive semi-definite viscous coefficient matrices at the left and right side of the interface in the normal direction. The coefficient $\beta^{(Int)}$ can be used to modify the strength of the IP penalty term, although excessively large values of $\beta^{(Int)}$ reduce the maximum stable time step. Reference [2, 31] selects $\beta^{(Int)}$ to be the maximum value for which the explicit stability constraint remains unaffected. The factor $\left(\mathcal{P}_{x_1}\right)_{(1)(1)}$ in the denominator represents the

normal local grid spacing, which is incorporated in the diagonal SBP operator $\mathcal{P}$.[14] This term is introduced to get the correct dimension, and, as for the standard IP finite element approach, it increases the strength of L with increased resolution.

7 Discussion: A theoretical cost analysis

A p-th order 3D tensor-product LGL element has $(p+1)^3$ collocation points. The total cost of the fully discrete, explicit-in-time operator, predominantly results from the inviscid and viscous differentiation operators. Thus, the operation count for a conventional non-staggered element [1,2] scales as $(p+1)^4$. By a similar accounting, the operation count for the semi-staggered operator scales as $(p+1)(p+2)^2$ and $(p+2)^4$ for the fully-staggered operator. The work ratio between the conventional algorithms and the two staggered approaches is given by

$$\left(\frac{p+2}{p+1}\right)^s \;=\; W_{st} \tag{73}$$

with $s=2$ (semi-staggered), and $s=4$ (fully-staggered), respectively (assuming that the explicit time stepping stability constraint is equivalent for all schemes).

The results shown in Section 8 demonstrate that the fully-staggered SSDC approach is significantly more accurate than the conventional LGL SSDC operator for the same solution polynomial and grid density. To determine which approach is more efficient, assume that two simulations are performed on the same grid, and that r_ϵ is the ratio of errors between the conventional and fully-staggered operators. A comparable accuracy can be achieved by increasing the number of elements used in the conventional approach. Thus, assume that N^e_{Conv} and N^e_{Stag} are the number of elements required by each approach to achieve the same error. The work ratio N^e_{Conv}/N^e_{Stag} for 1D elements of polynomial order p, required to overcome the differential in accuracy, is therefore $r_\epsilon \;=\; \left(N^e_{Conv}/N^e_{Stag}\right)^{p+1}$. Now assume that the error is homogeneously distributed in D spatial dimensions, and that a decrease in element size produces a proportional change in the explicit temporal stability constraint. The resulting expression for the cost ratio is given by

$$(r_\epsilon)^{\frac{D+1}{p+1}} \;=\; \frac{N^e_{Conv}}{N^e_{Stag}} \;=\; W_{hr}. \tag{74}$$

Figure 4 shows the ratio of cost $\frac{W_{st}}{W_{hr}}$ between the two approaches as a function of the polynomial order p. Five error ratios are assumed: $r_\epsilon = 2^\beta, 0 \le \beta \le 4$. The first comparison ($r_\epsilon = 1$) assumes the two approaches to be of comparable accuracy. The last $r_\epsilon = 16$ assumes that the staggered operator is 16 times more accurate. This simple estimate suggests that the fully staggered approach is cost effective, despite the increased operation count.

8 Numerical results: Accuracy and robustness

8.1 Isentropic Euler vortex propagation

The test case considered in this section is the (inviscid) propagation of a vortex for which an exact solution is known. This is an excellent test problem for verifying the accuracy and functionality of

[14] Herein, $(\mathcal{P}_{x_i})_{(1)(1)}$ with $i=1$ appears in the definition of L because the interface between the two elements is orthogonal to the x_1 direction [13,31].

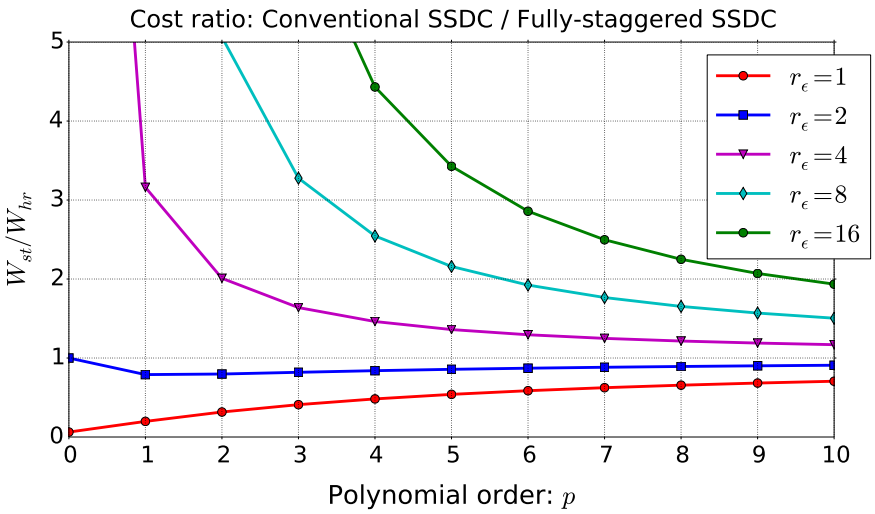

Figure 4. Cost comparison of conventional LGL [1, 2] and fully-staggered SSDC operators.

the inviscid components of a compressible Navier-Stokes solver. It is fully described by

$$\begin{aligned} f(x_1,x_2,x_3,t) &= 1-\left[(x_1-x_{1,0}-U_\infty\cos(\alpha)\,t)^2+(x_2-x_{2,0}-U_\infty\sin(\alpha)\,t)^2\right], \\ T(x_1,x_2,x_3,t) &= \left[1-\epsilon_v^2 M_\infty^2\tfrac{\gamma-1}{8\pi^2}\exp\left(f(x_1,x_2,x_3,t)\right)\right], \\ \rho(x_1,x_2,x_3,t) &= T^{\frac{1}{\gamma-1}}, \\ u_1(x_1,x_2,x_3,t) &= U_\infty\cos(\alpha)-\epsilon_v\tfrac{x_2-x_{2,0}-U_\infty\sin(\alpha)t}{2\pi}\exp\left(\tfrac{f(x_1,x_2,x_3,t)}{2}\right), \\ u_2(x_1,x_2,x_3,t) &= U_\infty\sin(\alpha)-\epsilon_v\tfrac{x_1-x_{1,0}-U_\infty\cos(\alpha)t}{2\pi}\exp\left(\tfrac{f(x_1,x_2,x_3,t)}{2}\right), \\ u_3(x_1,x_2,x_3,t) &= 0, \end{aligned} \tag{75}$$

where U_∞, M_∞, and $(x_{1,0}, x_{2,0}, x_{3,0})$ are the module of the freestream velocity, the Mach number, and the coordinates of the vortex center, respectively. In this study, the values $U_\infty = M_\infty c_\infty$, $\epsilon_v = 5.0$, $M_\infty = 0.5$, $\gamma = 1.4$, and $\alpha = 45^o$ are used; and the domain is described by

$$x_1 \in (-5,5), \quad x_2 \in (-5,5), \quad x_3 \in (-1,1), \quad (x_{1,0},x_{2,0},x_{3,0}) = (0,0,0), \quad t \geq 0.$$

The boundary conditions are prescribed by penalizing the numerical solution against the exact solution by using an SAT approach [33], whereas the interface coupling between two adjoining elements is imposed using the entropy stable treatment proposed in references 1, 13.

The accuracy of the following entropy stable schemes is investigated using uniform Cartesian and unstructured nonuniform grids:

- Fully-staggered SSDC algorithm with $p_{LG} = 1, 2, 3, 4, 5, 10$ and $p_{LGL} = 2, 3, 4, 5, 6, 11$.
- Conventional LGL SSDC algorithm [1, 13] with $p_{LGL} = 1, 2, 3, 4, 5, 10$.

8.1.1 Uniform Cartesian grid

Different grid resolutions are examined, and the vortex is halfway out of the domain when the error measure is evaluated. This measures the effect of the penalty boundary conditions and the

interior scheme. Tables 1–6 show the convergence study for a sequence of maximum nine nested grids.[15] The number of cells in each coordinate direction is indicated in the first column of these tables (i.e., "Resolution"). The L^2 norm of the error decay asymptotes towards the designed rate in each case (i.e., second order, third order, fourth order, fifth order, sixth order, and eleventh order, respectively), for both fully staggered and the conventional SSDC approaches. We highlight that the fully-staggered approach is significantly more accurate than the conventional algorithm for the same grid resolution. However, simple counting arguments based on inviscid flux evaluations, indicate that the cost of the staggered algorithm for a solution polynomial order p is comparable to that of an LGL operator [1, 2], with a solution polynomial order of $(p + 1)$.

Table 1 Error convergence is shown for the fully-staggered $p_{LG} = 1$, $p_{LGL} = 2$ and conventional LGL [1, 2] $p_{LGL} = 1$ SSDC algorithms for the isentropic Euler vortex propagation on uniform Cartesian grids.

	Fully-staggered, $p_{LG} = 1$, $p_{LGL} = 2$				Conventional, $p_{LGL} = 1$			
Resolution	L^2 error	L^2 rate	L^∞ error	L^∞ rate	L^2 error	L^2 rate	L^∞ error	L^∞ rate
$2 \times 2 \times 2$	1.42e-02	-	6.28e-02	-	9.78e-03	-	3.70e-02	-
$4 \times 4 \times 2$	8.73e-03	0.70	6.51e-02	-0.05	7.75e-03	0.33	5.11e-02	-0.46
$8 \times 8 \times 2$	3.86e-03	1.18	3.75e-02	0.80	7.41e-03	0.07	6.33e-02	-0.31
$16 \times 16 \times 2$	1.49e-03	1.37	1.52e-02	1.30	3.95e-03	0.91	4.08e-02	0.63
$32 \times 32 \times 2$	5.35e-04	1.47	6.07e-03	1.32	1.66e-03	1.25	1.88e-02	1.12
$64 \times 64 \times 2$	1.72e-04	1.64	1.95e-03	1.64	6.23e-04	1.42	7.38e-03	1.35
$128 \times 128 \times 2$	4.76e-05	1.85	5.30e-04	1.88	2.12e-04	1.56	2.49e-03	1.57
$256 \times 256 \times 2$	1.14e-05	2.06	1.27e-04	2.06	6.10e-05	1.79	6.96e-04	1.84
$512 \times 512 \times 2$	2.72e-06	2.07	3.22e-05	1.98	1.46e-05	2.07	1.65e-04	2.08

Table 2 Error convergence is shown for the fully-staggered $p_{LG} = 2$, $p_{LGL} = 3$ and conventional LGL [1, 2] $p_{LGL} = 2$ SSDC algorithms for the isentropic Euler vortex propagation on uniform Cartesian grids.

	Fully-staggered, $p_{LG} = 2$, $p_{LGL} = 3$				Conventional, $p_{LGL} = 2$			
Resolution	L^2 error	L^2 rate	L^∞ error	L^∞ rate	L^2 error	L^2 rate	L^∞ error	L^∞ rate
$2 \times 2 \times 2$	1.31e-02	-	9.28e-02	-	6.57e-03	-	6.44e-02	-
$4 \times 4 \times 2$	3.52e-03	1.90	2.20e-02	2.07	6.14e-03	0.10	7.24e-02	-0.17
$8 \times 8 \times 2$	8.83e-04	2.00	8.38e-03	1.40	2.66e-03	1.21	3.11e-02	1.22
$16 \times 16 \times 2$	1.79e-04	2.30	2.78e-03	1.59	6.91e-04	1.94	1.13e-02	1.46
$32 \times 32 \times 2$	3.10e-05	2.53	5.54e-04	2.33	2.01e-04	1.78	5.24e-03	1.11
$64 \times 64 \times 2$	5.30e-06	2.55	8.86e-05	2.64	2.66e-05	2.92	7.15e-04	2.87
$128 \times 128 \times 2$	7.80e-07	2.77	1.32e-05	2.74	4.35e-06	2.61	1.15e-04	2.64
$256 \times 256 \times 2$	1.14e-07	2.78	2.19e-06	2.60	6.57e-07	2.73	1.75e-05	2.71
$512 \times 512 \times 2$	1.42e-08	3.00	2.67e-07	3.03	8.57e-08	2.94	2.60e-06	2.75

[15] The number of grid cells is doubled every time in each coordinate direction.

Table 3 Error convergence is shown for the fully-staggered $p_{LG} = 3$, $p_{LGL} = 4$ and conventional LGL $[1, 2]$ $p_{LGL} = 3$ SSDC algorithms for the isentropic Euler vortex propagation on uniform Cartesian grids.

	Fully-staggered, $p_{LG} = 3$, $p_{LGL} = 4$				Conventional, $p_{LGL} = 3$			
Resolution	L^2 error	L^2 rate	L^∞ error	L^∞ rate	L^2 error	L^2 rate	L^∞ error	L^∞ rate
$2 \times 2 \times 2$	5.63e-03	-	3.30e-02	-	6.94e-03	-	8.21e-02	-
$4 \times 4 \times 2$	1.77e-03	1.67	2.12e-02	0.64	3.69e-03	0.91	5.18e-02	0.66
$8 \times 8 \times 2$	2.02e-04	3.13	3.60e-03	2.56	6.79e-04	2.44	1.12e-02	2.21
$16 \times 16 \times 2$	1.71e-05	3.56	3.22e-04	3.48	7.30e-05	3.22	1.76e-03	2.67
$32 \times 32 \times 2$	1.36e-06	3.66	2.76e-05	3.54	7.10e-06	3.36	1.60e-04	3.46
$64 \times 64 \times 2$	1.01e-07	3.75	1.84e-06	3.91	7.07e-07	3.33	1.94e-05	3.05
$128 \times 128 \times 2$	6.31e-09	4.00	1.15e-07	4.00	5.41e-08	3.71	1.80e-06	3.43
$256 \times 256 \times 2$	3.51e-10	4.17	6.41e-09	4.16	3.69e-09	3.88	1.45e-07	3.63
$512 \times 512 \times 2$	2.12e-11	4.05	4.48e-10	3.84	2.40e-10	3.94	1.12e-08	3.69

Table 4 Error convergence is shown for the fully-staggered $p_{LG} = 4$, $p_{LGL} = 5$ and conventional LGL $[1, 2]$ $p_{LGL} = 4$ SSDC algorithms for the isentropic Euler vortex propagation on uniform Cartesian grids.

	Fully-staggered, $p_{LG} = 4$, $p_{LGL} = 5$				Conventional, $p_{LGL} = 4$			
Resolution	L^2 error	L^2 rate	L^∞ error	L^∞ rate	L^2 error	L^2 rate	L^∞ error	L^∞ rate
$2 \times 2 \times 2$	4.14e-03	-	3.61e-02	-	5.76e-03	-	5.92e-02	-
$4 \times 4 \times 2$	6.04e-04	2.78	8.41e-03	2.10	1.41e-03	2.03	2.05e-02	1.53
$8 \times 8 \times 2$	3.17e-05	4.25	3.37e-04	4.64	1.17e-04	3.59	1.62e-03	3.66
$16 \times 16 \times 2$	1.68e-06	4.23	3.45e-05	3.29	7.24e-06	4.02	1.79e-04	3.18
$32 \times 32 \times 2$	6.40e-08	4.72	1.35e-06	4.68	3.91e-07	4.21	1.20e-05	3.90
$64 \times 64 \times 2$	2.26e-09	4.82	5.39e-08	4.65	1.76e-08	4.47	5.57e-07	4.43
$128 \times 128 \times 2$	7.36e-11	4.94	1.99e-09	4.76	7.16e-10	4.62	2.41e-08	4.53
$256 \times 256 \times 2$	-	-	-	-	2.19e-11	5.03	8.37e-10	4.85

Table 5 Error convergence is shown for the fully-staggered $p_{LG} = 5$, $p_{LGL} = 6$ and conventional LGL $[1, 2]$ $p_{LGL} = 5$ SSDC algorithms for the isentropic Euler vortex propagation on uniform Cartesian grids.

	Fully-staggered, $p_{LG} = 5$, $p_{LGL} = 6$				Conventional, $p_{LGL} = 5$			
Resolution	L^2 error	L^2 rate	L^∞ error	L^∞ rate	L^2 error	L^2 rate	L^∞ error	L^∞ rate
$2 \times 2 \times 2$	2.73e-03	-	3.49e-02	-	3.05e-03	-	5.75e-02	-
$4 \times 4 \times 2$	1.81e-04	3.91	1.34e-03	4.71	5.25e-04	2.54	5.62e-03	3.36
$8 \times 8 \times 2$	8.68e-06	4.38	1.98e-04	2.75	2.60e-05	4.33	7.85e-04	2.84
$16 \times 16 \times 2$	1.25e-07	6.12	2.76e-06	6.16	7.52e-07	5.11	2.46e-05	5.00
$32 \times 32 \times 2$	2.63e-09	5.57	5.60e-08	5.63	1.90e-08	5.31	6.30e-07	5.29
$64 \times 64 \times 2$	4.18e-11	5.98	1.00e-09	5.80	4.00e-10	5.57	1.81e-08	5.12
$128 \times 128 \times 2$	-	-	-	-	7.67e-12	5.71	3.71e-10	5.61

Table 6 Error convergence is shown for the fully-staggered $p_{LG} = 10$, $p_{LGL} = 11$ and conventional LGL $[1, 2]$ $p_{LGL} = 10$ SSDC algorithms for the isentropic Euler vortex propagation on uniform Cartesian grids.

	Fully-staggered, $p_{LG} = 10$, $p_{LGL} = 11$				Conventional, $p_{LGL} = 10$			
Resolution	L^2 error	L^2 rate	L^∞ error	L^∞ rate	L^2 error	L^2 rate	L^∞ error	L^∞ rate
$2 \times 2 \times 2$	1.23e-04	-	1.36e-03	-	1.33e-04	-	2.41e-03	-
$4 \times 4 \times 2$	4.35e-07	8.15	5.75e-06	7.88	1.83e-06	6.18	3.14e-05	6.26
$8 \times 8 \times 2$	6.17e-10	9.46	1.79e-08	8.33	3.30e-09	9.12	1.11e-07	8.15
$16 \times 16 \times 2$	2.07e-12	8.22	1.57e-11	10.15	1.27e-12	11.35	5.28e-11	11.03

8.1.2 Unstructured nonuniform grids

The goal of this study is to investigate whether the fully-staggered algorithm is effectively $(p+1)$-order accurate for more realistic meshes (p is the order of the polynomial supported by the LG points). As for the case of uniform Cartesian grids, different grid resolutions are examined, and the vortex is halfway out of the domain when the error measure is evaluated. A nested family of grids is constructed by replicating N times the "unstructured grid kernel" shown in Figure 5.

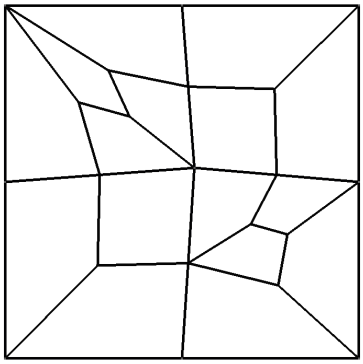

Figure 5. "Unstructured grid kernel" used to construct a sequence of nested grids for the inviscid vortex test case.

Tables 7–12 show the convergence study for a sequence of twelve nested grids. The number of "unstructured grid kernels" in each coordinate direction is indicated in the first column of these tables. For the fully-staggered SSDC algorithm, the L^2 norm of the error decay asymptotes towards the designed rate (i.e., $(p+1)$) and, in each case, is more accurate than the conventional LGL SSDC algorithm for the same grid resolution. The conventional path converges instead to p.

Table 7 Error convergence is shown for the fully-staggered $p_{LG} = 1$, $p_{LGL} = 2$ and conventional LGL [1,2] $p_{LGL} = 1$ SSDC algorithms for the isentropic Euler vortex propagation on highly nonuniform grids.

	Fully-staggered, $p_{LG} = 1$, $p_{LGL} = 2$				Conventional, $p_{LGL} = 1$			
Resolution	L^2 error	L^2 rate	L^∞ error	L^∞ rate	L^2 error	L^2 rate	L^∞ error	L^∞ rate
$1 \times 1 \times 2$	1.19e-02	-	1.34e-01	-	8.22e-03	-	8.77e-02	-
$2 \times 2 \times 2$	6.31e-03	0.91	8.16e-02	0.72	1.07e-02	-0.38	2.20e-01	-1.33
$3 \times 3 \times 2$	5.12e-03	0.51	7.39e-02	0.25	1.02e-02	0.11	1.37e-01	1.18
$4 \times 4 \times 2$	3.57e-03	1.25	5.52e-02	1.01	1.07e-02	-0.14	1.94e-01	-1.21
$5 \times 5 \times 2$	2.56e-03	1.49	4.94e-02	0.50	1.02e-02	0.21	2.02e-01	-0.18
$6 \times 6 \times 2$	1.87e-03	1.73	2.95e-02	2.83	8.82e-03	0.78	1.70e-01	0.96
$7 \times 7 \times 2$	1.52e-03	1.36	2.91e-02	0.08	7.36e-03	1.18	1.46e-01	0.98
$8 \times 8 \times 2$	1.26e-03	1.39	2.36e-02	1.58	6.36e-03	1.09	1.14e-01	1.81
$9 \times 9 \times 2$	1.04e-03	1.61	2.27e-02	0.33	5.82e-03	0.75	1.08e-01	0.47
$10 \times 10 \times 2$	8.76e-04	1.65	2.06e-02	0.93	5.43e-03	0.66	1.06e-01	0.20
$11 \times 11 \times 2$	7.52e-04	1.61	1.69e-02	2.06	5.06e-03	0.75	1.02e-01	0.38
$12 \times 12 \times 2$	6.54e-04	1.59	1.60e-02	0.63	4.70e-03	0.84	1.16e-01	-1.43
$13 \times 13 \times 2$	5.75e-04	1.61	1.62e-02	-0.16	4.39e-03	0.87	1.13e-01	0.29
$14 \times 14 \times 2$	5.09e-04	1.67	1.45e-02	1.54	4.11e-03	0.87	1.05e-01	1.06
$15 \times 15 \times 2$	4.53e-04	1.66	1.27e-02	1.83	3.87e-03	0.88	9.40e-02	1.56
$16 \times 16 \times 2$	4.07e-04	1.66	1.17e-02	1.33	3.65e-03	0.90	8.30e-02	1.92

Table 8 Error convergence is shown for the fully-staggered $p_{LG} = 2$, $p_{LGL} = 3$ and conventional LGL [1,2] $p_{LGL} = 2$ SSDC algorithms for the isentropic Euler vortex propagation on highly nonuniform grids.

	Fully-staggered, $p_{LG} = 2$, $p_{LGL} = 3$				Conventional, $p_{LGL} = 2$			
Resolution	L^2 error	L^2 rate	L^∞ error	L^∞ rate	L^2 error	L^2 rate	L^∞ error	L^∞ rate
$1 \times 1 \times 2$	5.25e-03	-	3.96e-02	-	9.21e-03	-	1.47e-01	-
$2 \times 2 \times 2$	1.62e-03	1.70	1.88e-02	1.07	3.95e-03	1.22	7.74e-02	0.92
$3 \times 3 \times 2$	1.38e-03	0.39	2.28e-02	-0.47	3.14e-03	0.56	6.92e-02	0.28
$4 \times 4 \times 2$	7.71e-04	2.03	2.18e-02	0.15	2.53e-03	0.76	7.05e-02	-0.07
$5 \times 5 \times 2$	3.21e-04	3.92	7.48e-03	4.80	1.65e-03	1.90	5.91e-02	0.79
$6 \times 6 \times 2$	2.04e-04	2.49	4.28e-03	3.07	1.14e-03	2.06	3.37e-02	3.08
$7 \times 7 \times 2$	1.47e-04	2.11	3.35e-03	1.58	8.75e-04	1.70	2.81e-02	1.19
$8 \times 8 \times 2$	1.08e-04	2.34	2.87e-03	1.15	6.86e-04	1.82	2.14e-02	2.02
$9 \times 9 \times 2$	8.10e-05	2.43	2.14e-03	2.49	5.37e-04	2.08	1.75e-02	1.73
$10 \times 10 \times 2$	6.18e-05	2.57	1.56e-03	3.01	4.26e-04	2.19	1.59e-02	0.90
$11 \times 11 \times 2$	4.76e-05	2.75	1.41e-03	1.06	3.50e-04	2.08	1.21e-02	2.82
$12 \times 12 \times 2$	3.71e-05	2.86	1.27e-03	1.20	2.95e-04	1.95	9.28e-03	3.08
$13 \times 13 \times 2$	2.95e-05	2.85	8.69e-04	4.75	2.54e-04	1.88	7.92e-03	1.97
$14 \times 14 \times 2$	2.39e-05	2.85	6.44e-04	4.05	2.21e-04	1.84	7.48e-03	0.78
$15 \times 15 \times 2$	1.97e-05	2.82	5.82e-04	1.45	1.95e-04	1.82	7.05e-03	0.85
$16 \times 16 \times 2$	1.64e-05	2.80	4.59e-04	3.67	1.74e-04	1.81	6.48e-03	1.31

Table 9 Error convergence is shown for the fully-staggered $p_{LG} = 3$, $p_{LGL} = 4$ and conventional LGL [1,2] $p_{LGL} = 3$ SSDC algorithms for the isentropic Euler vortex propagation on highly nonuniform grids.

	Fully-staggered, $p_{LG} = 3$, $p_{LGL} = 4$				Conventional, $p_{LGL} = 3$			
Resolution	L^2 error	L^2 rate	L^∞ error	L^∞ rate	L^2 error	L^2 rate	L^∞ error	L^∞ rate
$1 \times 1 \times 2$	2.33e-03	-	3.57e-02	-	4.76e-03	-	5.64e-02	-
$2 \times 2 \times 2$	4.73e-04	2.30	6.71e-03	2.41	1.02e-03	2.22	2.04e-02	1.47
$3 \times 3 \times 2$	2.39e-04	1.69	7.59e-03	-0.31	9.00e-04	0.32	2.19e-02	-0.18
$4 \times 4 \times 2$	8.94e-05	3.42	2.14e-03	4.40	4.70e-04	2.26	1.87e-02	0.54
$5 \times 5 \times 2$	4.59e-05	2.99	1.27e-03	2.34	2.79e-04	2.34	1.05e-02	2.59
$6 \times 6 \times 2$	2.27e-05	3.86	6.72e-04	3.49	1.67e-04	2.80	7.92e-03	1.55
$7 \times 7 \times 2$	1.32e-05	3.51	4.66e-04	2.37	9.27e-05	3.83	4.74e-03	3.33
$8 \times 8 \times 2$	8.58e-06	3.24	4.55e-04	0.18	5.82e-05	3.49	3.00e-03	3.43
$9 \times 9 \times 2$	5.76e-06	3.39	3.41e-04	2.44	4.05e-05	3.07	1.82e-03	4.23
$10 \times 10 \times 2$	3.93e-06	3.61	2.45e-04	3.16	3.04e-05	2.73	1.23e-03	3.71
$11 \times 11 \times 2$	2.76e-06	3.71	1.79e-04	3.30	2.34e-05	2.74	1.11e-03	1.13
$12 \times 12 \times 2$	2.01e-06	3.66	1.33e-04	3.35	1.82e-05	2.91	8.80e-04	2.65
$13 \times 13 \times 2$	1.50e-06	3.64	9.99e-05	3.62	1.43e-05	2.97	7.65e-04	1.76
$14 \times 14 \times 2$	1.14e-06	3.68	7.53e-05	3.82	1.16e-05	2.87	6.45e-04	2.30
$15 \times 15 \times 2$	8.81e-07	3.77	5.80e-05	3.78	9.57e-06	2.77	5.79e-04	1.55
$16 \times 16 \times 2$	6.91e-07	3.76	4.53e-05	3.81	8.01e-06	2.75	4.79e-04	2.96

Table 10 Error convergence is shown for the fully-staggered $p_{LG} = 4$, $p_{LGL} = 5$ and conventional LGL [1,2] $p_{LGL} = 4$ SSDC algorithms for the isentropic Euler vortex propagation on highly nonuniform grids.

	Fully-staggered, $p_{LG} = 4$, $p_{LGL} = 5$				Conventional, $p_{LGL} = 4$			
Resolution	L^2 error	L^2 rate	L^∞ error	L^∞ rate	L^2 error	L^2 rate	L^∞ error	L^∞ rate
$1 \times 1 \times 2$	6.59e-04	-	8.13e-03	-	2.02e-03	-	4.01e-02	-
$2 \times 2 \times 2$	1.08e-04	2.61	1.98e-03	2.04	2.90e-04	2.80	5.48e-03	2.87
$3 \times 3 \times 2$	5.77e-05	1.54	2.05e-03	-0.09	1.70e-04	1.32	8.78e-03	-1.16
$4 \times 4 \times 2$	2.09e-05	3.52	1.40e-03	1.32	8.33e-05	2.48	4.12e-03	2.63
$5 \times 5 \times 2$	5.91e-06	5.67	3.26e-04	6.54	3.27e-05	4.19	2.14e-03	2.93
$6 \times 6 \times 2$	2.52e-06	4.67	7.79e-05	7.85	1.18e-05	5.58	9.91e-04	4.23
$7 \times 7 \times 2$	1.23e-06	4.63	6.04e-05	1.66	8.90e-06	1.85	6.95e-04	2.30
$8 \times 8 \times 2$	6.58e-07	4.71	4.17e-05	2.77	5.62e-06	3.44	3.77e-04	4.59
$9 \times 9 \times 2$	3.90e-07	4.44	2.46e-05	4.49	3.59e-06	3.82	2.19e-04	4.59
$10 \times 10 \times 2$	2.43e-07	4.48	1.29e-05	6.14	2.39e-06	3.83	1.64e-04	2.75
$11 \times 11 \times 2$	1.56e-07	4.67	9.68e-06	2.99	1.66e-06	3.86	1.20e-04	3.31
$12 \times 12 \times 2$	1.02e-07	4.91	7.30e-06	3.24	1.20e-06	3.71	7.67e-05	5.12
$13 \times 13 \times 2$	6.75e-08	5.11	4.36e-06	6.44	9.03e-07	3.55	6.29e-05	2.47
$14 \times 14 \times 2$	4.65e-08	5.03	2.42e-06	7.97	6.93e-07	3.57	5.40e-05	2.06

Table 11 Error convergence is shown for the fully-staggered $p_{LG} = 5$, $p_{LGL} = 6$ and conventional LGL [1, 2] $p_{LGL} = 5$ SSDC algorithms for the isentropic Euler vortex propagation on highly nonuniform grids.

	Fully-staggered, $p_{LG} = 5$, $p_{LGL} = 6$				Conventional, $p_{LGL} = 5$			
Resolution	L^2 error	L^2 rate	L^∞ error	L^∞ rate	L^2 error	L^2 rate	L^∞ error	L^∞ rate
$1 \times 1 \times 2$	2.93e-04	-	5.48e-03	-	6.72e-04	-	1.35e-02	-
$2 \times 2 \times 2$	2.44e-05	3.58	5.74e-04	3.26	6.53e-05	3.36	2.53e-03	2.41
$3 \times 3 \times 2$	1.02e-05	2.15	4.46e-04	0.62	3.72e-05	1.39	1.67e-03	1.02
$4 \times 4 \times 2$	2.65e-06	4.70	8.64e-05	5.70	1.36e-05	3.49	7.67e-04	2.70
$5 \times 5 \times 2$	7.36e-07	5.75	2.93e-05	4.85	5.77e-06	3.86	3.68e-04	3.30
$6 \times 6 \times 2$	2.36e-07	6.24	1.24e-05	4.73	2.90e-06	3.78	1.83e-04	3.83
$7 \times 7 \times 2$	1.00e-07	5.54	4.80e-06	6.15	1.06e-06	6.51	7.48e-05	5.80
$8 \times 8 \times 2$	4.97e-08	5.26	2.57e-06	4.66	5.10e-07	5.50	3.09e-05	6.62
$9 \times 9 \times 2$	2.55e-08	5.67	2.08e-06	1.83	2.98e-07	4.56	1.93e-05	3.97
$10 \times 10 \times 2$	1.41e-08	5.64	1.25e-06	4.83	1.81e-07	4.74	1.03e-05	5.98
$11 \times 11 \times 2$	8.02e-09	5.90	6.86e-07	6.28	1.16e-07	4.66	6.76e-06	4.43
$12 \times 12 \times 2$	4.78e-09	5.94	3.84e-07	6.68	7.68e-08	4.75	5.05e-06	3.35
$13 \times 13 \times 2$	2.99e-09	5.86	2.35e-07	6.11	5.21e-08	4.84	4.48e-06	1.51
$14 \times 14 \times 2$	1.93e-09	5.88	1.76e-07	3.88	3.63e-08	4.87	3.62e-06	2.87

Table 12 Error convergence is shown for the fully-staggered $p_{LG} = 10$, $p_{LGL} = 11$ and conventional LGL [1, 2] $p_{LGL} = 10$ SSDC algorithms for the isentropic Euler vortex propagation on highly nonuniform grids.

	Fully-staggered, $p_{LG} = 10$, $p_{LGL} = 11$				Conventional, $p_{LGL} = 10$			
Resolution	L^2 error	L^2 rate	L^∞ error	L^∞ rate	L^2 error	L^2 rate	L^∞ error	L^∞ rate
$1 \times 1 \times 2$	1.73e-06	-	2.70e-05	-	2.87e-06	-	1.16e-04	-
$2 \times 2 \times 2$	1.23e-08	7.13	4.74e-07	5.83	6.50e-08	5.46	4.50e-06	4.69
$3 \times 3 \times 2$	2.71e-09	3.73	1.57e-07	2.72	1.41e-08	3.78	1.12e-06	3.43
$4 \times 4 \times 2$	3.12e-10	7.51	1.49e-08	8.19	1.46e-09	7.88	1.19e-07	7.79
$5 \times 5 \times 2$	3.52e-11	9.78	4.26e-09	5.62	2.16e-10	8.56	2.64e-08	6.76
$6 \times 6 \times 2$	4.19e-12	11.66	4.20e-10	12.71	2.99e-11	10.84	2.80e-09	12.30

8.2 Viscous shock

The second test case considered in this section is the propagation of a viscous shock for which an exact time-dependent solution is known. The compressible Navier-Stokes equations support an exact solution for the viscous shock profile, under the assumption that the Prandtl number is $Pr = \frac{3}{4}$. Mass and total enthalpy are constant across a shock. Furthermore, if $Pr = \frac{3}{4}$ then the momentum and energy equations are redundant. If we assume that the shock is propagating along the x_1 coordinate direction,[16] the single momentum equation across the shock is given by

$$\begin{array}{c} \alpha v \frac{\partial v}{\partial x_1} - (v-1)(v-v_f) = 0 \quad ; \quad -\infty \leq x_1 \leq \infty \quad , \quad t \geq 0; \\ v \;=\; \frac{u_1}{u_{1,left}} \; ; \; v_f = \frac{u_{1,right}}{u_{1,left}} \; ; \; \alpha \;=\; \frac{\gamma-1}{2\gamma} \frac{\mu}{Pr\, \dot{m}}, \end{array} \tag{76}$$

where $\dot{m}$ is the constant mass flow across the shock. An exact solution is obtained by solving the momentum equation (76) for the velocity profile, v:

$$x_1 \;=\; \tfrac{1}{2}\alpha \left(Log\,|(v-1)(v-v_f)| + \tfrac{1+v_f}{1-v_f} Log \left| \tfrac{v-1}{v-v_f} \right| \right). \tag{77}$$

A moving shock is recovered by applying a uniform translation to the solution. A full derivation of this solution appears in the thesis of Fisher [22]. In this study, the values $U_\infty = M_\infty c_\infty$, $M_\infty = 2.5$, $Re_\infty = 10$, and $\gamma = 1.4$ are used. The viscous shock, which at $t = 0$ is located at the center of the computational domain, is propagated in the direction parallel to the horizontal axis. The domain is described by

$$x_1 \in (-10, 10), \quad x_2 \in (-10, 10), \quad x_3 \in (-1, 1), \quad t \geq 0.$$

The boundary conditions on the faces perpendicular to the horizontal axis are prescribed by penalizing the numerical solution against the exact solution; periodic boundary conditions are used on the remaining four boundary faces of the computational domain. This is an excellent test problem for verifying the accuracy and functionality of the inviscid and viscous components of a compressible Navier-Stokes solver.

The accuracy of the following entropy stable schemes is investigated using uniform Cartesian and unstructured nonuniform grids:

- Fully-staggered SSDC algorithm with $p_{LG} = 1, 2, 3, 4, 5, 10$ and $p_{LGL} = 2, 3, 4, 5, 6, 11$.
- Conventional LGL SSDC algorithm [1, 13] with $p_{LGL} = 1, 2, 3, 4, 5, 10$.

8.2.1 Uniform Cartesian grids

Different grid resolutions are examined, and the viscous shock has been propagated halfway out of the domain when the error measure is evaluated. This measures the effect of the penalty boundary condition and the interior scheme. Tables 13–18 show the convergence study for a sequence of maximum nine nested grids (the number of grid cells is doubled in each direction every time). The number of cells in each coordinate direction is indicated in the first column of these tables (i.e., "Resolution"). The L^2 norm of the error decay asymptotes towards the designed rate in each case, for both fully-staggered and the conventional LGL SSDC schemes. As for the Euler vortex test case, we note that the fully-staggered approach is more accurate than the conventional algorithm for the

[16] This is assumption is just used to simplify the notation.

same grid resolution. However, simple counting arguments based on inviscid flux and viscous flux evaluations, indicate that the cost of the staggered algorithm for a solution polynomial order p is comparable to that of an LGL operator [1,2], with a solution polynomial order of $(p+1)$.

Table 13 Error convergence is shown for the fully-staggered $p_{LG}=1$, $p_{LGL}=2$ and the conventional LGL [1,2] $p_{LGL}=1$ SSDC algorithms for the viscous shock on uniform Cartesian grids.

	Fully-staggered, $p_{LG}=1$, $p_{LGL}=2$				Conventional, $p_{LGL}=1$			
Resolution	L^2 error	L^2 rate	L^∞ error	L^∞ rate	L^2 error	L^2 rate	L^∞ error	L^∞ rate
$2\times2\times2$	1.61e-01	-	6.15e-01	-	6.45e-02	-	2.31e-01	-
$4\times4\times2$	3.16e-02	2.35	1.24e-01	2.31	7.26e-02	-0.17	2.67e-01	-0.21
$8\times8\times2$	1.27e-02	1.32	5.56e-02	1.16	3.64e-02	1.00	1.77e-01	0.59
$16\times16\times2$	3.23e-03	1.97	1.87e-02	1.57	1.36e-02	1.42	7.76e-02	1.19
$32\times32\times2$	8.78e-04	1.88	6.20e-03	1.60	4.23e-03	1.69	2.42e-02	1.68
$64\times64\times2$	2.25e-04	1.96	1.84e-03	1.75	1.12e-03	1.91	7.60e-03	1.67
$128\times128\times2$	5.62e-05	2.00	4.76e-04	1.95	2.79e-04	2.01	1.97e-03	1.95
$256\times256\times2$	1.38e-05	2.02	1.18e-04	2.01	6.81e-05	2.04	4.52e-04	2.13
$512\times512\times2$	3.43e-06	2.01	2.85e-05	2.05	1.67e-05	2.03	1.03e-04	2.13

Table 14 Error convergence is shown for the fully-staggered $p_{LG}=2$, $p_{LGL}=3$ and the conventional LGL [1,2] $p_{LGL}=2$ SSDC algorithms for the viscous shock on uniform Cartesian grids.

	Fully-staggered, $p_{LG}=2$, $p_{LGL}=3$				Conventional, $p_{LGL}=2$			
Resolution	L^2 error	L^2 rate	L^∞ error	L^∞ rate	L^2 error	L^2 rate	L^∞ error	L^∞ rate
$2\times2\times2$	2.15e-02	-	9.04e-02	-	7.58e-02	-	2.08e-01	-
$4\times4\times2$	8.66e-03	1.31	3.14e-02	1.52	2.29e-02	1.73	1.26e-01	0.73
$8\times8\times2$	1.65e-03	2.39	8.80e-03	1.84	9.27e-03	1.30	8.48e-02	0.57
$16\times16\times2$	4.01e-04	2.04	2.88e-03	1.61	2.62e-03	1.82	3.14e-02	1.43
$32\times32\times2$	4.11e-05	3.29	2.77e-04	3.38	3.44e-04	2.93	4.15e-03	2.92
$64\times64\times2$	5.33e-06	2.95	3.72e-05	2.90	4.12e-05	3.06	5.91e-04	2.81
$128\times128\times2$	7.18e-07	2.89	5.21e-06	2.83	5.18e-06	2.99	7.64e-05	2.95
$256\times256\times2$	1.04e-07	2.79	7.51e-07	2.79	6.69e-07	2.95	9.81e-06	2.96
$512\times512\times2$	1.35e-08	2.94	1.55e-07	2.28	8.93e-08	2.91	1.28e-06	2.94

Table 15 Error convergence is shown for the fully-staggered $p_{LG} = 3$, $p_{LGL} = 4$ and the conventional LGL [1,2] $p_{LGL} = 3$ SSDC algorithms for the viscous shock on uniform Cartesian grids.

	Fully-staggered, $p_{LG} = 3$, $p_{LGL} = 4$				Conventional, $p_{LGL} = 3$			
Resolution	L^2 error	L^2 rate	L^∞ error	L^∞ rate	L^2 error	L^2 rate	L^∞ error	L^∞ rate
$2 \times 2 \times 2$	2.19e-02	-	8.39e-02	-	5.00e-02	-	3.15e-01	-
$4 \times 4 \times 2$	3.97e-03	2.46	1.55e-02	2.43	1.13e-02	2.15	1.26e-01	1.32
$8 \times 8 \times 2$	5.12e-04	2.96	3.49e-03	2.15	2.98e-03	1.92	3.43e-02	1.87
$16 \times 16 \times 2$	2.65e-05	4.27	1.52e-04	4.52	1.56e-04	4.25	1.79e-03	4.26
$32 \times 32 \times 2$	1.96e-06	3.76	1.38e-05	3.46	1.17e-05	3.74	1.75e-04	3.35
$64 \times 64 \times 2$	1.45e-07	3.76	1.12e-06	3.63	7.79e-07	3.91	1.31e-05	3.74
$128 \times 128 \times 2$	1.09e-08	3.73	8.53e-08	3.71	4.89e-08	3.99	7.85e-07	4.07
$256 \times 256 \times 2$	7.08e-10	3.95	9.73e-09	3.13	3.03e-09	4.01	4.70e-08	4.06

Table 16 Error convergence is shown for the fully-staggered $p_{LG} = 4$, $p_{LGL} = 5$ and the conventional LGL [1,2] $p_{LGL} = 4$ SSDC algorithms for the viscous shock on uniform Cartesian grids.

	Fully-staggered, $p_{LG} = 4$, $p_{LGL} = 5$				Conventional, $p_{LGL} = 4$			
Resolution	L^2 error	L^2 rate	L^∞ error	L^∞ rate	L^2 error	L^2 rate	L^∞ error	L^∞ rate
$2 \times 2 \times 2$	6.27e-03	-	2.59e-02	-	3.75e-02	-	1.32e-01	-
$4 \times 4 \times 2$	6.72e-04	3.22	4.10e-03	2.66	6.14e-03	2.61	6.88e-02	0.94
$8 \times 8 \times 2$	1.33e-04	2.34	8.25e-04	2.31	3.86e-04	3.99	5.21e-03	3.72
$16 \times 16 \times 2$	5.96e-06	4.48	3.87e-05	4.41	4.68e-05	3.04	7.04e-04	2.89
$32 \times 32 \times 2$	1.58e-07	5.23	1.10e-06	5.14	9.90e-07	5.56	2.23e-05	4.98
$64 \times 64 \times 2$	5.07e-09	4.96	4.38e-08	4.65	2.90e-08	5.09	7.67e-07	4.86
$128 \times 128 \times 2$	1.69e-10	4.91	1.40e-09	4.96	9.32e-10	4.96	2.38e-08	5.01
$256 \times 256 \times 2$	6.23e-12	4.76	5.69e-11	4.62	3.09e-11	4.91	1.07e-09	4.48

Table 17 Error convergence is shown for the fully-staggered $p_{LG} = 5$, $p_{LGL} = 6$ and the conventional LGL [1,2] $p_{LGL} = 5$ SSDC algorithms for the viscous shock on uniform Cartesian grids.

	Fully-staggered, $p_{LG} = 5$, $p_{LGL} = 6$				Conventional, $p_{LGL} = 5$			
Resolution	L^2 error	L^2 rate	L^∞ error	L^∞ rate	L^2 error	L^2 rate	L^∞ error	L^∞ rate
$2 \times 2 \times 2$	7.63e-03	-	3.14e-02	-	2.81e-02	-	2.16e-01	-
$4 \times 4 \times 2$	6.93e-04	3.46	4.29e-03	2.87	1.69e-03	4.06	7.02e-03	4.94
$8 \times 8 \times 2$	3.73e-05	4.22	2.11e-04	4.35	2.18e-04	2.96	3.29e-03	1.10
$16 \times 16 \times 2$	3.30e-07	6.82	2.74e-06	6.26	1.79e-06	6.92	2.85e-05	6.85
$32 \times 32 \times 2$	7.59e-09	5.44	6.09e-08	5.49	4.39e-08	5.35	1.15e-06	4.63
$64 \times 64 \times 2$	1.29e-10	5.87	1.22e-09	5.64	6.70e-10	6.03	1.80e-08	5.99
$128 \times 128 \times 2$	2.08e-12	5.96	2.40e-11	5.66	1.08e-11	5.96	3.35e-10	5.75

Table 18 Error convergence is shown for the fully-staggered $p_{LG} = 10$, $p_{LGL} = 11$ and the conventional LGL [1,2] $p_{LGL} = 10$ SSDC algorithms for the viscous shock on uniform Cartesian grids.

	Fully-staggered, $p_{LG} = 10$, $p_{LGL} = 11$				Conventional, $p_{LGL} = 10$			
Resolution	L^2 error	L^2 rate	L^∞ error	L^∞ rate	L^2 error	L^2 rate	L^∞ error	L^∞ rate
$2 \times 2 \times 2$	1.69e-03	-	7.22e-03	-	3.05e-03	-	1.46e-02	-
$4 \times 4 \times 2$	5.99e-06	8.14	3.34e-05	7.76	3.70e-05	6.36	5.75e-04	4.67
$8 \times 8 \times 2$	3.95e-08	7.25	2.48e-07	7.07	1.27e-07	8.19	2.29e-06	7.97
$16 \times 16 \times 2$	1.94e-11	10.99	1.48e-10	10.72	6.58e-11	10.91	1.64e-09	10.45
$32 \times 32 \times 2$	4.96e-13	5.29	7.91e-12	4.22	4.77e-13	7.11	1.70e-11	6.58

8.2.2 Unstructured nonuniform grids

A family of nested grids is constructed for the grid convergence study, by replicating N times the "unstructured grid kernel" shown in Figure 6. The viscous shock test case is again used to assess the accuracy of the fully-staggered approach on fully nonuniform grids. Tables 19–24 show the convergence study for a sequence of maximum six nested grids. As was the case in the previous study performed with the inviscid propagation of the Euler vortex, the fully-staggered SSDC approach is more accurate than the conventional SSDC algorithm for the same grid resolution. Furthermore, for the fully-staggered algorithm, the L^2 norm of the error decay asymptotes towards the designed rate (i.e., $(p+1)$) whereas the conventional path converges to order p.

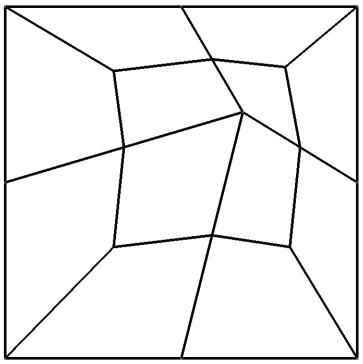

Figure 6. "Unstructured grid kernel" used to construct a sequence of nested grids for the viscous shock test case.

Table 19 Error convergence is shown for the fully-staggered $p_{LG} = 1$, $p_{LGL} = 2$ and the conventional LGL [1, 2] $p_{LGL} = 1$ SSDC algorithms for the viscous shock on highly nonuniform unstructured grids.

	Fully-staggered, $p_{LG} = 1$, $p_{LGL} = 2$				Conventional, $p_{LGL} = 1$			
Resolution	L^2 error	L^2 rate	L^∞ error	L^∞ rate	L^2 error	L^2 rate	L^∞ error	L^∞ rate
$2 \times 2 \times 2$	1.89e-02	-	1.43e-01	-	5.07e-02	-	2.56e-01	-
$4 \times 4 \times 2$	7.85e-03	1.27	6.85e-02	1.06	2.57e-02	0.98	2.05e-01	0.32
$8 \times 8 \times 2$	2.45e-03	1.68	3.08e-02	1.15	1.16e-02	1.15	1.04e-01	0.98
$16 \times 16 \times 2$	6.46e-04	1.92	8.35e-03	1.88	6.18e-03	0.91	7.80e-02	0.42
$32 \times 32 \times 2$	1.58e-04	2.03	2.15e-03	1.96	3.04e-03	1.02	4.12e-02	0.92
$64 \times 64 \times 2$	4.04e-05	1.97	6.39e-04	1.75	1.92e-03	0.67	2.77e-02	0.57

Table 20 Error convergence is shown for the fully-staggered $p_{LG} = 2$, $p_{LGL} = 3$ and the conventional LGL [1, 2] $p_{LGL} = 2$ SSDC algorithms for the viscous shock on highly nonuniform unstructured grids.

	Fully-staggered, $p_{LG} = 2$, $p_{LGL} = 3$				Conventional, $p_{LGL} = 2$			
Resolution	L^2 error	L^2 rate	L^∞ error	L^∞ rate	L^2 error	L^2 rate	L^∞ error	L^∞ rate
$2 \times 2 \times 2$	5.23e-03	-	4.10e-02	-	1.28e-02	-	1.44e-01	-
$4 \times 4 \times 2$	1.03e-03	2.34	1.51e-02	1.44	4.67e-03	1.46	9.41e-02	0.62
$8 \times 8 \times 2$	1.54e-04	2.74	2.67e-03	2.49	1.23e-03	1.92	3.53e-02	1.41
$16 \times 16 \times 2$	2.34e-05	2.72	5.03e-04	2.41	2.02e-04	2.61	5.88e-03	2.59
$32 \times 32 \times 2$	3.74e-06	2.65	8.29e-05	2.60	3.63e-05	2.48	7.34e-04	3.00
$64 \times 64 \times 2$	5.30e-07	2.82	1.25e-05	2.73	8.31e-06	2.13	1.37e-04	2.42

Table 21 Error convergence is shown for the fully-staggered $p_{LG} = 3$, $p_{LGL} = 4$ and the conventional LGL [1, 2] $p_{LGL} = 3$ SSDC algorithms for the viscous shock on highly nonuniform unstructured grids.

	Fully-staggered, $p_{LG} = 3$, $p_{LGL} = 4$				Conventional, $p_{LGL} = 3$			
Resolution	L^2 error	L^2 rate	L^∞ error	L^∞ rate	L^2 error	L^2 rate	L^∞ error	L^∞ rate
$2 \times 2 \times 2$	1.60e-03	-	1.74e-02	-	5.49e-03	-	1.15e-01	-
$4 \times 4 \times 2$	1.79e-04	3.16	2.96e-03	2.56	1.21e-03	2.19	3.80e-02	1.60
$8 \times 8 \times 2$	1.15e-05	3.96	1.42e-04	4.39	7.51e-05	4.01	2.03e-03	4.23
$16 \times 16 \times 2$	8.67e-07	3.73	1.38e-05	3.36	6.23e-06	3.59	3.13e-04	2.69
$32 \times 32 \times 2$	6.45e-08	3.75	1.25e-06	3.47	6.13e-07	3.34	2.90e-05	3.44
$64 \times 64 \times 2$	4.65e-09	3.79	1.01e-07	3.63	7.13e-08	3.11	2.71e-06	3.42

Table 22 Error convergence is shown for the fully-staggered $p_{LG} = 4$, $p_{LGL} = 5$ and the conventional LGL [1, 2] $p_{LGL} = 4$ SSDC algorithms for the viscous shock on highly nonuniform unstructured grids.

	Fully-staggered, $p_{LG} = 4$, $p_{LGL} = 5$				Conventional, $p_{LGL} = 4$			
Resolution	L^2 error	L^2 rate	L^∞ error	L^∞ rate	L^2 error	L^2 rate	L^∞ error	L^∞ rate
$2 \times 2 \times 2$	3.46e-04	-	3.82e-03	-	2.35e-03	-	6.95e-02	-
$4 \times 4 \times 2$	4.68e-05	2.88	7.66e-04	2.32	1.52e-04	3.95	4.63e-03	3.91
$8 \times 8 \times 2$	1.76e-06	4.73	3.83e-05	4.32	1.22e-05	3.63	6.35e-04	2.87
$16 \times 16 \times 2$	6.61e-08	4.74	1.97e-06	4.28	3.89e-07	4.98	1.34e-05	5.57
$32 \times 32 \times 2$	2.22e-09	4.90	7.09e-08	4.79	1.53e-08	4.66	6.96e-07	4.26
$64 \times 64 \times 2$	7.45e-11	4.80	3.23e-09	4.46	7.95e-10	4.27	4.03e-08	4.11

Table 23 Error convergence is shown for the fully-staggered $p_{LG} = 5$, $p_{LGL} = 6$ and the conventional LGL [1, 2] $p_{LGL} = 5$ SSDC algorithms for the viscous shock on highly nonuniform unstructured grids.

	Fully-staggered, $p_{LG} = 5$, $p_{LGL} = 6$				Conventional, $p_{LGL} = 5$			
Resolution	L^2 error	L^2 rate	L^∞ error	L^∞ rate	L^2 error	L^2 rate	L^∞ error	L^∞ rate
$2 \times 2 \times 2$	2.28e-04	-	3.77e-03	-	6.79e-04	-	9.36e-03	-
$4 \times 4 \times 2$	8.23e-06	4.79	2.03e-04	4.22	5.46e-05	3.64	3.18e-03	1.56
$8 \times 8 \times 2$	2.25e-07	5.19	1.05e-05	4.26	5.13e-07	6.73	2.74e-05	6.86
$16 \times 16 \times 2$	4.02e-09	5.81	2.32e-07	5.51	1.67e-08	4.94	1.17e-06	4.55
$32 \times 32 \times 2$	6.37e-11	5.98	5.05e-09	5.52	3.52e-10	5.57	3.10e-08	5.24

Table 24 Error convergence is shown for the fully-staggered $p_{LG} = 10$, $p_{LGL} = 11$ and the conventional LGL [1, 2] $p_{LGL} = 10$ SSDC algorithms for the viscous shock on highly nonuniform unstructured grids.

	Fully-staggered, $p_{LG} = 10$, $p_{LGL} = 11$				Conventional, $p_{LGL} = 10$			
Resolution	L^2 error	L^2 rate	L^∞ error	L^∞ rate	L^2 error	L^2 rate	L^∞ error	L^∞ rate
$2 \times 2 \times 2$	1.43e-06	-	2.92e-05	-	8.30e-06	-	5.38e-04	-
$4 \times 4 \times 2$	9.84e-09	7.18	2.71e-07	6.75	3.70e-08	7.81	2.70e-06	7.64
$8 \times 8 \times 2$	7.05e-12	10.45	4.24e-10	9.32	2.40e-11	10.59	2.89e-09	9.87

8.3 Taylor-Green vortex

The goal of this section is to demonstrate that nonlinearly stable schemes do not require stabilization techniques (e.g., de-aliasing, filtering, limiting, over-integration procedures) for successful computations of under-resolved turbulent flows.

The Taylor-Green vortex test case is used as a benchmark model problem, and is solved on the periodic cube $[-\pi L \leq x, y, z \leq +\pi L]$. The initial condition is given by the following analytical expressions

$$\begin{aligned} u_1 &= V_0 \sin\left(\frac{x_1}{L}\right) \cos\left(\frac{x_2}{L}\right) \cos\left(\frac{x_3}{L}\right), \\ u_2 &= -V_0 \cos\left(\frac{x_1}{L}\right) \sin\left(\frac{x_2}{L}\right) \cos\left(\frac{x_3}{L}\right), \\ u_3 &= 0, \\ p &= p_0 + \frac{\rho_0 V_0^2}{16} \left[\cos\left(\frac{2x_1}{L}\right) + \cos\left(\frac{2x_2}{L}\right)\right] \left[\cos\left(\frac{2x_3}{L}\right) + 2\right], \end{aligned} \tag{78}$$

where u_1, u_2, u_3 are the components of the velocity in the x_1-, x_2-, and x_3-directions, p is the pressure, and ρ is the density. The flow is initialized to be isothermal, i.e., $p/\rho = p_0/\rho_0 = RT_0$. The Reynolds number for this flow is defined as $Re = (\rho_0 V_0 L)/\mu$, where μ is the dynamic viscosity. Starting from the initial condition, the nonlinear interactions of different flow scales yield vortex breakdowns. This nonlinear process is initially anisotropic and laminar; but subsequently, it develops into fully anisotropic turbulence that decays with the typical spectral energy distribution.

Because our framework solves the compressible Navier-Stokes equations, we choose a Mach number of $M = 0.08$, which leads to a flow field that is essentially incompressible. This allows for a fair comparison with some of the incompressible simulations reported in literature. Herein, two Reynolds numbers are considered: $Re = 800$ and $Re = 1,600$. The Prandtl number is set to $Pr = 0.71$.

8.3.1 $Re = 800$

In this section, we report the results for $Re = 800$ on a uniform Cartesian grid with four hexahedrons in each coordinate direction. Therefore, the total number of elements in the grid is also $N^e = 4^3 = 64$. We compute the numerical solution with the sixteenth- ($p_G = 15$, $p_{LGL} = 16$), and seventeenth-order ($p_G = 16$, $p_{LGL} = 17$) accurate fully-staggered algorithms. The numerical solutions presented herein are compared with the direct numerical simulation (DNS) of Brachet et al. [34]. Figure 7 shows the kinetic energy dissipation rate of our computations and the reference data. The computation with a formally seventeenth-order accurate scheme compares very well with the DNS results, even on this very coarse grid.

8.3.2 $Re = 1,600$

The simulation is run using a fully unstructured grid that contains 42 hexahedrons. The distribution of the element in the 2D plane is shown in Figure 8.

Figure 9 shows the kinetic energy dissipation rate of our computations and the reference data of Carton de Wiart et al. [35]. The grid is too coarse to accurately resolve the flow field, however, the computation with a formally seventeenth-order accurate scheme is stable through all the simulation.

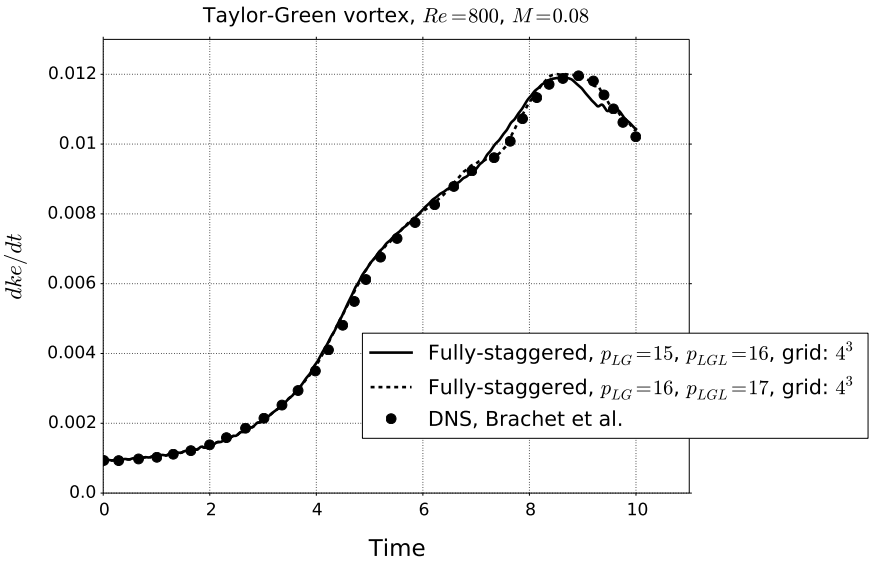

Figure 7. Evolution of the time derivative of the kinetic energy for the Taylor-Green vortex at $Re = 800$, $M = 0.08$; fully-staggered SSDC algorithm.

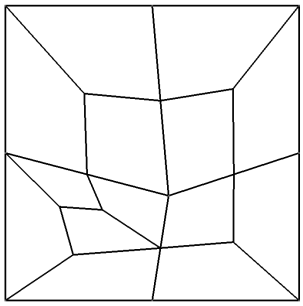

Figure 8. Plane distribution of the elements used for the Taylor-Green vortex at $Re = 1,600$, $M = 0.08$.

This is a feat unattainable with alternative approaches based on high-order accurate linear stable schemes.

8.4 Computation of a square cylinder in a supersonic free stream

The development of a high-order accurate entropy stable discretization aims to provide the next generation of robust high-fidelity numerical solvers for complex fluid flow simulations, for which standard suboptimal algorithms suffer greatly or fail completely. By computing the flow past a 3D square cylinder at $Re_\infty = 10^4$ and $M_\infty = 1.5$, we provide numerical evidence of such robustness for the complete entropy stable high-order spatial discretization. This supersonic flow is characterized by a very large range of length scales, strong shocks, and expansion regions that interact with each other, leading to complex flow patterns. During the past three decades, this fluid flow problem has been thoroughly investigated by several researchers for aerodynamic applications (see for instance,

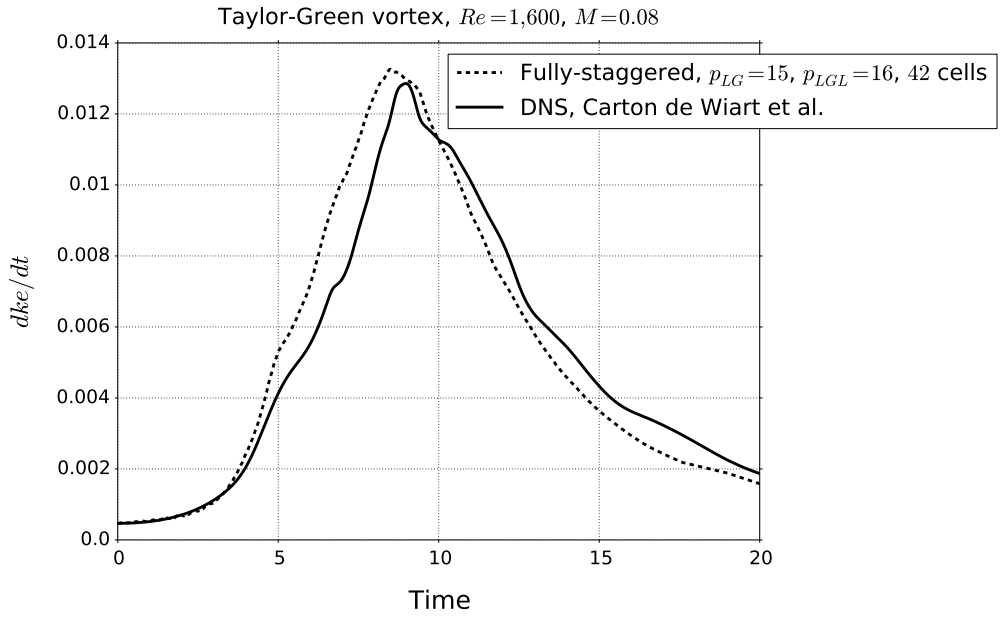

Figure 9. Evolution of the time derivative of the kinetic energy for the Taylor-Green vortex at $Re = 1,600$, $M = 0.08$; fully-staggered SSDC algorithm.

references 36, 37).

The domain of interest spans one square cylinder edge in the x_3 direction, and at the two planes perpendicular to this coordinate direction, periodic boundary conditions are used. The flow is computed using an unstructured grid with 43,936 hexahedrons. A fourth-order accurate ($p_{LG} = 3$, $p_{LGL} = 4$) fully staggered entropy stable discretization without any stabilization technique is used. The body surface is considered adiabatic and the wall boundary conditions are imposed using the entropy stable approach presented in reference 2. The solution is initialized using a uniform flow at $M_\infty = 1.5$ with zero angle of attack. This test case was also used in reference 2 to assess the robustness of the conventional SSDC algorithm.

A strong shock is formed in front of the bluff body in the beginning of the simulation. Subsequently, the discontinuity moves upstream until it reaches a "stationary" position that is about 2.15 square cylinder edges from the frontal surface of the body. During this phase, additional weaker shocks, which originate from the four sharp corners of the body, interact with the subsonic regions formed near the walls. This complicated flow pattern, yields the formation of shocklets in the wake of the square cylinder.

A global view of the "high order grid," the Mach number, density, temperature and entropy contours at $t = 100$ are shown in Figure 10. The shock has already reached a stationary position at $t = 100$, and the flow past the square cylinder is completely unsteady, characterized by subsonic and supersonic regions. The formation of shocklets in the near wake region are clearly visible.

An extensive parametric study of Mach numbers ($1.1 < M < 1.8$) and grids ($10K - 40K$ elements) was performed using the supersonic square cylinder. All high Mach number simulations performed to date suggest that the staggered and conventional approaches have comparable robustness. The failure mode for both approaches is a negative density that develops in the vicinity

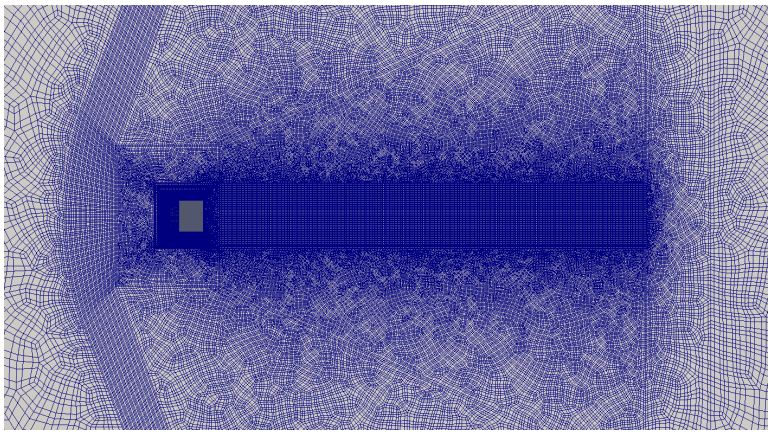

(a) High order grid.

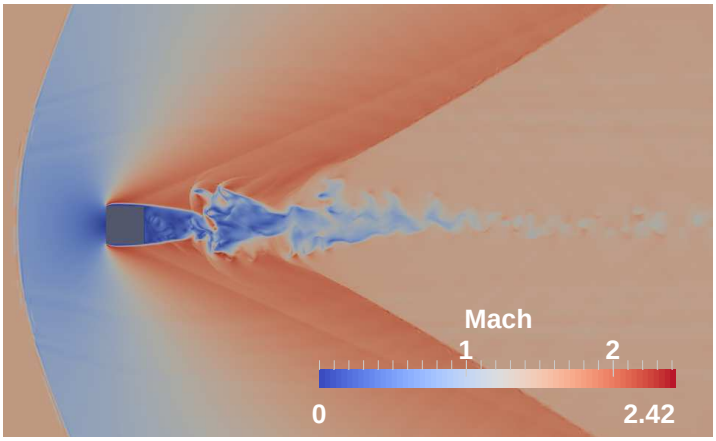

(b) Mach number; $\Delta M = 0.0095$.

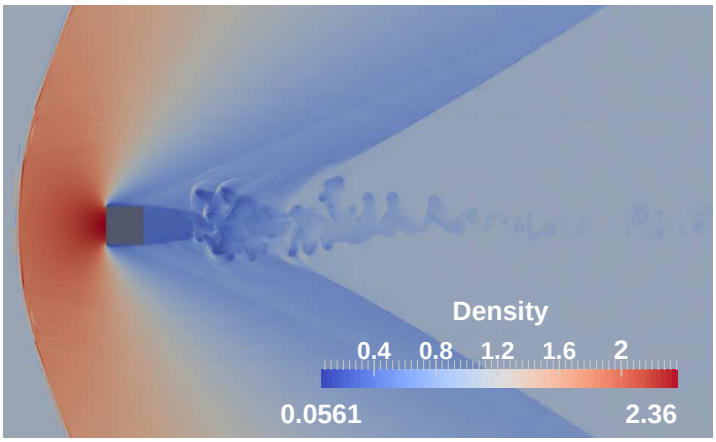

(c) Density; $\Delta\rho = 0.0090$.

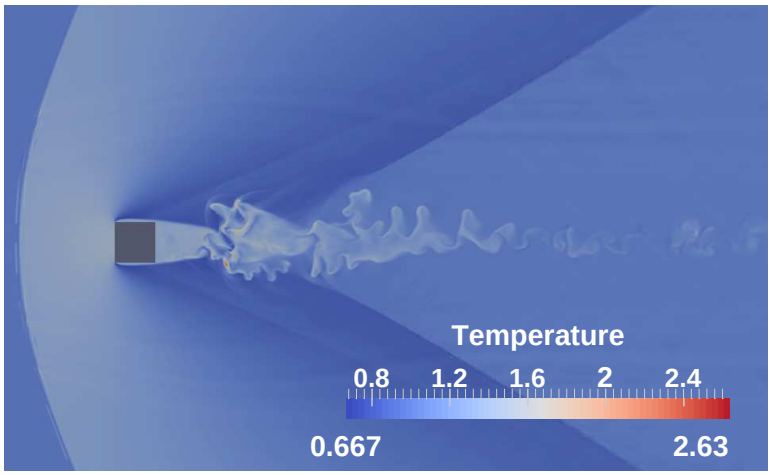

(d) Temperature; $\Delta T = 0.0077$.

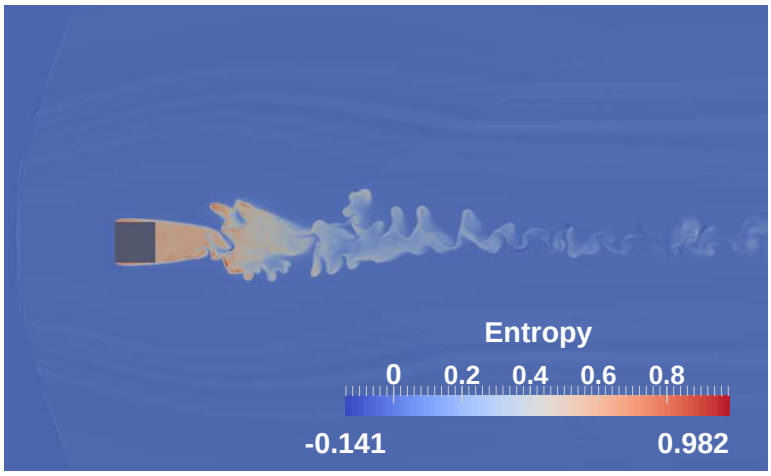

(e) Entropy; $\Delta s = 0.0044$.

Figure 10. Unsteady flow past a 3D square cylinder at $Re_\infty = 10^4$ and $M_\infty = 1.5$; fourth-order accurate fully-staggered SSDC method ($p_{LG} = 3$, $p_{LGL} = 4$) without stabilization technique; $t = 100$.

of a strong shock.

9 Conclusions

A summation-by-parts, simultaneous-approximation-term (SBP-SAT) framework is used to develop a generalized entropy stable spectral element formulation that includes a broader selection of collocation points. A necessary condition for an entropy-stable, staggered operator is a restriction/prolongation interpolation pair that satisfies a precise Galerkin constraint (see equation (16)). This constraint is automatically satisfied when interpolating between the LG and LGL points, provided the polynomial order of the LGL points exceeds that of the LG points (as well as other less desirable combinations). Thus, the primary goals herein are to 1) extend the entropy stable mechanics to a staggered configuration that collocates the solution variables at the Legendre-Gauss (LG) points and the fluxes at the Legendre-Gauss-Lobatto (LGL) points, and 2) to establish the competitive advantages (if any) of the new entropy stable staggered algorithm relative to the algorithms presented in references 1, 2.

Conventional energy analysis as well as entropy analysis are used on the 1D viscous Burgers' equation, to prove the nonlinearly stability of the staggered operators for arbitrary order, diagonal-norm SBP operators. The comparison of the energy and entropy estimates on Burgers' equation provides insight on how to proceed with the entropy stability analysis of the compressible Navier-Stokes equations for staggered operators. Next, the entropy analysis techniques presented in references 1, 2 are used to develop an entropy conservative, staggered grid, spectral collocation operator for the 3D compressible Navier-Stokes equation. Entropy conservative/stable inviscid interface operators are then developed for the staggered formulation. The viscous interface coupling is based on an LDG/IP approach analogous to the coupling operators presented in references 1,2. The resulting spectral collocation operators are design order accurate for arbitrary order, conservative on the LGL points, and satisfy the additional secondary constraint of entropy stability. Extension to curvilinear meshes [22, 23] and entropy stable solid wall BCs [13, 31] follow immediately.

Extensive numerical tests for the 3D Euler and compressible Navier-Stokes equations reveal that the new staggered grid entropy stable algorithms are significantly more accurate than the collocated Legendre-Gauss-Lobatto operators of equivalent polynomial order, that are presented in references 1, 2. They are however, more costly to implement. The cost of a flux evaluation for the staggered algorithm of solution polynomial order p is comparable to that of an Legendre-Gauss-Lobatto points operator [1, 2] of solution polynomial order $(p + 1)$. Preliminary studies using an explicit temporal integrator indicate that the increased accuracy of the staggered approach nearly offsets the additional cost. Further investigation is required to fully establish the cost efficacy of over-collocated fluxes (including the spectral difference and the flux reconstruction operators), relative to conventional collocated fluxes. An ongoing investigation continues that includes 1) the effects of implicit temporal integrators and 2) data movement on current and next generation hardware; computationally intensive yet extremely accurate, low memory footprint algorithms could be competitive in the future.

This work provides an essential step towards an operational entropy stable framework of arbitrary order. An obvious extension of this work is the development of entropy stable, h- and/or p-refinement operators. Both scenarios require data interpolation from adjoining interfaces onto a common intermediate mortar, with quadrature points that do not in general coincide. A long term goal includes entropy stable operators for other element types including triangles, prisms and tetrahedra.

References

1. Carpenter, M. H.; Fisher, T. C.; Nielsen, E. J.; and Frankel, S. H.: Entropy stable spectral collocation schemes for the Navier–Stokes equations: Discontinuous interfaces. *SIAM Journal on Scientific Computing*, vol. 36, no. 5, 2014, pp. B835–B867.

2. Parsani, M.; Carpenter, M. H.; and Nielsen, E. J.: Entropy stable wall boundary conditions for the three-dimensional compressible Navier–Stokes equations. *Journal of Computational Physics*, vol. 292, 2015, pp. 88–113.

3. Atkins, H. L.; and Shu, C.-W.: Quadrature-free implementation of discontinuous Galerkin method for hyperbolic equations. *AIAA Journal*, vol. 36, no. 5, 1998, pp. 775–782.

4. Gassner, G. J.: A kinetic energy preserving nodal discontinuous Galerkin spectral element method. *International Journal for Numerical Methods in Fluids*, vol. 76, no. 1, 2014, pp. 28–50.

5. Kopriva, D. A.; and Gassner, G. J.: On the quadrature and weak form choices in collocation type discontinuous Galerkin spectral element methods. *Journal of Scientific Computing*, vol. 44, no. 2, 2010, pp. 136–155.

6. Bernardi, C.; and Maday, Y.: A collocation method over staggered grids for the Stokes problem. *International Journal for Numerical Methods in Fluids*, vol. 8, no. 5, 1988, pp. 537–557.

7. Kopriva, D. A.; and Kolias, J. H.: A conservative staggered-grid Chebyshev multidomain method for compressible flows. *Journal of Computational Physics*, vol. 125, no. 1, 1996, pp. 244–261.

8. Cai, W.; Gottlieb, D.; and Harten, A.: Cell averaging Chebyshev methods for hyperbolic problems. *Computers and Mathematics with Applications*, vol. 24, no. 5-6, 1992, pp. 37–49.

9. Liu, Y.; Vinokur, M.; and Wang, Z. J.: Spectral difference method for unstructured grids I: Basic formulation. *Journal of Computational Physics*, vol. 216, no. 2, 2006, pp. 780–801.

10. May, G.; and Jameson, A.: A spectral difference method for the Euler and Navier–Stokes equations on unstructured meshes. *44th AIAA Aerospace Sciences Meeting and Exhibit*, AIAA 2006-304, 2006.

11. Huynh, H. T.: A flux reconstruction approach to high-order schemes including discontinuous Galerkin methods. *18th AIAA Computational Fluid Dynamics Conference*, AIAA 2007-4079, 2007.

12. Vincent, P. E.; Castonguay, P.; and Jameson, A.: A new class of high-order energy stable flux reconstruction schemes. *Journal of Scientific Computing*, vol. 47, no. 1, 2011, pp. 50–72.

13. Parsani, M.; Carpenter, M. H.; and Nielsen, E. J.: Entropy stable discontinuous interfaces coupling for the three-dimensional compressible Navier–Stokes equations. *Journal of Computational Physics*, vol. 290, 2015, pp. 132–138.

14. Hesthaven, J. S.; and Warburton, T.: *Nodal discontinuous Galerkin methods: Algorithms, analysis, and applications*. Texts in Applied Mathematics, Springer, 2008.

15. Svärd, M.; and Özcan, H.: Entropy-stable schemes for the Euler equations with far-field and wall boundary conditions. *Journal of Scientific Computing*, vol. 58, no. 1, 2014, pp. 61–89.

16. Lax, P.; and Wendroff, B.: Systems of conservation laws. *Communications on Pure and Applied Mathematics*, vol. 13, no. 2, 1960, pp. 217–237.

17. Bernardi, C.; Maday, Y.; and Patera, A. T.: *A new nonconforming approach to domain decomposition: The mortar element method*, Collège de France Seminar, Vol. XI (Paris, 1989–1991), Pitman Research Notes in Mathematics Series, Longman Scientific and Technical, Harlow, vol. 299. 1994, pp. 13–51.

18. Lax, P. D.: *Hyperbolic systems of conservation laws and the mathematical theory of shock waves*. SIAM, Philadelphia, 1973.

19. Fisher, T. C.; and Carpenter, M. H.: High-order entropy stable finite difference schemes for nonlinear conservation laws: Finite domains. *Journal of Computational Physics*, vol. 252, 2013, pp. 518–557.

20. Svärd, M.; and Mishra, S.: Entropy stable schemes for initial-boundary-value conservation laws. *Zeitschrift für Angewandte Mathematik und Physik*, vol. 63, no. 6, 2012, pp. 985–1003.

21. Carpenter, M. H.; and Gottlieb, D.: Spectral methods on arbitrary grids. *Journal of Computational Physics*, vol. 129, 1996, pp. 74–86.

22. Fisher, T. C.: High-order L^2 stable multi-domain finite difference method for compressible flows. Ph.D. Thesis, Purdue University, 2012.

23. Fisher, T. C.; Carpenter, M. H.; Nordström, J.; Yamaleev, N. K.; and Swanson, R. C.: Discretely conservative finite-difference formulations for nonlinear conservation laws in split form: Theory and boundary conditions. *Journal of Computational Physics*, vol. 234, 2013, pp. 353–375.

24. Dafermos, C. M.: *Hyperbolic conservation laws in continuum physics*. Springer-Verlag, Berlin, 2010.

25. Tadmor, E.: Entropy stability theory for difference approximations of nonlinear conservation laws and related time-dependent problems. *Acta Numerica*, vol. 12, 2003, pp. 451–512.

26. Godunov, S. K.: An interesting class of quasilinear systems. *Doklady Akademii Nauk SSSR*, vol. 139, no. 3, 1961, pp. 521–523. English translation: Soviet Math. 2, pp. 947–949 (1961).

27. Mock, M. S.: Systems of Conservation Laws of Mixed Type. *Journal of Differential Equations*, vol. 37, no. 1, 1980, pp. 70–88.

28. Harten, A.: On the symmetric form of systems of conservation laws with entropy. *Journal of Computational Physics*, vol. 49, 1983, pp. 151–164.

29. Ismail, F.; and Roe, P. L.: Affordable, entropy-consistent Euler flux functions II: Entropy production at shocks. *Journal of Computational Physics*, vol. 228, 2009, pp. 5410–5436.

30. Carpenter, M. H.; and Fisher, T. C.: Entropy stable spectral collocation schemes for the Navier-Stokes equations: Discontinuous interfaces. NASA TM 218039, 2013.

31. Parsani, M.; Carpenter, M. H.; and Nielsen, E. J.: Entropy stable wall boundary conditions for the compressible Navier–Stokes equations. NASA TM 218282, 2014.

32. Merriam, M. L.: An entropy-based approach to nonlinear stability. NASA TM 101086, 1989.

33. Carpenter, M. H.; Gottlieb, D.; and Abarbanel, S.: Time-stable boundary conditions for finite-difference schemes solving hyperbolic systems: Methodology and application to high-order compact schemes. *Journal of Computational Physics*, vol. 111, 1994, pp. 220–236.

34. Brachet, M. E.; Meiron, D.; Orszag, S.; Nickel, B.; Morf, R.; and Frisch, U.: The Taylor–Green vortex and fully developed turbulence. *Journal of Statistical Physics*, vol. 34, no. 5-6, 1984, pp. 1049–1063.

35. de Wiart, C.; Hillewaert, K.; Duponcheel, M.; and Winckelmans, G.: Assessment of a discontinuous Galerkin method for the simulation of vortical flows at high Reynolds number. *International Journal for Numerical Methods in Fluids*, vol. 74, no. 7, 2014, pp. 469–493.

36. Nakagawa, T.: Vortex shedding behind a square cylinder in transonic flows. *Journal of Fluid Mechanics*, vol. 178, 1987, pp. 303–323.

37. Birch, T.; Prince, S. A.; and Simpson, G. M.: An experimental and computational study of the aerodynamics of a square cross-section body at supersonic speeds. RTO-MP-069(I), DERA, 2003.

38. Fisher, T. C.; Carpenter, M. H.; Nordström, J.; Yamaleev, N. K.; and Swanson, R. C.: Discretely conservative finite-difference formulations for nonlinear conservation laws in split form: Theory and boundary conditions. NASA TM 2011-217307, 2011.

39. Kopriva, D. A.: *Implementing spectral methods for partial differential equations*. Springer, New York, 2009.

40. Golub, G. H.; and Loan, C. F. V.: *Matrix Computations*. Johns Hopkins Studies in the Mathematical Sciences, The Johns Hopkins University Press, 1996.

Appendix A

Summation-by-parts

A.1 Complementary grids

Define on the interval $-1 \leq x \leq 1$, the vector of discrete points

$$\mathbf{x} \;=\; (x_1, x_1, \ldots, x_{N-1}, x_N)^\top, \quad -1 \;\leq\; x_1, x_2, \ldots, x_{N-1}, x_N \;\leq 1. \tag{A1}$$

Because the approximate solution is constructed at these points, they are referred to as *solution points*. Furthermore, define a set of intermediate points prescribing bounding control volumes about each solution point. These $(N+1)$ points are referred to as *flux points* as they are similar in nature to the control volume edges employed in the finite-volume method. The distribution of the flux points depends on the discretization operator. The spacing between the flux points is implicitly contained in the SBP operator $\mathcal{P}$. In fact, the diagonal elements of $\mathcal{P}$ are equal to the spacing between flux points (see figure 1),

$$\begin{aligned} \overline{\mathbf{x}} = (\overline{x}_0, \overline{x}_1, \ldots \overline{x}_N)^\top, \quad \overline{x}_0 = x_1, \quad \overline{x}_N = x_N, \\ \overline{x}_i - \overline{x}_{i-1} = \mathcal{P}_{(i)(i)}, \quad i = 1, 2, \ldots, N. \end{aligned} \tag{A2}$$

In operator notation, this is equivalent to

$$\Delta\overline{\mathbf{x}} = \mathcal{P}\mathbf{1}, \quad \mathbf{1} = (1, 1, \ldots, 1)^\top, \tag{A3}$$

and Δ is as defined in equation (A6). Note that in equation (A2), the solution and flux points coincide at the left and right extremes of the domain. Thus

$$\overline{f}_0 = f(q_1), \quad \overline{f}_N = f(q_N). \tag{A4}$$

This duality is needed to define unique operators and is important in proving entropy stability.

A.2 Telescopic flux form

All SBP derivative operators $\mathcal{D}$ can be manipulated into the telescopic flux form,

$$\frac{\partial \mathbf{f}}{\partial x}(\mathbf{q}) = \mathcal{P}^{-1}\mathcal{Q}\mathbf{f} + \mathcal{T}_{p+1} \;=\; \mathcal{P}^{-1}\Delta\overline{\mathbf{f}} + \mathcal{T}_{p+1}, \tag{A5}$$

where the $N \times (N+1)$ matrix Δ is defined as

$$\Delta = \begin{pmatrix} -1 & 1 & 0 & 0 & 0 & 0 \\ 0 & -1 & 1 & 0 & 0 & 0 \\ 0 & 0 & \ddots & \ddots & 0 & 0 \\ 0 & 0 & 0 & -1 & 1 & 0 \\ 0 & 0 & 0 & 0 & -1 & 1 \end{pmatrix}. \tag{A6}$$

The Δ operator calculates the undivided difference of the two adjacent fluxes. The existence of a telescopic form for all SBP operators is reiterated in the following lemma, presented without proof. (The original proof appears elsewhere [38].)

Lemma A.1. *All differentiation matrices that satisfy the SBP convention given in equation* (2) *are telescoping operators in the $\mathcal{P}$-norm and can be expressed as in equation* (A5)*.*

This telescopic flux form admits a generalized SBP property. All SBP operators defined in equation (2) can be manipulated to transfer the action of the discrete derivative onto a test function with an equivalent order of approximation. The telescopic flux form defined in equation (A5) combined with the flux consistency condition (A4) results in a more generalized relation,

$$\boldsymbol{\phi}^\top \mathcal{P}\mathcal{P}^{-1}\Delta\overline{\mathbf{f}} = \boldsymbol{\phi}^\top(\widetilde{\mathcal{B}} - \widetilde{\Delta})\overline{\mathbf{f}} = f(q_N)\phi_N - f(q_1)\phi_1 - \boldsymbol{\phi}\widetilde{\Delta}\overline{\mathbf{f}}, \tag{A7}$$

where

$$\widetilde{\Delta} = \begin{pmatrix} 0 & -1 & 0 & 0 & 0 & 0 \\ 0 & 1 & -1 & 0 & 0 & 0 \\ 0 & 0 & \ddots & \ddots & 0 & 0 \\ 0 & 0 & 0 & 1 & -1 & 0 \\ 0 & 0 & 0 & 0 & 1 & 0 \end{pmatrix}, \quad \widetilde{\mathcal{B}} = \begin{pmatrix} -1 & 0 & 0 & 0 & 0 & 0 \\ 0 & 0 & 0 & 0 & 0 & 0 \\ 0 & 0 & \ddots & \ddots & 0 & 0 \\ 0 & 0 & 0 & 0 & 0 & 0 \\ 0 & 0 & 0 & 0 & 0 & 1 \end{pmatrix},$$

and

$$\frac{1}{\delta x}\boldsymbol{\phi}^\top\widetilde{\Delta} = \left(\frac{d\boldsymbol{\phi}}{dx}\right)^\top + \mathcal{O}(N^{-1}),$$

with δx the local grid spacing. This is equivalent to the commonly used explanation of SBP in indicial form,

$$\sum_{i=1}^{N}\phi_i\left(\overline{f}_i - \overline{f}_{i-1}\right) = f(q_N)\phi_N - f(q_1)\phi_1 - \sum_{i=1}^{N-1}\overline{f}_i\left(\phi_{i+1} - \phi_i\right). \tag{A8}$$

The action of the derivative is still moved onto the test function but at first order accuracy. Note that although this generalized property is used herein to construct entropy conservative fluxes, it is also instrumental for satisfying the Lax-Wendroff theorem [18] in weak form.

A.3 α-split fluxes

Conservative or chain-rule fluxes constructed on the solution points $\mathbf{x}$ by using the SBP derivative operators, have a discretely equivalent representation on the flux points $\overline{\mathbf{x}}$ [23] (see Figure 1). Consider the general flux of the form $f(u) = V(u)W(u)$. Next, α-split the flux into a combination of conservative and chain-rule form and discretize with any diagonal norm SBP operator. The resulting α-split discrete operator has an equivalent telescoping flux representation of the form [23, 38]

$$\alpha\mathcal{P}^{-1}\mathcal{Q}\mathcal{V}\mathbf{w} + (1-\alpha)\left(\mathcal{V}\mathcal{P}^{-1}\mathcal{Q}\mathbf{w} + \mathcal{W}\mathcal{P}^{-1}\mathcal{Q}\mathbf{v}\right) \;=\; \mathcal{P}^{-1}\Delta\overline{\mathbf{f}}. \tag{A9}$$

(Again, $\mathcal{V}$ and $\mathcal{W}$ are diagonal matrices with the $\mathbf{v}$ and $\mathbf{w}$ vectors injected onto the matrix diagonals.) The telescoping flux is constructed point-wise by using the expression

$$\begin{gathered}\overline{f}_i \;=\; 2\sum_{k=i+1}^{N}\sum_{l=1}^{i} q_{\ell k}\left[\alpha\frac{v(u_\ell)w(u_\ell) + v(u_k)w(u_k)}{2} \;+\; (1-\alpha)\frac{v(u_\ell)w(u_k) + v(u_k)w(u_\ell)}{2}\right], \\ 1 \le i \le N-1, \qquad \overline{f}_0 = v(u_1)w(u_1), \quad \overline{f}_N = v(u_N)w(u_N),\end{gathered} \tag{A10}$$

where the coefficient $q_{\ell k}$ corresponds to the (ℓ, k) row and column in $\mathcal{Q}$, respectively.

Appendix B

Polynomial methods

B.1 Definitions

Define on the interval $-1 \leq x \leq 1$, the vectors of discrete point values,

$$\begin{aligned} \widetilde{\mathbf{x}} &= [\widetilde{x}_1, \widetilde{x}_2, \ldots, \widetilde{x}_{M-1}, \widetilde{x}_M]^\top, \quad -1 \leq \widetilde{x}_1, \widetilde{x}_2, \ldots, \widetilde{x}_{M-1}, \widetilde{x}_M \leq 1, \\ \mathbf{x} &= [x_1, x_2, \ldots, x_{N-1}, x_N]^\top, \quad -1 \leq x_1, x_2, \ldots, x_{N-1}, x_N \leq 1. \end{aligned} \tag{B1}$$

Herein, the discrete points $\widetilde{\mathbf{x}}$ and $\mathbf{x}$ are chosen to be the Legendre-Gauss (LG) points and the Legendre-Gauss-Lobatto (LGL) points, respectively.

Next, define the interpolation operators that move data between $\widetilde{\mathbf{x}}$ and $\mathbf{x}$. Assume that an infinitely smooth function $f(x)$ is defined on the interval $-1 \leq x \leq 1$. Reading the function f and derivative $\partial f/\partial x$ at the discrete points $\widetilde{\mathbf{x}}$ and $\mathbf{x}$, we define the vectors

$$\begin{aligned} \mathbf{f}(\widetilde{\mathbf{x}}) &= [f(\widetilde{x}_0), f(\widetilde{x}_1), \ldots, f(\widetilde{x}_{M-1}), f(\widetilde{x}_M)]^\top, \\ \mathbf{f}(\mathbf{x}) &= [f(x_0), f(x_1), \ldots, f(x_{N-1}), f(x_N)]^\top, \\ \frac{d\mathbf{f}}{dx}(\widetilde{\mathbf{x}}) &= \left[\frac{df}{dx}(\widetilde{x}_0), \frac{df}{dx}(\widetilde{x}_1), \ldots, \frac{df}{dx}(\widetilde{x}_{M-1}), \frac{df}{dx}(\widetilde{x}_M)\right]^\top, \\ \frac{d\mathbf{f}}{dx}(\mathbf{x}) &= \left[\frac{df}{dx}(x_0), \frac{df}{dx}(x_1), \ldots, \frac{df}{dx}(x_{N-1}), \frac{df}{dx}(x_N)\right]^\top. \end{aligned} \tag{B2}$$

Define the Lagrange basis polynomials relative to the discrete points, $\widetilde{\mathbf{x}}$, as

$$L_j(x) = \prod_{\substack{k=1 \\ k \neq j}}^{M} \frac{x - \widetilde{x}_k}{\widetilde{x}_j - \widetilde{x}_k}, \qquad 1 \leq j \leq M, \tag{B3}$$

with a similar definition for the discrete points $\mathbf{x}$

$$L_j(x) = \prod_{\substack{k=1 \\ k \neq j}}^{N} \frac{x - x_k}{x_j - x_k}, \qquad 1 \leq j \leq N. \tag{B4}$$

With a slight abuse of notation, define the vector of Lagrange basis polynomials relative to the vectors $\widetilde{\mathbf{x}}$ and $\mathbf{x}$ as

$$\begin{aligned} \mathbf{L}(x; \widetilde{\mathbf{x}}) &= (\mathbf{L}_0(x; \widetilde{\mathbf{x}}), \mathbf{L}_1(x; \widetilde{\mathbf{x}}), \ldots, \mathbf{L}_{M-1}(x; \widetilde{\mathbf{x}}), \mathbf{L}_M(x; \widetilde{\mathbf{x}}))^\top, \\ \mathbf{L}(x; \mathbf{x}) &= (\mathbf{L}_0(x; \mathbf{x}), \mathbf{L}_1(x; \mathbf{x}), \ldots, \mathbf{L}_{N-1}(x; \mathbf{x}), \mathbf{L}_N(x; \mathbf{x}))^\top. \end{aligned} \tag{B5}$$

This notation makes explicit reference to the set of collocation points from which the basis polynomials are derived. Finally, the vector of Lagrange basis polynomials can be evaluated at any set of points, thus creating a second-order tensor (matrix). For example, evaluating $\mathbf{L}(x; \widetilde{\mathbf{x}})$ at the points $\mathbf{x}$ would yield

$$\mathbf{L}(\mathbf{x}; \widetilde{\mathbf{x}}) = (\mathbf{L}_0(\mathbf{x}; \widetilde{\mathbf{x}}), \mathbf{L}_1(\mathbf{x}; \widetilde{\mathbf{x}}), \ldots, \mathbf{L}_{M-1}(\mathbf{x}; \widetilde{\mathbf{x}}), \mathbf{L}_M(\mathbf{x}; \widetilde{\mathbf{x}}))^\top, \tag{B6}$$

where each element of the M vector being an N vector, e.g.,

$$\mathbf{L}_j(\mathbf{x};\widetilde{\mathbf{x}}) \;=\; (L_j(x_0;\widetilde{\mathbf{x}}), L_j(x_1;\widetilde{\mathbf{x}}), \cdots, L_j(x_{N-1};\widetilde{\mathbf{x}}), L_j(x_N;\widetilde{\mathbf{x}}))^\top. \tag{B7}$$

Note that $\mathbf{L}(\widetilde{\mathbf{x}};\widetilde{\mathbf{x}}) = \delta_{ij}$, where δ_{ij} represents the Kronecker's delta.

B.2 Differentiation

The interpolation polynomial $f_N(x)$ (of order $p = N-1$) that collocates $f(x)$ at the points $\widetilde{\mathbf{x}}$ is given by

$$f(x) \approx f_N(x) = \mathbf{L}(x;\widetilde{\mathbf{x}})^\top \mathbf{f}(\widetilde{\mathbf{x}}). \tag{B8}$$

The objective is to construct collocation derivative operators in terms of the Lagrange basis polynomials on the interval.

Theorem B.1. *The derivative operator that exactly differentiates an arbitrary p-th order polynomial ($p = N-1$) at the collocation points $\widetilde{\mathbf{x}}$ is*

$$\mathcal{D} = (d_{ij}) = \left(\frac{dL_j}{dx}(y_i;\widetilde{\mathbf{x}})\right). \tag{B9}$$

Proof. Differentiating equation (B8) once yields the expression

$$\frac{df_N(x)}{dx} = \left(\frac{d\mathbf{L}}{dx}(x;\widetilde{\mathbf{x}})\right)^\top \mathbf{f}(\widetilde{\mathbf{x}}). \tag{B10}$$

Evaluating equation (B10) at a set of points (e.g., $\widetilde{\mathbf{x}}$), results in an expression of the form $\frac{d\mathbf{f}}{dx} = \mathcal{D}\mathbf{f}$, from which equation (12) follows immediately. □

Thus, the differentiation operator, $\mathcal{D}$, for the collocation points $\widetilde{\mathbf{x}}$ can be expressed in terms of the derivative of the Lagrange basis polynomials $\mathbf{L}(x;\widetilde{\mathbf{x}})$. A Galerkin technique can also be used to derive an equivalent differentiation operator.

Theorem B.2. *The derivative operator that exactly differentiates an arbitrary p-th order polynomial ($p = N-1$) at the collocation points $\widetilde{\mathbf{x}}$ is*

$$\mathcal{D} = (d_{ij}) = \widehat{\mathcal{P}}^{-1}\,\widehat{\mathcal{Q}}. \tag{B11}$$

Proof. First note that in addition to expression (B10), the exact derivative, $\frac{df(x)}{dx}$, of the function $f(x)$ can be approximated by

$$\frac{df}{dx}(x) \approx \frac{df_N}{dx}(x) = \mathbf{L}(x;\widetilde{\mathbf{x}})^\top \frac{d\mathbf{f}}{dx}(\widetilde{\mathbf{x}}). \tag{B12}$$

In general, expressions (B10) and (B12) are not equivalent. The Galerkin statement demands that the integral error between the two expressions be orthogonal to a set of Lagrange polynomials. Specifically that

$$\int_{-1}^{1} \mathbf{L}(x;\widetilde{\mathbf{x}}) \left(\mathbf{L}(x;\widetilde{\mathbf{x}})^\top \frac{d\mathbf{f}}{dx}(\widetilde{\mathbf{x}}) \;-\; \left(\frac{d\mathbf{L}}{dx}(x;\widetilde{\mathbf{x}})\right)^\top \mathbf{f}(\widetilde{\mathbf{x}})\right) dx \;=\; 0 \tag{B13}$$

which can be expressed in the equivalent form

$$\widehat{\mathcal{P}}\frac{d\mathbf{f}}{dx}(\widetilde{\mathbf{x}}) \;=\; \widehat{\mathcal{Q}}\mathbf{f}(\widetilde{\mathbf{x}}) \tag{B14}$$

with

$$\begin{array}{rcccl} \widehat{\mathcal{P}} & = & (p_{ij}) & = & \int_{-1}^{1} \mathbf{L}(x;\widetilde{\mathbf{x}})\mathbf{L}(x;\widetilde{\mathbf{x}})^{\top}\, dx, \\ \widehat{\mathcal{Q}} & = & (q_{ij}) & = & \int_{-1}^{1} \mathbf{L}(x;\widetilde{\mathbf{x}})\big(\frac{d\mathbf{L}}{dx}(x;\widetilde{\mathbf{x}})\big)^{\top}\, dx. \end{array} \tag{B15}$$

Equation (B11) would follow immediately if $\widehat{\mathcal{P}}$ is symmetric positive definite (SPD), and therefore invertible. The fact that $\widehat{\mathcal{P}}$ is symmetric follows immediately from definition (B15). Positive definiteness is more subtle. Following the definition of SPD, we pre- and post-multiply $\widehat{\mathcal{P}}$ by an arbitrary discrete vector ψ, yielding

$$\boldsymbol{\psi}^{\top}\widehat{\mathcal{P}}\boldsymbol{\psi} \;=\; \int_{-1}^{1} \boldsymbol{\psi}^{\top}\mathbf{L}(x;\widetilde{\mathbf{x}})\mathbf{L}(x;\widetilde{\mathbf{x}})^{\top}\boldsymbol{\psi}\, dx \;=\; \int_{-1}^{1} \psi(x)^2\, dx, \tag{B16}$$

an expression, which is strictly greater than zero, unless $\boldsymbol{\psi}$ is the null vector. Thus, the matrix $\widehat{\mathcal{P}}$ is SPD, therefore invertible, and (B11) follows immediately. □

Remark. Once we have established that $\widehat{\mathcal{P}}$ is invertible, we can proven (B11) directly by showing that $\widehat{\mathcal{P}}\,\mathcal{D} = \widehat{\mathcal{Q}}$. This is accomplished by simplifying, after substituting the definitions of $\widehat{\mathcal{P}}$, $\mathcal{D}$ and $\widehat{\mathcal{Q}}$.

A proof that $\widehat{\mathcal{Q}}$ is nearly skew-symmetric is as follows.

Theorem B.3. *The matrix* $\widehat{\mathcal{Q}} \;=\; \int_{-1}^{1} \mathbf{L}(x;\widetilde{\mathbf{x}})\big(\frac{d\mathbf{L}}{dx}(x;\widetilde{\mathbf{x}})\big)^{\top} dx$ *is structurally of the form*

$$\widehat{\mathcal{Q}} + \widehat{\mathcal{Q}}^{\top} = \mathcal{B}. \tag{B17}$$

Thus, by virtue of the structure of $\widehat{\mathcal{P}}$ and $\widehat{\mathcal{Q}}$, the differentiation operator, $\mathcal{D}$, is indeed an SBP operator defined by (2).

Proof. Integrating by parts the definition of $\widehat{\mathcal{Q}}$ yields the expression

$$\begin{array}{rcl} \widehat{\mathcal{Q}} \;=\; \int_{-1}^{1} \mathbf{L}(x;\widetilde{\mathbf{x}})\big(\frac{d\mathbf{L}}{dx}(x;\widetilde{\mathbf{x}})\big)^{\top}\, dx & = & \mathbf{L}(+1;\widetilde{\mathbf{x}})\,\mathbf{L}(+1;\widetilde{\mathbf{x}})^{\top} - \mathbf{L}(-1;\widetilde{\mathbf{x}})\,\mathbf{L}(-1;\widetilde{\mathbf{x}})^{\top} \\ & - & \int_{-1}^{1} \big(\frac{d\mathbf{L}}{dx}(x;\widetilde{\mathbf{x}})\big)\mathbf{L}(x;\widetilde{\mathbf{x}})^{\top}\, dx. \end{array} \tag{B18}$$

All Lagrange polynomials based on the LGL collocation points vanish on the boundaries for $1 < i, j < N$. Thus, the boundary matrices reduce to the form

$$\mathbf{L}(+1;\widetilde{\mathbf{x}})\,\mathbf{L}(+1;\widetilde{\mathbf{x}})^{\top} - \mathbf{L}(-1;\widetilde{\mathbf{x}})\,\mathbf{L}(-1;\widetilde{\mathbf{x}})^{\top} \;=\; \delta_{iN}\,\delta_{jN} - \delta_{i1}\,\delta_{j1}.$$

Writing equation (B18) in indicial nomenclature leads to $q_{ij} + q_{ji} = \delta_{iN}\,\delta_{jN} - \delta_{i1}\,\delta_{j1}$, which is the desired result. □

B.2.1 Collocation and mass lumping

A Legendre collocation operator may be constructed by approximating the integrals in equations (B15) by the LGL quadrature formula. Let

$$\boldsymbol{\eta} = (\eta_1, \eta_2, \dots \eta_{N-1}, \eta_N)^\top \tag{B19}$$

be the nodes of the LGL quadrature formula (i.e., the zeroes of the polynomial $\frac{d\left(P_{n-1}(x)(1-x^2)\right)}{dx}$ [39]), and let ω_l, $1 \le l \le N$ be the quadrature weights. Define $\mathbf{L}(\eta_l; \mathbf{x})$ as the vector of Lagrange basis polynomials evaluated at the quadrature point η_l; i.e.,

$$\mathbf{L}(\eta_l; \mathbf{x}) \;=\; (L_1(\eta_l; \mathbf{x}), L_2(\eta_l; \mathbf{x}), \dots, L_N(\eta_l; \mathbf{x}))^\top.$$

Using these definitions, the mass and stiffness matrices $\mathcal{P}$ and $\mathcal{Q}$ are given by the expressions

$$\mathcal{P} \;=\; \textstyle\sum_l \mathbf{L}(\eta_l; \mathbf{x})(\mathbf{L}(\eta_l; \mathbf{x}))^\top \omega_l, \quad \mathcal{Q} \;=\; \sum_l \mathbf{L}(\eta_l; \mathbf{x})\left(\frac{d\mathbf{L}}{dx}(\eta_l; \mathbf{x})\right)^\top \omega_l. \tag{B20}$$

Theorem B.4. *The matrix $\mathcal{P}$ is diagonal for collocations points located at the LGL quadrature points, i.e., $\mathbf{x} = \boldsymbol{\eta}$. Furthermore, the diagonal coefficients of $\mathcal{P}$ are the integration weights ω_l, $1 \le l \le N$ used in the quadrature [21].*

Proof. Recall that the Lagrange polynomials evaluated at the knot points satisfy the property $L_i(x_j) = \delta_{ij}$. Thus, the result follows immediately from the definition of the norm $\mathcal{P} = \sum_l \mathbf{L}(\eta_l; \mathbf{x})(\mathbf{L}(\eta_l; \mathbf{x}))^\top \omega_l$. □

Remark. Replacing the full $\mathcal{P}$-norm in (B15) with a lower-order diagonal operator is sometimes referred to as "mass lumping".

Note that in general, $\widehat{\mathcal{P}} \neq \mathcal{P}$. The LGL formula is exact for polynomials of degree $2p-1$, where $p = N-1$. However, $\int_{-1}^{1} \mathbf{L}(x; \mathbf{x})(\mathbf{L}(x; \mathbf{x}))^\top \, dx$ is of degree $2p$. Thus, the integration differs for the highest order term (i.e., $2p$-th order term). Indeed, the two matrix norms differ by a rank one perturbation, i.e $\widehat{\mathcal{P}} = \mathcal{P} + \gamma_p \mathcal{D}^p \mathbf{e_0} (\mathcal{D}^p \mathbf{e_0})^\top$ where $\mathbf{e_0} = (1, 0, \cdots, 0)^\top$, $\mathcal{D}^p$ is the highest derivative supported by the polynomial, and γ_p depends on polynomial order.

The matrices $\widehat{\mathcal{Q}}$ and $\mathcal{Q}$ are equivalent. This follows from the fact of the two matrices are defined by the polynomials $\int_{-1}^{1} \mathbf{L}(x; \mathbf{x})\left(\frac{d\mathbf{L}}{dx}(x; \mathbf{x})\right)^\top \, dx$ that have a combined rank of $2p-1$. Therefore, integration is exact when using the LGL integration formula.

The uniqueness of the differentiation matrix $\mathcal{D}$ yields the expression

$$\mathcal{D} = \widehat{\mathcal{P}}^{-1} \widehat{\mathcal{Q}} = \mathcal{P}^{-1} \mathcal{Q}.$$

This statement does not contradict the fact that $\widehat{\mathcal{P}} \neq \mathcal{P}$. Indeed, the Sherman-Morrison formula [40] can be used to show that the difference (i.e., $\widehat{\mathcal{P}}^{-1} - \mathcal{P}^{-1}$) lies in the null space of the singular $\mathcal{Q}$ matrix.

B.3 Interpolation

We seek interpolation operators that take the discrete values $\mathbf{f}(\widetilde{\mathbf{x}})$ of an arbitrary polynomial function $f_M(x)$, from one set of points to another, (e.g., interpolating $f_M(x)$ from $\widetilde{\mathbf{x}}$ to $\mathbf{x}$). Define the two sets of discrete points as follows:

$$\begin{aligned} \widetilde{\mathbf{x}} &= (\widetilde{x}_1, \widetilde{x}_2, \cdots, \widetilde{x}_{M-1}, \widetilde{x}_M)^\top, \quad -1 \le \widetilde{x}_1, \widetilde{x}_2, \cdots, \widetilde{x}_{M-1}, \widetilde{x}_M \le 1, \\ \mathbf{x} &= (x_1, x_2, \cdots, x_{N-1}, x_N)^\top, \quad -1 \le x_1, x_2, \cdots, x_{N-1}, x_N \le 1. \end{aligned} \tag{B21}$$

A Galerkin approach is used to build the interpolation operators.

Theorem B.5. *An interpolation pair that translates polynomial information between two sets of points* $\widetilde{\mathbf{x}}$ *and* $\mathbf{x}$ *can be expressed as*

$$\mathcal{I}_{N\to M} \;=\; \widetilde{\mathcal{P}}^{-1}\,\mathcal{R}_{M-N}, \quad \mathcal{I}_{M\to N} \;=\; \widehat{\mathcal{P}}^{-1}\,\mathcal{R}_{M-N}^{\top} \tag{B22}$$

with

$$\widetilde{\mathcal{P}} = \int_{-1}^{1} \mathbf{L}(x;\widetilde{\mathbf{x}})\mathbf{L}(x;\widetilde{\mathbf{x}})^{\top} dx, \quad \widehat{\mathcal{P}} = \int_{-1}^{1} \mathbf{L}(x;\mathbf{x})\mathbf{L}(x;\mathbf{x})^{\top} dx, \quad \mathcal{R}_{M-N} = \int_{-1}^{1} \mathbf{L}(x;\widetilde{\mathbf{x}})\mathbf{L}(x;\mathbf{x})^{\top} dx. \tag{B23}$$

Proof. First define two distinct polynomial representations of the same function $f(x)$, using Lagrange polynomials and discrete function values. Assume that M and N are not equal. The polynomial representations are

$$f(x) \;\approx\; f_M(x) \;=\; \mathbf{L}(x;\widetilde{\mathbf{x}})^{\top}\mathbf{f}(\widetilde{\mathbf{x}}), \quad f(x) \;\approx\; f_N(x) \;=\; \mathbf{L}(x;\mathbf{x})^{\top}\mathbf{f}(\mathbf{x}). \tag{B24}$$

Next, demand that the two polynomials approximations of $f(x)$ be as close as possible in an integral sense. Two Galerkin statements for the minimization of the differences in polynomials are

$$\int_{-1}^{1} \mathbf{L}(x;\widetilde{\mathbf{x}}) \left(\mathbf{L}(x;\widetilde{\mathbf{x}})^{\top}\mathbf{f}(\widetilde{\mathbf{x}}) \;-\; \mathbf{L}(x;\mathbf{x})^{\top}\mathbf{f}(\mathbf{x}) \right) dx \;=\; 0, \tag{B25}$$

$$\int_{-1}^{1} \mathbf{L}(x;\mathbf{x}) \left(\mathbf{L}(x;\widetilde{\mathbf{x}})^{\top}\mathbf{f}(\widetilde{\mathbf{x}}) \;-\; \mathbf{L}(x;\mathbf{x})^{\top}\mathbf{f}(\mathbf{x}) \right) dx \;=\; 0, \tag{B26}$$

and enforce integral minimization of interpolation error between two distinct sets of Lagrange polynomials, (i.e., those constructed with respect to $\widetilde{\mathbf{x}}$ and $\mathbf{x}$).

Rearranging equation (B25) and (B26) yields

$$\mathbf{f}(\widetilde{\mathbf{x}}) \;=\; \widetilde{\mathcal{P}}^{-1}\,\mathcal{R}_{M-N}\,\mathbf{f}(\mathbf{x}) \;=\; \mathcal{I}_{N\to M}\,\mathbf{f}(\mathbf{x}), \quad \mathbf{f}(\mathbf{x}) \;=\; \widehat{\mathcal{P}}^{-1}\,\mathcal{R}_{M-N}^{\top}\,\mathbf{f}(\widetilde{\mathbf{x}}) \;=\; \mathcal{I}_{M\to N}\,\mathbf{f}(\widetilde{\mathbf{x}}) \tag{B27}$$

with

$$\widetilde{\mathcal{P}} = \int_{-1}^{1} \mathbf{L}(x;\widetilde{\mathbf{x}})\mathbf{L}(x;\widetilde{\mathbf{x}})^{\top} dx, \quad \widehat{\mathcal{P}} = \int_{-1}^{1} \mathbf{L}(x;\mathbf{x})\mathbf{L}(x;\mathbf{x})^{\top} dx, \quad \mathcal{R}_{M-N} = \int_{-1}^{1} \mathbf{L}(x;\widetilde{\mathbf{x}})\mathbf{L}(x;\mathbf{x})^{\top} dx. \tag{B28}$$

We have already established the invertibility of $\widehat{\mathcal{P}}$ and $\widetilde{\mathcal{P}}$. □

Remark. Equation (B22) immediately implies

$$\widetilde{\mathcal{P}}\,\mathcal{I}_{N\to M} \;=\; \mathcal{I}_{N\to M}^{\top}\widehat{\mathcal{P}}. \tag{B29}$$

B.3.1 Mass lumping LGL norms

Entropy stability is achieved with a mass-lumped diagonal operator $\mathcal{P}$ (i.e., equation (B20)). Equation (B29) plays a pivotal role in all staggered entropy proofs. Thus, an equivalent relation that holds for $\mathcal{P} = \sum_l \mathbf{L}(\eta_l;\mathbf{x})(\mathbf{L}(\eta_l;\mathbf{x}))^\top \omega_l$ must be derived.

A Legendre collocation interpolation operators may be constructed by approximating the integrals in equations (B23) with the LG and LGL quadrature formula.

Theorem B.6. *The mass lumped expression*

$$\widetilde{\mathcal{P}}\,\mathcal{I}_{LGL\to LG} \;=\; \mathcal{I}_{LG\to LGL}^\top \mathcal{P} \tag{B30}$$

with $\mathcal{P} = \sum_l \mathbf{L}(\eta_l;\mathbf{x})(\mathbf{L}(\eta_l;\mathbf{x}))^\top \omega_l$ is valid provided the number of LGL points exceeds by at least one the number of LG points (i.e., $N > M$).

Proof. Define $\mathcal{D}^N$ as the matrix $\mathcal{D}$ raised to the power N. Substituting the relationship $\widehat{\mathcal{P}} = \mathcal{P} + \gamma_N\,\mathcal{D}^N\mathbf{e_0}\big(\mathcal{D}^N\mathbf{e_0}\big)^\top$ into equation (B29) yields the expression

$$\widetilde{\mathcal{P}}\,\mathcal{I}_{LGL\to LG} \;=\; \mathcal{I}_{LG\to LGL}^\top\Big(\mathcal{P} + \gamma_N\,\mathcal{D}^N\mathbf{e_0}\big(\mathcal{D}^N\mathbf{e_0}\big)^\top\Big) \;=\; \mathcal{I}_{LG\to LGL}^\top\mathcal{P} + \gamma_N\,\mathcal{I}_{LG\to LGL}^\top\mathcal{D}^N\mathbf{e_0}\big(\mathcal{D}^N\mathbf{e_0}\big)^\top. \tag{B31}$$

If the vector condition $\big(\mathcal{D}^N\mathbf{e_0}\big)^\top\mathcal{I}_{LG\to LGL} = 0$ holds, then (B30) is satisfied.

Let $\boldsymbol{\xi}$ be a matrix of basis vectors of polynomial degree M on the LG points. The action of the interpolation operator $\mathcal{I}_{LG\to LGL}$ on $\boldsymbol{\xi}$ is a rotation of each basis vector from the LG to LGL points. Note that the rotation does not change the polynomial order of any of the vectors.

Now, recall that the vector $\mathcal{D}^N\mathbf{e_0}$ is the undivided difference on the LGL. Thus, if $N > M$, then the undivided difference of a polynomial of degree $\leq M$ will be the zero vector for each of the M basis vectors. Because the vectors are arbitrary, the vector condition $\big(\mathcal{D}^N\mathbf{e_0}\big)^\top\mathcal{I}_{LG\to LGL} = 0$ must hold. □

Remark. For the work presented herein, $M = p$ and $N = p + 1$.

REPORT DOCUMENTATION PAGE

Form Approved
OMB No. 0704–0188

1. REPORT DATE *(DD-MM-YYYY)*	2. REPORT TYPE	3. DATES COVERED *(From - To)*
01-12-2015	Technical Memorandum	03/2015-07/2015

4. TITLE AND SUBTITLE
Entropy Stable Staggered Grid Spectral Collocation for the Burgers' and Compressible Navier-Stokes Equations

5a. CONTRACT NUMBER

5b. GRANT NUMBER

5c. PROGRAM ELEMENT NUMBER

6. AUTHOR(S)
Carpenter, Mark H., Parsani, Matteo, Fisher, Travis C., and Nielsen, Eric J.

5d. PROJECT NUMBER

5e. TASK NUMBER

5f. WORK UNIT NUMBER
794072.02.07.02.03

7. PERFORMING ORGANIZATION NAME(S) AND ADDRESS(ES)
NASA NASA Langley Research Center
Hampton, Virginia 23681-2199

8. PERFORMING ORGANIZATION REPORT NUMBER
L–20597

9. SPONSORING/MONITORING AGENCY NAME(S) AND ADDRESS(ES)
National Aeronautics and Space Administration
Washington, DC 20546-0001

10. SPONSOR/MONITOR'S ACRONYM(S)
NASA

11. SPONSOR/MONITOR'S REPORT NUMBER(S)
NASA-TM–2015–218990

12. DISTRIBUTION/AVAILABILITY STATEMENT
Subject Category 02
Availability: NASA STI Program (757) 864-9658

13. SUPPLEMENTARY NOTES

14. ABSTRACT
Staggered grid, entropy stable discontinuous spectral collocation operators of any order are developed for Burgers' and the compressible Navier-Stokes equations on unstructured hexahedral elements. This generalization of previous entropy stable spectral collocation work [1, 2], extends the applicable set of points from tensor product, Legendre-Gauss-Lobatto (LGL) to a combination of tensor product Legendre-Gauss (LG) and LGL points. The new semi-discrete operators discretely conserve mass, momentum, energy and satisfy a mathematical entropy inequality for both Burgers' and the compressible Navier-Stokes equations in three spatial dimensions. They are valid for smooth as well as discontinuous flows. The staggered LG and conventional LGL point formulations are compared on several challenging test problems. The staggered LG operators are significantly more accurate, although more costly to implement. The LG and LGL operators exhibit similar robustness, as is demonstrated using test problems known to be problematic for operators that lack a nonlinearly stability proof for the compressible Navier-Stokes equations (e.g., discontinuous Galerkin, spectral difference, or flux reconstruction operators).

15. SUBJECT TERMS
Entropy stability, Staggered Grids, Discontinuous methods on any order, Robustness, Burgers' equation, Compressible Navier-Stokes, Summation-By-Parts, Simultaneous-Approximation-Term, Interpolation, Unstructured Grids

16. SECURITY CLASSIFICATION OF:			17. LIMITATION OF ABSTRACT	18. NUMBER OF PAGES	19a. NAME OF RESPONSIBLE PERSON
a. REPORT	b. ABSTRACT	c. THIS PAGE			STI Help Desk (email: help@sti.nasa.gov)
U	U	U	UU		19b. TELEPHONE NUMBER *(Include area code)* (757) 864-9658